THE ANALYSIS OF 3D PRINTED IMPLANTS

by

Arya Nicum

Submitted in accordance with the requirements for the degree

of

Master of Philosophy (MPhil)

University College London

Faculty of Medical Sciences

Division of Surgery and Interventional Science

December 2024

Declaration

I, Arya Nicum, confirm that the work presented in this thesis is my own. Where information has been derived from other sources; I confirm that this has been indicated in the thesis.

Signature

_____

Date

_____

Abstract

3D printing is an additive manufacturing technique which is rapidly being adopted across engineering. This is due to the benefits that 3D printing enables when comparing to conventional methods, such as design control enabling manufacturers to produce custom devices, complex structures for improved initial stability and osseointegration, and parts with differing features, all within a single step in the manufacturing workflow. Two prevalent metal-based methods of 3D printing are the metal powder-based techniques, Selective Laser Melting (SLM) and Electron Beam Melting (EBM). These methods utilise a laser or electron beam to selectively melt powder particles repeatedly layer-by-layer to form a fully dense part.

However, with the speed of adoption of 3D printing, there remains several unknown impacts of final-production implants, and particularly the porous structures. The overarching aim of this thesis is to investigate the influence of these different manufacture methods on the physical features of 3D printed implants, with a particular focus on the complex porous structures specifically on 3D printed acetabular cups, and begin to consider the clinical and regulatory impacts of this new technology in orthopaedics, to ensure patient safety is maintained in this transition.

To achieve this, various analysis techniques including Scanning Electron Microscopy (SEM) and Micro-Computed Tomography (Micro-CT) have been applied to characterise both custom-made and off-the-shelf 3D printed acetabular implants and their porous structures.

Chapter 3 discusses the dimensional features of the struts of these structures as well as the level of porosity found in this layer. Despite the different approaches to the porous layer design between manufacturers resulting in a variation in the dimensional features, porosity was largely not statistically significant between

manufacturers, demonstrating that manufacturers appear to work to a shared goal (porosity varied from medians of 49% to 82%), while optimal porosity is yet to be determined. Chapter 4 investigates the presence of a known by-product of 3D printing, surface adhered particles, and found that these were present within the porous layer regardless of manufacturer and 3D printing type, and SLM exhibited twelve times the number of particles present and smaller particles than found for EBM (24.3μm and 53.8μm, respectively). The results from this report aims to provide some fundamental evidence to inform both surgeons and implant manufacturers, and also regulatory bodies on the engineering and clinical properties of 3D printed orthopaedic implants.

Impact Statement

3D printing is an innovative manufacturing technique which is rapidly being adopted for the production of orthopaedic implants, including off-the-shelf acetabular cups for hip arthroplasty. Also, there is an increasing number of hip arthroplasty procedures being performed every year due to an ageing population and also the surgery is being offered to younger patients (<60 years old). In the UK in 2018, it was reported that 3D printed implants accounted for 13% of all uncemented acetabular revision cases and so in recent years 3D printed cups have become routine for these procedures. However, with the novelty of 3D printing, there lacks the appropriate standards and regulation as they struggle to stay up to date with the pace at which this method is being developed and utilised, and the respective advancements and limitations. This report aims to present insights on the investigation of these properties and features present in 3D printed implants.

There was a development and optimisation of two methodologies for the chapters. Micro-computed tomography (Micro-CT) was combined with the medical imaging software Synopsys Simpleware for a novel approach to examining the features of the porous layers of 3D printed orthopaedic implants, including the dimensional characteristics of the struts and the levels of porosity. Additionally, a partially automated and computational method was developed in Python combined with a manual method using ImageJ to characterise the surface of these struts within the porous structure to evaluate the presence of surface adhered particles, that were present on all cups.

The results of this thesis are an important step for both academic research as well as for implant manufacturers. These studies and their respective methodologies were

among the first of their kind and begin to fill the gaps in current literature and build on the current techniques used for analysis of several types additively manufactured implants, such as knee, spine, craniomaxillofacial implants among others. The aim of this report was to investigate and characterise the features of the porous regions of these implants and therefore the evidence found can start to inform surgeons and manufacturers of the features and limitations of 3D printed orthopaedic implants and assist in the development and revision of homogenised regulations and standards of these devices. Ultimately, the results in this report will help patients and their safety, which is always the primary goal of these investigations.

Acknowledgements

I would like to thank my supervisory team for their guidance. I have been very grateful for the opportunity to undertake these studies.

Specifically, I would like to express my gratitude to Dr Harry Hothi, for his constant willingness, encouragement and inspiration, and for remaining committed to my project despite the internal challenges. I will always be grateful for all of his time and feedback, and this thesis would have not been possible without his support.

My thanks also go to Sara and Angelika who helped me to find the positives and brightening up the office environment.

Finally, all my gratitude goes to my family and closest friends, who have all been there to listen and support my choices at every uncertain moment over the last couple of years.

Table of Contents

List of Figures

Figure 2.13: (a) SEM Images of a regular or cellular and an irregular 3D-printed porous structure and the corresponding manufacture method (Electron Beam Melting (EBM) and Selective Laser Melting (SLM)). (b) Computer rendered meshes formed using Micro-CT data from AM acetabular cups from four separate manufacturers with varying porous structures. Comparisons between porous structures available from different manufacturers can be made [102].

Figure 2.14: A panel of SEM images depicting surface adhered particles (indicated) in the porous layer of 3D-printed acetabular cups, and the variability of the particles with AM method; Electron Beam Melting (EBM) and Selective Laser Melting (SLM). All Images at x200 magnification [102].

Figure 2.15: Images displaying the extremes of surface adhered powder particles within the porous layer. (a) Almost completely consolidated particles protruding from the strut surface compared with (b) almost completely unmelted particles only just attached to the strut surface. Images at 200x magnification [102].

Figure 2.16: A 3D-printed implant (e.g. (a) an acetabular cup). A Micro-CT scan of the implant can assist in determining (b) the diameter of the implant and provide (c) isolated slices of the internal structure for measurement of (d) the thickness of the porous region, (e) the dense region and (f) the total thickness. [102]

Figure 2.17: (a) Obtaining a roundness measurement using a Coordinate Measuring Machine (CMM). (b) Obtaining a measurement of surface roughness using a Surface Profilometer [102].

Figure 2.18: (a) Image generated from Micro-CT data to show voids in the dense region of a 3D-printed acetabular cup. From these images, void location and frequency can be analysed. This will be followed by (b) void size and shape evaluation [102].

Figure 2.19: (a) A render of a custom 3D-printed acetabular cup created using Micro-CT data and imported into an analysis software (Simpleware, Synopsys, Exeter, UK). From this data, (b) the porous layer is examined and isolated, and (c) a mesh model of the structure is generated. (d) A single mesh unit can then be extracted, followed by (e) best fit modelling with a sphere, to assist in calculating the porosity of the porous layer [102].

Figure 3.00: The study design showing the analysis steps that were performed on unused, 3D-printed, custom and off-the-shelf implants that imaged using micro-computed tomography, where the dimensional features and porosity were determined by analysis in Simpleware, followed by suitable statistical analysis.

Figure 3.01: Macroscopic images of the twelve custom acetabular cups examined in this study, 3D printed by six manufacturers. For each cup, two different views are presented.

Figure 3.02: Macroscopic images of the porous backside of six off-the-shelf acetabular cups examined in this study, 3D printed by one manufacturer.

Figure 4.05: (a) The locations at which SEM images were taken using Cup_4A as an example; (b) How ImageJ was used to identify surface adhered particles and measure their area, from which the particle diameter was determined [125].

Figure 4.06: A) Examples using the circle tool in ImageJ to measure the specific particles. B) The areas measured for the 10 chosen particles were converted into diameters and compared with the measurements found by the code to check for concurrent values. Examples in (A) are indicated. These steps were applied to all cups counted and measured using the computerised method.

Figure 4.07: A representative grid of SEM images of the implants examined in this study (Electron Beam Melting (EBM) vs Selective Laser Melting (SLM)). Surface adhered particles (SAP) are indicated by arrows. All images are at 200x magnification and were taken at the Introducer Screw hole location. Blue circles highlight an additional observation of undulations in the struts potentially indicating layer thickness.

Figure 4.08: A representative grid of SEM images of the implants examined in this study (Electron Beam Melting (EBM) vs Selective Laser Melting (SLM)). Surface adhered particles (SAP) are indicated by arrows. All images are at 200x magnification and were taken at the Bulk Screw hole location.

Figure 4.09: A representative grid of SEM images of the implants examined in this study (Electron Beam Melting (EBM) vs Selective Laser Melting (SLM)). Surface adhered particles (SAP) are indicated by arrows. All images are at 200x magnification and were taken at the Bulk Porosity location. Blue circles highlight an additional observation of undulations in the struts potentially indicating layer thickness.

Figure 4.10: A representative grid of SEM images of the implants examined in this study (Electron Beam Melting (EBM) vs Selective Laser Melting (SLM)). Surface adhered particles (SAP) are indicated by arrows. All images are at 200x magnification and were taken at the Rim location.

Figure 4.11: A panel of SEM Images demonstrating the change of focus to highlight the particles present at the surface and subsurface for the different cups. All images taken at 200x magnification.

Figure 4.12: A box plot showing the difference in Particles per mm^2 at the surface level between cups manufactured by Electron Beam Melting (EBM) vs Selective Laser (SLM). A Kruskal-Wallis test showed there to be a difference in the number of particles per mm^2 on the surface of each cup ($p=0.0001$). [125] Cup 3A and 3B are highlighted as they exhibit differing results to the remainder of the SLM cups.

Figure 4.13: A panel of cups manufactured by EBM and SLM, showing stark differences between the particles per mm^2 and particle diameter between the manufacture methods. The contrast in level of adhesion of the particles is also highlighted in the red circles. All images are taken at 200x magnification.

List of Tables

Table 3.07: The comparisons between each of the cups for this particular parameter, where there were no statistically significant p-values.

Table 4.01: The Median(Range) for Particles per mm^2 and Diameter at the surface and subsurface levels, and corresponding p-values. Statistically significant p-values are indicated by an asterisk. Cups manufactured by EBM and SLM are also highlighted, as well as the results of Cup 3A and 3B in particular.

Table 4.02: Types and sizes of other clinically relevant particles in orthopaedics, e.g. wear debris from certain hip implant components and combinations. The particles observed and measured in this study are italicised [52,106,125,152–154].

1 | Introduction

1.1 | Motivation

Total hip arthroplasty (THA) is considered to be one of the most common and successful surgeries, and hip replacements often last up to 25 years [1]. This procedure is used to restore the hip joint biomechanics and treat conditions including osteoarthritis, traumatic hip fractures and congenital hip disorders.

In Europe it has been reported that over 600,000 total hip arthroplasty procedures take place each year, with over 1.4 million performed worldwide, and it is projected that this number will only continue to grow over the coming years. This is due to an ageing population, as well as the surgery being increasingly used to treat younger patients with longer life expectancies, therefore generating a demand for implants with longer service lives.

3D printing is a new and innovative manufacturing technique and has exhibited several advantages to facilitate new designs and produce medical implants, specifically in orthopaedics. It is being implemented for the mass manufacture of off-the-shelf acetabular cups, with the benefits of complex geometries that can be achieved with 3D printing when compared to conventional methods, such as the porous layer on the backside of the component to encourage bone ingrowth and also the design and production of patient-specific devices to treat massive acetabular defects in the pelvis. It is projected that 3D printed devices will achieve longer lifespans and have better clinical outcomes than conventionally manufactured implants, but there are few investigations where this is demonstrated thus far. The features as well as the drawbacks of this technology must also be better understood, and the respective regulatory bodies have yet to fully adapt and update their guidance to manufacturers.

Therefore, studies involving the examination of unused 3D printed to improve the understanding of the features of these implants and in particular the new porous layer that can be fabricated and its potential implications must be performed in order to smoothly transition to this manufacture method and ensure patient safety in the process.

1.2 | Aim

To evaluate the features of 3D printed orthopaedic implants, and in particular unused, off-the-shelf and custom acetabular cups, to assure patient safety as 3D printing continues to grow in use. Primarily investigating the influence of the manufacture method on the physical properties of the porous regions on 3D printed acetabular cups.

1.3 | Objectives

To develop a new investigation method able to analyse the dimensional properties of the porous structure of custom 3D-printed acetabular components, including using established and state-of-the-art techniques, such as X-ray micro-computed tomography in combination with a novel medical imaging software (Chapter 3).

To further interrogate the porous structures 3D-printed acetabular components using (1) imaging via scanning electron microscopy followed by (2) ImageJ and a newly developed partially automated method in Python for surface adhered particle identification, quantification and measurement (Chapter 4).

To clinically assess the results of the previous chapters and how they fit within the current literature and can be further investigated in the future (Chapter 5).

1.4 | Thesis Outline

This thesis begins with a literature review (Chapter 2) on the fundamentals of hip arthroplasty and the engineering principles of three-dimensional (3D) printing and its application in medicine and hip arthroplasty, followed by four experimental chapters.

Chapter 3 describes the development of a methodology for the dimensional analysis of porous structures of pristine custom 3D-printed acetabular components is presented using micro-computed tomography and a complementing medical imaging software.

Chapter 4 discusses the further characterisation of these porous structures; the analysis of the surface of the struts that make up the lattices, applying a primarily manual method, followed by the development, validation and implementation, of a computational method. This examination is performed on unused off-the-shelf 3D-printed acetabular implants.

Chapter 5 approaches the clinical relevance of the results of each of these chapters. The different types of porous structures and their current performance in vivo are discussed followed by the clinical impacts of surface adhered particles in patients and how this should be investigated going forward.

Future Works are discussed in Chapter 6, and the thesis is concluded in Chapter 7.

2 | Literature Review

2.1 | The Hip Joint

2.1.1 | Hip Anatomy and Biomechanics

The hip joint (or ‘coxa’) is a type of diarthrodial joint and is often referred to as a ‘ball-and-socket’ joint: where the head of the thigh bone (femur) is called the ball and the concave, hemispherical feature of the hip bone (acetabulum) is the socket, together constituting the acetabulofemoral joint. The flat bone formed by the pubis, ischium and ilium is the hip, or ‘coxal’, bone, and the sacrum and coccyx together constitute the pelvis.

There is a smooth layer of cartilage tissue that covers over both the femoral head and the inside of the acetabulum in a healthy hip joint, which allows cushioning when the joint is subjected to the everyday compressive forces, enabling the ball to glide smoothly in the socket. Additionally, the hip is lubricated with synovial fluid (produced by synovial membranes), further allowing low friction and continuous motion. The stability of the hip joint is secured by an articular capsule, several ligaments (three extracapsular, one intracapsular), tendons and muscles, to prevent dislocation of the joint [2]. The medial and lateral circumflex femoral arteries supply the hip joint with blood, and these are structures of the deep artery in the thigh and anastomose in the lower femoral neck and form a ring. The sciatic, femoral and obturator nerves mainly provide the innervation to the joint [3] (Figure 2.01 [4]).

During the range of everyday activities, the hip joint supports the body, by distributing and managing the weight and ensuring balance during dynamic loading. There are three main axes on which the hip muscles act, all of which pass through the centre of rotation of the hip joint, which is located at the centre of the femoral head. The hip joint enables a wide range of movement due to its anatomical structure, which

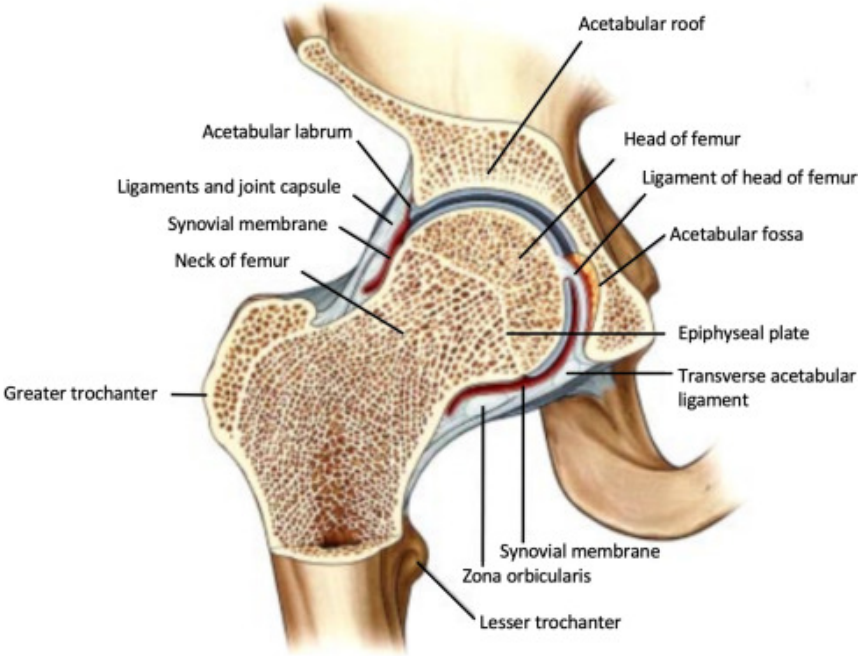

Figure 2.01: Labelled coronal section view of the hip joint [4].

results in the main directions of motion along and around these three axes: flexion and extension in the sagittal plane, abduction and adduction in the coronal plane, and intra and extra-rotation in the transverse plane. These can be visualised in Figure 2.02.

The definitions of these ranges of movement are as follows:

Flexion is the movement of the thigh coming towards the abdomen in a range of 0 to 130 degrees and is controlled by the iliopsoas and quadricep muscles.

Extension is the opposite of flexion and is regulated using the gluteus maximus muscle, with a range of 0 to 30 digress.

Abduction is the movement of the positioning the leg away from the body, as controlled by the primary hip abductors, the gluteal muscles, and has a range extending from 0 to 45 degrees.

Adduction is the reverse of this motion, returning the leg back towards the body. This motion is controlled by the adductor longus, brevis and magnus and the range is between 0 and 30 degrees.

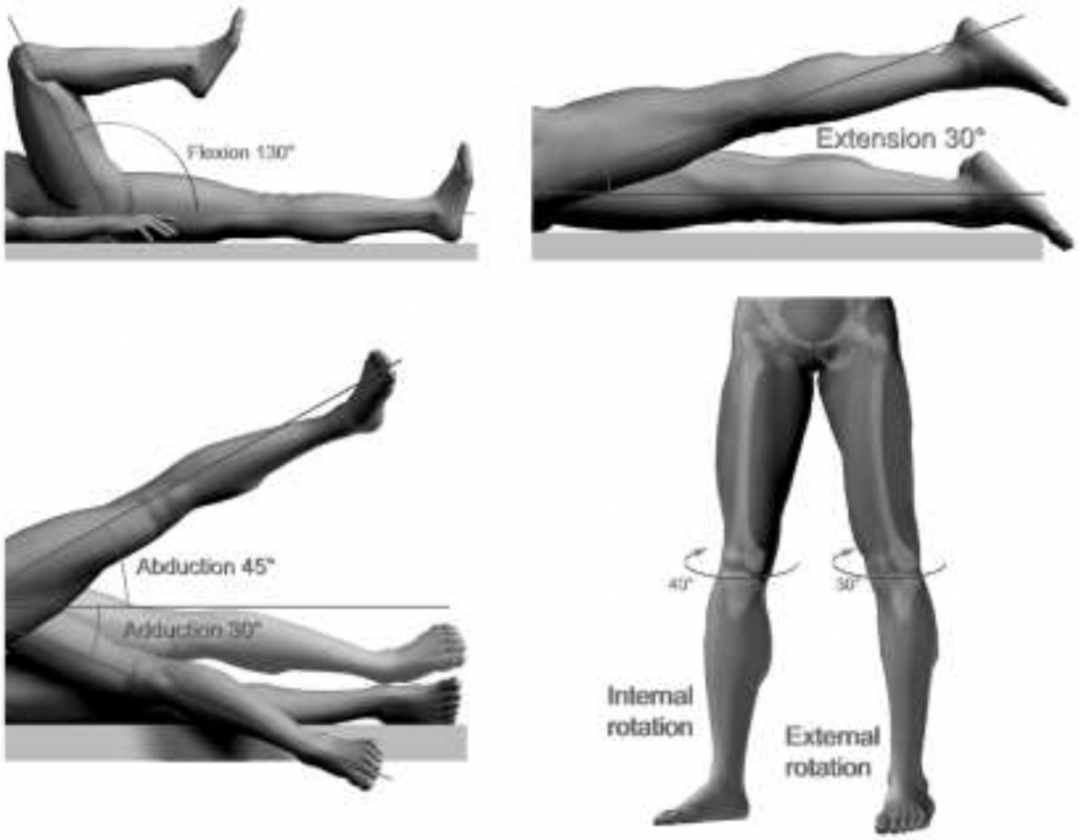

Figure 2.02: The different movements of the hip joint [2].

Additionally, a combination of the gluteal muscles controls the internal and external rotations, allowing the hip to turn both inward to a maximum of 30 degrees and outward to a maximum of 40 degrees [2].

2.1.2 | Hip Pathology

As the hip is one of the primary weight-bearing joints in the body, there are many different chronic and acute pathological conditions that could lead to hip arthroplasty. With normal everyday activities, it has been estimated that the internal forces experienced by the hip joint range from 2.6 and 5.6 times the weight of the body during walking and 1.9 and 6.0 times for climbing the stairs [5].

Primary Osteoarthritis (OA) is the most common chronic condition. This is a degenerative condition of the damage or complete loss of the articular cartilage resulting in the articulation of the bones in the hip joint against each other without the

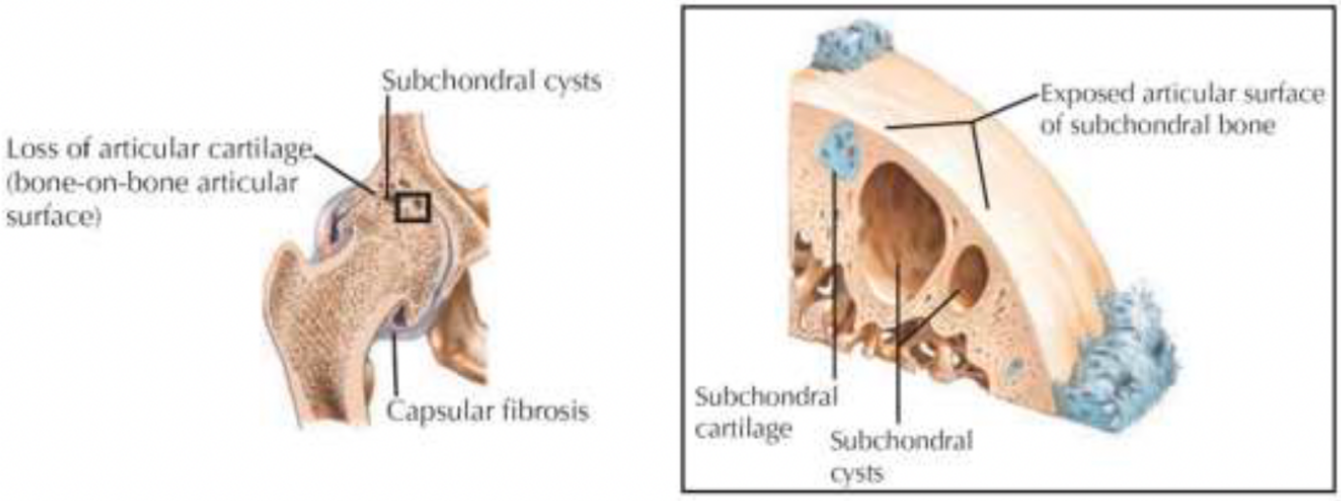

Figure 2.03: An example of an osteoarthritic hip [3].

protective cartilage layer (Figure 2.03 [3]). The associated processes of OA include muscle weakness, periarticular laxity of the ligaments, subchondral cysts, and synovial inflammation. The risk factors often associated with primary OA include obesity, family predisposition, age and overloading joints, however the exact root cause remains unknown. The main symptoms experienced by patients with OA often include joint pain and stiffness, and impairment of their mobility [6–9], and primary osteoarthritis accounts for between 60-92% of the main reasons for hip surgery worldwide [10–15].

Additionally, there are other conditions which can cause a change in the load distribution across the joint leading to secondary arthritis. These conditions include osteonecrosis, congenital disorders such as developmental hip dysplasia, and disorders occurred as a result of trauma such as fracture of the acetabulum or femoral neck [2,7]. In some cases, it has also been highlighted that supposed primary OA can be secondary to certain developmental abnormalities [16].

The specific conditions mentioned above are described as follows:

Osteonecrosis, or avascular necrosis, can be a cause for total hip arthroplasty. This disease is due to a problem with blood supply leading to the death of osteocytes and vital bone marrow. Osteonecrosis can be related to previous traumatic or non-traumatic events experienced by the patient such as fracture or dislocation of the hip, alcoholism or cortisone therapy, as well as being idiopathic and developing in the absence of any serious health event. The treatment of this condition is responsible for approximately 5-12% of THA cases completed in the United Kingdom annually [17,18].

Developmental Hip Dysplasia is a congenital condition, characterised by deficiencies and anatomical abnormalities of the acetabulum and proximal femur. This disorder occurs when the hip joint forms incorrectly in newborn babies and infants, leading to repeated dislocations, considerable pain and potential loss of function of the joint. Elevated loads and contact stresses on the joint can result in early onset OA and ultimately total hip arthroplasty is the recommended standard of care at end stage OA [19].

Subsequent to a traumatic event to the hip such as fracture of the acetabulum or femoral neck, another common disorder, post-traumatic arthrosis can occur, resulting in the need for total hip arthroplasty [20,21]. Additional conditions that could require surgery include rheumatologic diseases, such as rheumatoid arthritis [22] and ankylosing spondylitis [23]. Both of these autoimmune conditions are long term disorders that generate generalised inflammation in the joints leading the patient to experience pain, swelling and joint stiffness and later leading to OA. Bone tumours of the proximal femur can also require total hip arthroplasty for treatment [2].

2.2 | Total Hip Arthroplasty (THA)

2.2.1 | Introduction

Hip replacement surgery or hip arthroplasty is a popular and well-established medical procedure. It constitutes replacing the diseased hip joint with artificial prostheses. The replacement components consist of an artificial acetabular cup and femoral head, which aim to mimic the low friction environment of the original joint, through the use of biocompatible materials with low coefficients of friction, low wear resistance and sufficient mechanical properties to withstand the loads experienced by a hip joint.

The advent and development of this surgery has had a radical effect on patients suffering with painful and limiting hip joint conditions, by restoring their mobility, enabling the completion of the activities of daily life and improving their overall quality of life. The revolutionary impact of this procedure has led to it being dubbed ‘the operation of the (twentieth) century’ [24].

In Europe, over 600,000 hip arthroplasties are estimated to have been performed annually, with up to 1.4 million being performed worldwide [25]. Between 2016 and 2018 approximately 300,000 hip surgeries were performed in the UK, where the majority of patients were female (59.8%), with an overall median (interquartile range) age of 69 (61-76) years old. Osteoarthritis was listed as the reason for primary surgery in 97.7% of cases performed [13], and looking forward, it is projected that the demand for hip arthroplasty will increase by up to 134% in the UK alone by 2030 [26]. In England, the number of hip replacements by the NHS per 100,000 of the population rose from 272.6 in 2002, to 539.7 in 2018 [27]. A significant explanation for this is due to an increasing life expectancy, where of the 81,130 hip and 93,911 knee replacement procedures completed between April 2018-2019, >90% were over

50 years old [28]. Other factors such as rising cases of obesity placing more strain on joints also contribute to the growing frequency of these surgeries [29].

When comparing the registry data for the United States, 602,582 hip arthroplasties were performed between 2012 and 2018, and female patients also formed the majority of cases (59%), and the overall mean (standard deviation) age of patients was 66 (11) years old [10]. Looking forward in the US, it is expected that the number of operations will grow by 174% by 2030 [30].

Similar trends for the demographic of hip arthroplasty patients have also been reported in other countries such as Australia, where the number of hip procedures dramatically increased by 83% between 2003 and 2018. Comparably, the surgery was more common among female patients (54.9%) and the overall mean age was 68 years old [11].

Despite the trend of patients with a slightly older overall mean age, hip arthroplasties are increasingly becoming a treatment option for younger patients with longer life expectancies and more active lifestyles. Therefore, there is the demand for components with a longer lifespan and improved performance.

Recent survival data reported on the survivorship of these implants observed an all-cause implant survivorship ‘89.4%at 15-years, 70.2% at 20-years and 57.9% at 25-years follow up’. This is the metric based on implant revision for any cause that led to the procedure, and this data highlighted the impressive effectiveness of hip arthroplasty as a successful surgery, but also that there is still a number of overall cases that will experience implant failure [1].

Advances in the technology of implants and their design is an important area of research focus, to improve the longevity and performance of implants and reduce the occurrence of revision surgeries.

2.2.2 | Implants for Total Hip Arthroplasty

Current hip replacements are often made up of four different components; a metal socket (the acetabular cup), a ceramic or plastic liner which sits inside the cup, a metal or ceramic ball (the femoral head) which shares an articulating bearing surface with the liner, and a long femoral stem also made from metal, which is attached to the femoral head via a tapered neck and is implanted into the femur. In most modern designs, the stem and neck are a one-piece component, but in some designs this piece is modular and can have different options. An alternative to a total hip replacement is through hip resurfacing which involves a metal surface replacement femoral implant combined with a metal acetabular socket, but this implant and treatment option is currently less common (Figure 2.04) [3,13].

The different materials and modularity of the parts for the implants allow the most suitable combination to achieve the best wear resistance and mechanical properties for the bearing surface. These combinations include metal-on-metal (MoM), metal-on-polyethylene (MoP), ceramic-on-ceramic (CoC), ceramic-on-polyethylene (CoP) and ceramic-on-metal (CoM).

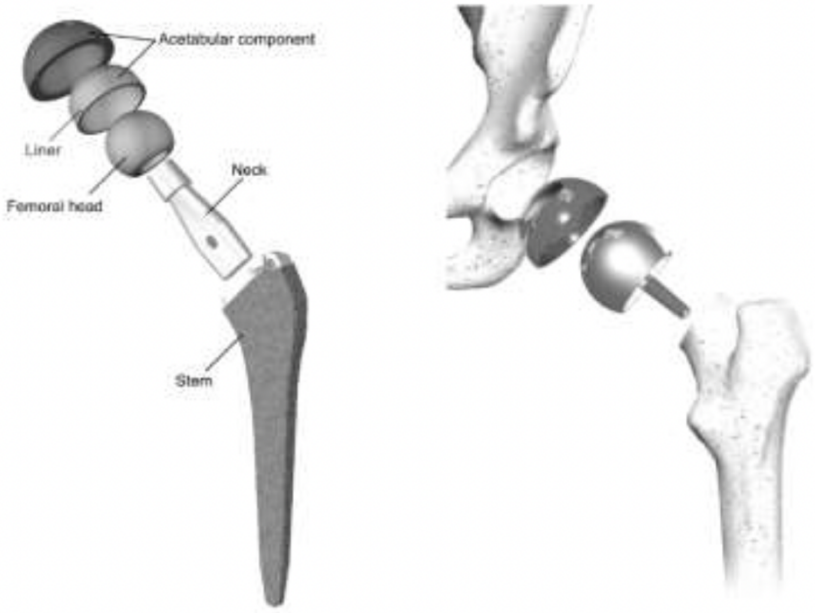

Figure 2.04: Components of a total hip replacement prosthesis (left) and hip resurfacing (right) [2].

Often fixation of the femoral stem in the femoral canal and the acetabular cup into the pelvis are achieved using one of two techniques. Cemented involves fixation using an acrylic-based cement and the uncemented technique achieves fixation by press-fitting the prosthesis against or within the bone.

When using cement, a certain type of epoxy cement is prepared and pressurised into the prepped clean and dry bone bed to ensure a uniform medium for the cement to fill the free space within the bone cavity between the bone and implants. Cemented implants are more commonly used in elderly patients (above the age of 75 years old), patients who are less active, or patients with low quality surrounding bone stock, or where a reduced ability for bone growth are present.

In the case of uncemented fixation, an implant with a roughened, coated or porous surface can assist in anchoring the implant to the bone, combined with additional flanges or screws (on acetabular cups). This method and type of implant us more commonly used in younger patients (below the age of 70 years old), patients with more active lifestyles and more bone stock of a better quality. It is important to consider that younger patients are more likely to undergo a revision surgery, and this

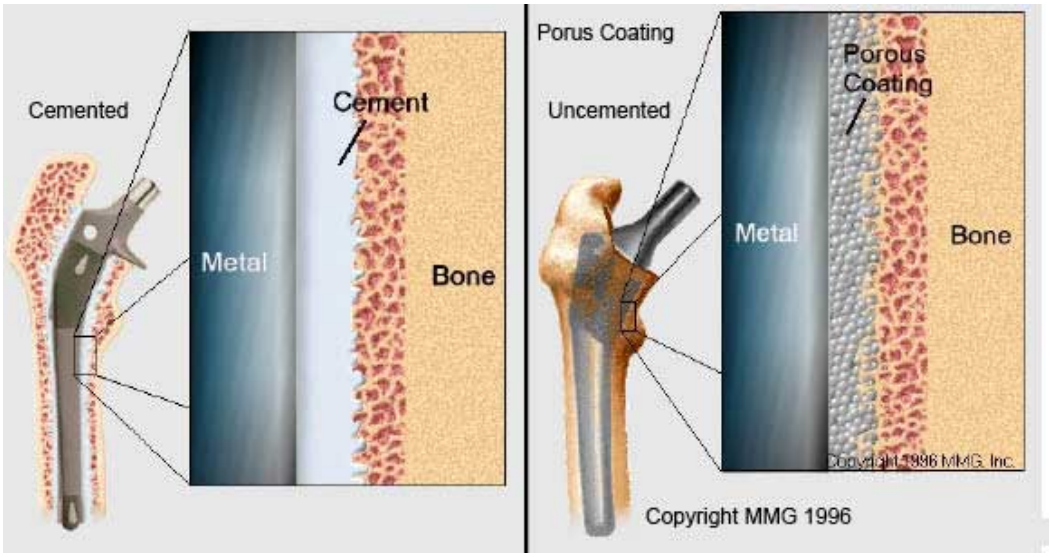

Figure 2.05: Diagrams demonstrating the different fixation methods – cemented and uncemented, for a femoral stem as an example [31].

would be more complex if a cemented implant is applied in the primary procedure (Figure 2.05 [31]).

2.2.3 | The Importance of Bone

Bone is important in the context of implants as it can influence the initial and long-term fixation of the device post-implantation. It is a hard and dynamic connective tissue that is able to remodel when subject to external forces such as loads and stresses. The primary functions of bone in the body are to provide a rigid framework throughout the body (skeletal formation) to support and protect vital internal organs, and also construct a system of rigid structures as attachment sites for the corresponding muscles and ligaments to facilitate movement and motion of the body [32].

Bone has a macrostructure that can be classified into two categories: compact or cortical bone, and trabecular or cancellous bone. Cortical bone is often what forms longer bones such as the femur in its cylindrical shaft, surrounding the bone marrow, and its differing thickness along these bones can impact the risk of fracture. This type of bone is almost completely solid with approximately 3-5% porosity for cells and proliferation. In contrast to cortical bone, trabecular bone exhibits a porosity of approximately 50-90% and is formed of structural rod-like struts termed trabecular which have dimensions of approximately 100μm in thickness. This type of bone therefor exhibits a higher surface area for blood vessels and connective tissue and allows the proliferation of cells. Additionally, this open structure provides some internal mechanical support by enabling the distribution of load and for the absorption of energy on impact which is particularly significant around joints, and therefore provides and explanation for why this type of bone is found in these areas of the body [32–35].

The mechanical properties and quality of bone stock can vary widely with age, activity level and anatomical side of the bone. Additionally, the presence of an artificial prosthesis can alter the original equilibrium of the joint, and so a suitable integration of the device and the surrounding bone can lead to more successful outcomes [32]. Therefore, when considering the biomechanical properties of bone, the strength and the elastic modulus of bone have a critical impact on defining the bone pathology and a significant influence on the design and material choice of artificial implants.

2.2.4 | Complications and Failure of THA leading to Total Hip Revision (THR)

Hip arthroplasty is a very common and successful surgical procedure, but there are still several cases where the operation must be revised due to a range of factors including the failure of one or more of the implant components. This percentage poses an economic burden which is estimated to range from £10,893 ± £5,476 for dislocated

implants up to £21,937 ± £10,965 for infected implants [36]. Despite the surgeon reporting a single reason for revision of the operation, in most cases there are several contributing factors, including surgical such as implant mal-position, patient factors such as obesity or high activity levels and implant factors such as a problem with the implant design or biocompatibility issues with the implant material. In the UK between 2003 and 2018, a primary reason for revision was listed as ‘unexplained pain’ and this accounted for 16.9% (19,541 of 115,77) of cases recorded in this period [13]. Some potential explanations for this reason for revision are detailed below.

Wear and loosening

Aseptic loosening is one of the most common causes for failure of total hip arthroplasty and is loosening of the implant as a result of chronic inflammation in the absence of infection due to particles from wear at the implant-bone interface. When two articulating surfaces are in contact and undergo relative motion, material wear can occur and this can occur at multiple interfaces in a joint replacement, and in replacement hip, the main articulating interface is between the femoral head an acetabular component (liner or cup) and therefore will experience wear. A second type of wear can occur when a ‘third body’ particle such as bone, cement or metal particles, infiltrates the articulating interface. A third type of wear can occur in a joint replacement between two surfaces which are not supposed to articulate in relative motion, such as the ‘backside wear’ of a polyethylene liner against the metal acetabular cup in which it is seated, or where there is impingement on the side of the acetabular cup from the femoral neck.

Clinically, the consequences of the wear of hip implants include:

(1) The dimensions of the component surfaces subjected to the unexpected wear are altered and can impact the biomechanics and range of motion of the joint, and potentially lead to dislocation.

(2) Material wear of the components can generate particulate debris and result in chronic inflammation, periprosthetic osteolysis, loosening and potentially pseudo-tumour formation, and this can have both local and wider systemic effects [37].

The characteristics of the wear debris, such as the cytotoxicity of the material, the size and the morphology of the debris, the volume and rate of release of the particle

and the complexity of the path for particle migration all impact their osteolytic effect [38].

Repeated loading, micromotion at the articulating surfaces, progressive wear and periprosthetic osteolysis over the lifetime of the implant can lead to compromised quality of the surrounding bone stock, resulting in micromotion and eventually loosening and failure of the implant, requiring revision hip surgery (Figure 2.06 [39]). Aseptic loosening was recorded as the main reason for revision hip surgery for cases and represented 43.5% (50,375 out of 115,777) of the total hip revision cases in the UK reported between 2003 and 2018 [13].

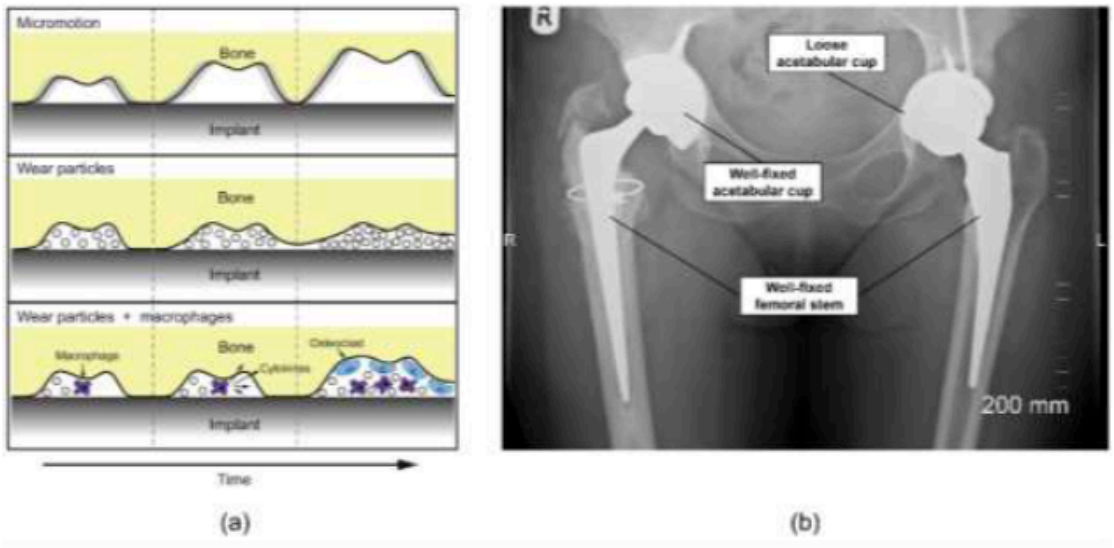

Figure 2.06: (a) Aseptic loosening pathways: (top) progressive micromotion of the implant; (middle) wear products interfering with direct bone-implant contact; (bottom) wear particles activating macrophages, leading to bone resorption [39]. (b) Antero-posterior (AP) plain radiograph showing a loose acetabular cup that was revised.

Infection

Infection can occur after a hip replacement procedure as a result of contamination during the operation or the potential release of bacteria into the bloodstream from other sources in the body such as the bladder, lungs or bowel [38]. There are three

categories of periprosthetic infections; acute infections which occur within 6 weeks post operatively (type 1), a delayed or chronic infection that occurs after 6 weeks post operatively (type 2) and late haematogenous infections which are carried by the blood (type 3) [40]. Examinations including blood tests, medical imaging and aspiration biopsies are all fundamental in determining the presence and type of infection [41].

Once the implant is infected, a biofilm forms around the infected implant, therefore rendering treatment via antibiotics impossible as they are unable to overcome this film and destroy the bacteria responsible for the infection. This therefore requires the removal and replacement of the implant, which can be achieved in either a single operation, or in two stages, where first a spacer fitted with an antibiotic is placed into the infected joint for 6 weeks before the final operation [37].

In the UK, from 2003 to 2018, infection was reported as the reason for revision for 13.8% of the 115,77 cases [13].

Dislocation

Dislocation of a total hip arthroplasty is the occurrence of the femoral head dislodging from the acetabular component of the implants (the cup or liner). There is a ligament in the original natural hip joint linking the femoral head and acetabulum which is not replaced during total hip arthroplasty, and the femoral head is kept in place within the acetabular component through correct positioning of the implant during the procedure and making use of the muscles and ligaments surrounding the pelvis [38]. It is more common for dislocation of total hip arthroplasty to occur in the first six to eight weeks following surgery (75% of dislocation cases occur in this period), due to the incomplete healing of the damaged surrounding soft tissue and

have been reported to occur most frequently in female patients over the age of 70 years old [37]. Dislocation that occurs early in the healing process of THA is often resolved by sedating the patient and manual manipulation of the joint to reposition the implant. Dislocation can also occur later on after surgery and for cases of dislocations that occur after six months post-surgery, it is likely that it will become recurrent, therefore requiring the need for revision surgery.
In the UK, dislocation was reported as the reason for revision in 14.4% (16,646 out of 115,777) of the revision THA cases recorded between 2003 and 2018 [13].

Fracture

Periprosthetic fracture is bone fracture that occurs in the immediate vicinity of a hip implant and tends to involve the implant and then often requires surgery as treatment. In most cases of periprosthetic fracture, there is fracture involving the femoral stem rather than near the pelvis and involving the component of the acetabular cup. During this surgery, the bone fracture is normally stabilised, but in some cases where the fracture is severe and alters the position or condition of the implants, total hip revision surgery is also required. Some patients are at a higher risk of periprosthetic fracture, and these include more elderly patients suffering with osteoporosis (reduced bone mass) or have poor quality bone stock for pathological reasons. Additionally, it is expected that the incidence of periprosthetic fracture will rise as the service life of the implant and levels of activity of patients increase [38].
Periprosthetic fracture was reported as the reason for revision in 10.1% (11,662 out of 115,777) of the revision THA cases recorded in the UK between 2003 and 2018 [13].

2.2.5 | Conventionally Manufactured Acetabular Implants

Current implants for total hip arthroplasties are made up of an uncemented press-fit titanium alloy or cemented cobalt-chrome (Co-Cr) alloy (or stainless steel) femoral stem, attached to a Co-Cr alloy or ceramic femoral head which articulates at the bearing surface in a polyethylene or ceramic liner. This liner is fitted on a titanium or Co-Cr alloy acetabular cup, which is press-fitted and often screwed into the acetabulum in the pelvis [42]. There are several combinations available to surgeons when selecting from the available implant designs and material options from manufacturers and looking at the performance of a specific implant is a helpful indicator in this selection. However, there is sometimes limited or no public information on their performance in patients, and also the success, and respective failure, of an implant is dependent on a number of factors. In particular, these are the 'surgeon', the 'implant' and the 'patient', and are termed 'SIP' factors.

The primary method of fixation in total hip arthroplasty cases recorded for the UK in 2018 involved the uncemented fixation of both the femoral stem and acetabular cup and represented 37.6% of cases (410,296 out of 1,091,892 of total THA cases). MoP was the most common bearing coupling type adopted for all fixation methods, and hybrid combinations involved a cemented femoral stem and an uncemented acetabular cup, and reverse hybrid is the opposite of this (Figure 2.07 [13]).

2.2.6 | Implant Material and Manufacture

The manufacture method of conventional acetabular implants is most commonly techniques such as forging and casting, and also various subtractive methods including milling and computer numerical controlled (CNC) machining. These methods often begin with a block of the raw material (metal alloy) which is either melted (forging and casting) or subject to the subtractive methods to obtain the final part [43,44]. In most cases for conventional acetabular cups, this is how the overall

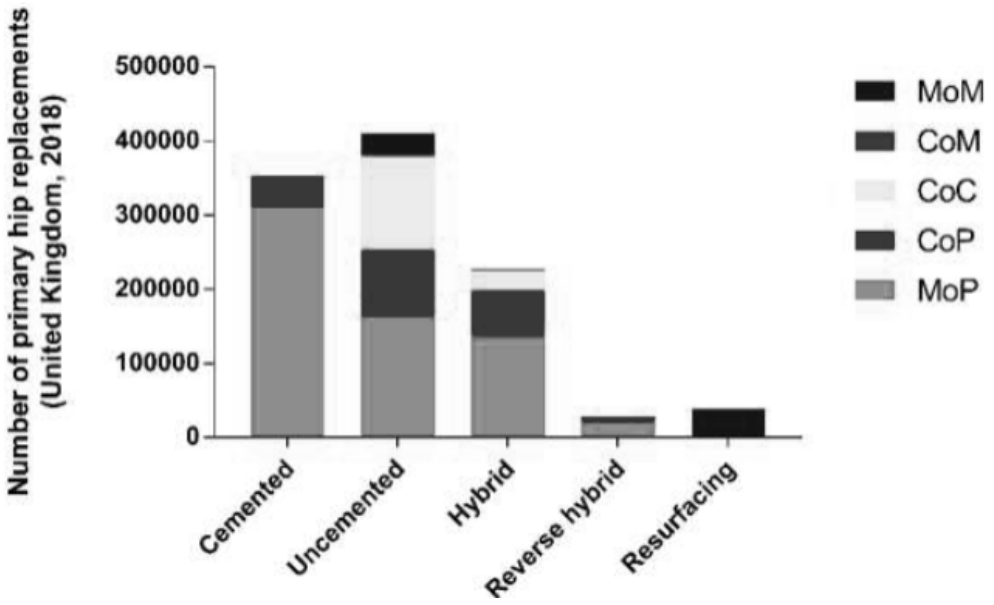

Figure 2.07: Number of primary hip replacements performed in the United Kingdom in 2018 by fixation method and bearing type [13].

hemispherical shape of the implant is produced, and then it will undergo further post-processing where treatments such as coatings are applied.

The titanium alloy Ti-6Al-4V is the most common chosen material for uncemented acetabular implants, due to its excellent biocompatibility as well as its mechanical properties and corrosion resistance [45,46].

After the main body of the acetabular cup is produced (the ‘dome’) the external bone-facing backside is finished using several techniques such as wet or coarse blasting to roughen areas of the surface. The inner side of the cup is also finished through polishing to ensure satisfactory seating and locking of the liner. Finally, a porous coating is applied to the roughened outer side of the acetabular cup during one of the final stages of production, through different methods [44].

2.2.7 | Implant Design

Many manufacturers over the last 20 years have progressively introduced their ‘highly porous’ designs for the bone-facing backside of an acetabular implant in an attempt to overcome the drawbacks of traditional coatings for these implants. ‘Highly’

or ‘ultra-porous’ coatings are used by manufacturers when the associated implant exhibits a porous structure with a porosity of > 60% and/or pore size > 400 μm [47,48]. These structures are particularly useful in promoting the initial stability and subsequent osseointegration of the surrounding bone stock, through a low elastic modulus and a high coefficient of friction [49].

The most commonly used conventionally manufactured acetabular cups employing porous solutions are summarised in Table 2.01. The percentage proportions were calculated based on the number of cases of uncemented acetabular implants used in primary and revision total hip arthroplasties in the UK in 2018, which were 67,568 and 3,799 cases, respectively. The respective totals of primary and revision total hip

Table 2.01: Summary of the most used conventionally manufactured uncemented porous acetabular implants, the morphometric features (porosity, pore size) of their porous structure and their percentage use in 2018 in the UK.

Company*	**Design**	**Coating / Porous Structure**	**Porosity (%); pore size (μm)**	**Primary (%)****	**Revision (%)****
B.Braun	Plasmacup Plasmafit	Plasmapore	35; 50 – 200	0.2 0.5	n/a <0.1
DePuy Synthes	Pinnacle	Gription Porocoat	63; 300 45; 250	4.6 26.6	12.8 1.8
Implantcast	Ecofit	ImplaFix	15 – 30; n/a	n/a	n/a
Medacta	MPact	Mectagrip	n/a; 100 – 350	0.2	< 0.1
MicroPort Orthopaedics	Dynasty Procotyl L	BioFoam Porous Ti Beaded	60 – 70; 530 30; n/a	n/a 0.6	n/a 0.1
Smith+Nephew	Polarcup R3 Reflection	Ti Plasma StikTite RoughCoat	15 – 20; n/a 60; 200 20 – 40; 170	0.1 8.3 < 0.1	< 0.1 2.2 n/a
Stryker	Trident 1	Tritanium	65; 250 – 650	2.2	15.6
Zimmer Biomet	G7 Ringloc Trilogy Continuum TM Modular^ TM Revision^	Porous Plasma Spray Regenerex Fiber Metal Trabecular Metal^	n/a; >100 67; 300 ~50; <400 ~80; 440	1.2 < 0.1 8.6 4.7 0.5 < 0.1	4.3 0.7 1.5 10.8 15.6 8.3

*B. Braun (Melsungen, DE); DePuy Synthes (Warsaw, IN, US); Implantcast (Buxtehude, DE); Medacta (Castel San Pietro, CH); MicroPort Orthopedics (Arlington, TN, US); Smith-Nephew (Memphis, TN, US); Stryker (Mahwah, NJ, US); Zimmer Biomet (Warsaw, IN, US). **The sum is not 100% because non-porous or HA-coated acetabular implants have been excluded. ^TM: Trabecular Metal; the porous structure is made of tantalum.

surgeries were 97,792 and 7,889, respectively, where the gap in numbers is a result of the surgery using a cemented or non-porous acetabular component or femoral stem [13].

2.4 | Three-Dimensional (3D) Printing

Additive manufacturing (AM) or 3D printing is an increasingly popular manufacture method in several engineering industries. AM is the process of joining materials to make parts designed with a computer aided design (CAD) software, when compared to subtractive or conventional manufacturing methodologies [50]. Manufacture via 3D printing is the direct fabrication of a part layer by layer using a source material in the form of a wire or powder feedstock and a heat source to provide thermal energy.

AM is increasingly becoming the choice of manufacture for several industries due to the many benefits it has from an engineering and manufacturing perspective, when comparing to conventional methods. A clear benefit of 3D printing, especially when comparing to the alternative conventional methods, is the ability to print complex and intricate porous structures. These structures are useful and applicable to many engineering industries for different, but often advantageous reasons. For example, in aerospace, a fundamental objective when designing new parts for an aircraft is to optimise the weight-saving capability. 3D printing provides the unique freedom with the design to manufacture components with complex internal geometries and keep them lightweight without compromising the mechanical properties. This is crucial in an industry such as aerospace as it has one of the highest standards for component performance [51].

Another key advantage in many industries is the ease of the CAD to print process where the final part can be constructed in a single step despite the design involving numerous different architectures (e.g. a fully dense region integrated with areas of

porous lattice structures). This rules out the need for expensive tooling and moulds that would otherwise be needed to manufacture these parts, as well as time-consuming additional steps to combine different components of the same part or applying surface treatments to form regions with a different topology [51].
For the same reasons, this technology is could have an equally beneficial effect on the manufacture of orthopaedic implants.

2.4.1 | Selective Laser Melting (SLM) and Electron Beam Melting (EBM)

The AM methods Selective Laser Melting (SLM) or Electron Beam Melting (EBM) are both powder-based 3D printing methods and types of Powder Bed Fusion (PBF), where either a laser or an electron beam are utilised alongside a powder bed for construction of the part. As per the ASTM standard defining terms for characterising additive manufacturing, these methods utilise metal powders alongside a high energy beam, selectively fusing powder particles to construct the desired part layer-by-layer. With each layer, the powder bed is raised and the build platform lowered to allow new powder to be deposited. Building of the part is achieved by melting and re-melting of previous layers [50]. The process of SLM is carried out in a chamber filled with an inert gas (argon), using laser beam to melt the powder particles and manufacture the part. EBM uses a wide electron beam, larger than the equivalent used in SLM, and is completed in a heated vacuum chamber to prevent the formation of brittle oxides or residual stresses during production, which would impede the structural integrity of the final part [52]. This makes this process more time-consuming than SLM, but near-net-shape and ready to use components are produced via both methods. Despite high initial costs, these methods remain advantageous when compared with conventional methods due to superior design

control to manufacture complex structures for improved bony fixation [53,54], essential in orthopaedics.

Regardless of the metal alloy used, the quality of the powder feedstock for the printer is the first of many important factors that will contribute to the final properties of the finished implant (Figure 2.08). The characteristics of the powder such as size, shape, material composition and surface morphology are all dependent on the method of powder manufacture. Examples of this include, gas atomisation, water atomisation, rotating electrode atomisation and centrifugal atomisation, and these methods influence properties such as flowability (the ability of the powder to ‘flow’ effectively when being deposited onto the build plate during printing), and packing density (how close the powder particles can pack together) [55,56]. The diameter of powder particles used in EBM is also significantly larger than those used in SLM, to accommodate a larger energy beam and ensure optimisation of each process for a high-quality printed component. Typically powders with approximate diameter ranges of 15-45μm and 45-106μm are used in SLM and EBM [57]. A smaller powder particle size has led to a smoother surface finish due to smaller agglomerations that form at the surface as well as a smaller thickness of each build layer [58]. It is also important that the chemical composition of the powder meets the required alloy specification, specifically in this case as the metal powder feedstock can be recycled, leading to potential contamination from gases present such as oxygen. Additionally, it has been shown that the with 21 reuse cycles of the powder, the weight can increase up to

0.19% due to oxygen content [59], and this could result in the formation of oxides and embrittle the titanium alloy [60].

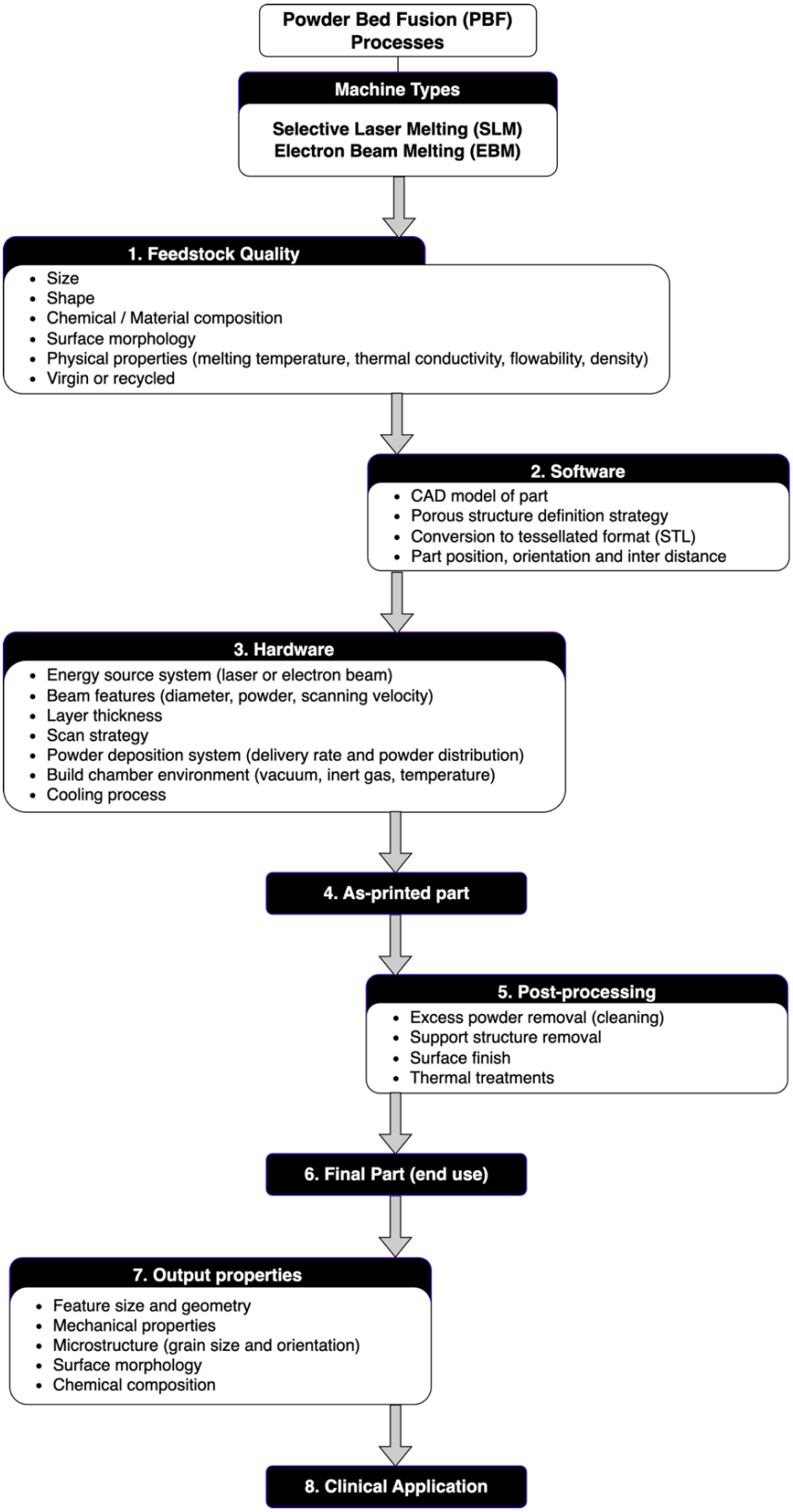

Figure 2.08: Flowchart of the powder bed fusion process showing the main variables involved. The output properties of the final part are determined by feedstock quality (metal powder), software and hardware specifics, and post-processing.

Another important variable that contributes to the properties and quality of the final printed part is the software system and the CAD of the part (Figure 2.08). This is converted into a surface tessellation form (STL) and sliced into layers of the cross-section of the part so that the correct information is used to print each layer. However, it is likely that this conversion can sometimes result in a loss of resolution of the design and become a source of error for the geometry of the final part [61,62]. A final variable pf these processes is the hardware and physical processes of the type of powder bed fusion technique (Figure 2.08). SLM utilises a laser as the heat source, which melts the powder when photons are absorbed. EBM uses an electron beam which is generated in a similar way to that found in a scanning electron microscope, and the powder is melted via the transfer of kinetic energy from the column of electrons, but this also results in an increasingly negative charge on the powder bed. Therefore, the electron beam used is larger and combined with helium gas to dissipate the charge, leading to a larger size of initial powder being used and a larger minimum feature side that can be produced. Despite this, both SLM and EBM are suitable manufacture meshes and lattice structures appropriate for orthopaedics such as in acetabular implants [63]. A summary of the technical differences between SLM and EBM are explained in Table 2.02 [58,64–67].

2.4.2 | Rationale for 3D Printing in Orthopaedics

The majority of total hip arthroplasties are still carried out using conventionally manufactured acetabular cups. Despite this, acetabular implants manufactured using 3D printing techniques are growing in popularity and increasingly being adopted for both primary and revision cases. Some of the advantages and disadvantages associated with these manufacture methods have been outlined in Table 2.03.

Table 2.02: Comparison of the main technical parameters and differences of Selective laser Melting and Electron Beam Melting [58,64–67].

	Selective Laser Melting	**Electron Beam Melting**
Heat Source	Laser Beam (up to 1 kW)	Electron Beam (60 kW)
Scan Speed	Limited by galvanometer inertia	Fast, magnetically driven
Powder Size	10 – 45 µm	45 – 106 µm
Minimum beam size	50 mm	140 mm
Beam/Melt pool dimension	0.5 – 1.5 µm	2 – 3 µm
Layer Thickness	20 – 100 µm	50 – 200 µm
Chamber Atmosphere	Argon or nitrogen	Vacuum (+ helium)
Temperature	Build platform at 100 – 200 ˚C	Chamber at 400 – 1000 ˚C
Powder Pre-heating	Using infrared or resistive heaters	Using electron beam
Surface Finish	Excellent to moderate (~ 20 µm)	Moderate to poor (~ 35 µm)
Residual Stresses	Yes	No

A noticeable advantage when considering 3D printing in terms of manufacturing is the ability to construct complex porous structures with specifically designed pore shapes and struts, designed to seamlessly integrate with the dense main body of the part (acetabular dome). This is in contrast to conventional techniques which require a secondary stage to add a coating or treat the outer side of the cup to form some porosity, ultimately with much more limited control over the final properties when comparing to the novel 3D printing method. Additionally, another key benefit is that customisation of implants is much more efficiently achieved through 3D printing than conventionally.

However, when looking at clinical outcomes and longevity, conventionally manufactured implants have a long track record in this industry, with plenty of reliable data on performance and medium and long-term clinical results, in contrast to 3D printed cups. Despite this, aseptic loosening is still reported as one of the most common reasons for revisions and suitable long-term solutions for this challenge are still undetermined [68–70].

Table 2.03: Advantages and disadvantages of 3D Printing and conventional manufacturing methods for acetabular implants in hip arthroplasty.

	3D Printing	Conventional Manufacturing

Advantages	• Enhanced design control
	  • Printing of complex structures (porous lattice) for improved fixation
	  • Easily adjust design
	  • Wall Thickness optimisation
	  • Suitable for customisation / patient-specific
		• Trusted process and designs
		• Widespread clinical use
		• Well-known and long-term clinical outcomes

Disadvantages	• Potential clinical risks and impacts are unknown • Few investigations exist on impact of these implants • Studies that do exist suffer from small sample sizes and short-term clinical outcomes	• Poor fixation remains an issue in THA • Limited design control • Limited ability for customisation

Custom Acetabular Cups

3D printed customised acetabular implants suitably address the clinical unmet need of the poor outcomes associated with the use of conventionally made acetabular cups manufactured specifically for massive acetabular defects, such as jumbo cups, triflange implants, and the combination of cages and augments (Figure 2.09) [71–75]. These defects occur as a result of significant reduction in bone stock after a revision surgery of a failed implant, and this will continue to reduce with each procedure. In spite of the reasonable decrease in revision surgeries performed in the UK, (from 10,511 to 7,889 between 2012 and 2018, respectively) it is possible that up to 60% of these procedures involve the acetabulum and severe acetabular defects and pelvic discontinuity [13,76]. The management and treatment of massive acetabular defects is challenging due to the range in surviving pelvic bone stock and quality between each patient, which has ultimately resulted in poor clinical outcomes including unsuitable bone fixation of conventional acetabular implants in these defects of complex shapes and low availability of host bone with a sufficient blood supply. Examples of these poor clinical outcomes include the preferred implants for

Figure 2.09: Outer (backside) and internal surface of (a) custom and (b) off-the-shelf 3D-printed acetabular implants. Antero-posterior (AP) plain radiographs are also shown.

the treatment of these defects, including antiprotrusio cages and triflange cups, which have high failure rates of up to 29% [77,78].

The advent of 3D printing enabling acetabular cups for these kinds of massive defects with the potential to overcome the challenges discussed; patient-specific designs and sufficient control to manufacture a highly porous structure to achieve a well-fitting implant and enhanced bony ingrowth [79].

Off-the-shelf Acetabular Cups

The ability to have design control and print a complex porous structure for improved osseointegration forms the basis of the main clinical rationale to mass produce off-the-shelf acetabular cups via 3D printing (Figure 2.09). This is primarily because

loosening of the implant from the surrounding bone is one of the most common reasons for implant failure and hip revision surgery and this is due to a range of factors including poor bone quality, inherent metabolic bone diseases, and reduced initial bone stock due to any previous conditions or surgeries [80,81]. 3D printing facilitates increased design control and flexibility, enabling the print of highly porous structures for enhanced bony fixation, and with the ability to attempt to closely match the characteristics of bone such as pore size and also mechanical properties such as the elastic modulus of bone, to also prevent problems associated with stress shielding. Additionally, with the porous structure that is produced via 3D printing, this enables a surface of a higher coefficient of friction, leading to increased friction between the surrounding bone and the implant, which can have a positive impact on the initial stability and fixation [82,83]. It has been reported that similar morphometric and morphological properties to cancellous bone could promote the initial stability, osseointegration and bone ingrowth, and therefore overcoming several of the challenges of implants manufactured conventionally [84].

3D printing can also be utilised to design implants that will optimise the size, and perhaps more significantly, the joint biomechanics of the new prosthesis. Femoral heads with a size of 36 mm are often chosen by surgeons as this size can provide greater stability in the joint, but these are often unsuitable for most female patients unless the acetabular implant can be manufactured to have a thinner wall thickness [85,86]. It is possible that 3D printing can facilitate this dimensional feature and enable surgeons to use larger femoral heads (e.g. 36 mm) in combination with smaller acetabular cups (e.g. 48 mm). Despite this potential advantage, the extent of the positive impact of this design modification on the biomechanics of the implant

and joint still requires further research, but preliminary investigations indicate that this is an effective choice [87].

Engineering Perspective

The most useful benefit of using 3D printing to manufacture implants compared with conventional techniques, is enabling the manufacturers with the design freedom of the implant through the computer aided design (CAD) process. Complex structures can be produced and also integrated with other design features in a single step, and hence potentially reducing the steps in the workflow and assembly of these implants. In the example of an acetabular cup, the intricate porous layer can be manufactured simultaneously to the dense shell wall of the main body of the implant, all in a one-step process within the printer. This eliminates the need for specific tooling and moulds used in conventional methods and potentially reducing the cost of the final product [70,88]. When considering the cost of 3D printing compared with conventional implants, the curve representing the cost-per-part as a function of the number of devices manufactured remains relatively constant for 3D printing, versus a decreasing hyperbole for conventional methods (Figure 2.10). This indicates that 3D printing has a lower cost-per-part than conventional methods when the number of parts produces is below a certain threshold, but as this method becomes increasingly used, this threshold will rise [70]. Also, it is important to note that even with the increased complexity that can be achieved using 3D printing, this has not been shown to increase the cost of the final part, and in some cases is less than conventional methods to a certain extent of complexity (Figure 2.10).

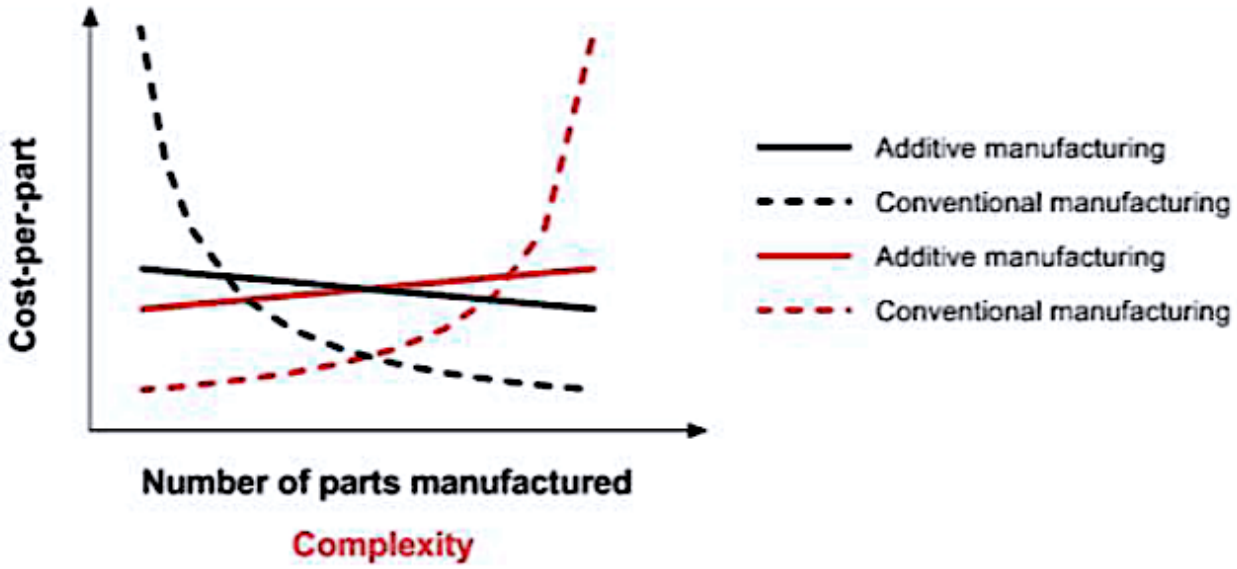

Figure 2.10: Graph showing the cost-per-part of additive manufactured and conventionally manufactured parts as function of the increasing number of parts produced and increasing complexity of the part.

Looking in the long term, it is possible that the choice of 3D printing for implant manufacture could improve the overall sustainability of this industry due to the reduction of source material and therefore material wastage. The reduction in raw material usage has been estimated to be up to 75% [89]. Also, this manufacture method has the potential to enable iterative production re-designs without the requirement for new tooling and moulds, however, these changes would still require resubmission and approval from the respective regulatory body. Nevertheless, the ability to have this capability accessible and on-demand is an important step in modernising the design approach to these implants [82,88].

However, most importantly when considering the manufacture of orthopaedic implants, 3D printing can facilitate a complex architecture and design control over the porous lattice for close alignment to trabecular bone and can be produced with the integration of both the porous and dense regions.

2.5 | 3D Printing in Orthopaedics

Over the last decade, three-dimensional (3D) printing of orthopaedic implants has increased in popularity, with many major manufacturers utilising the technology for their products. It is predicted that the market will grow by ~$1.35 billion by 2028 and will continue to increase as the technology becomes more advanced and cost-effective [90]. A key driver in this projected growth of the market is the ever-increasing number of orthopaedic surgeries that take place every year globally.

3D-printing is being employed in orthopaedics due to several benefits over conventional manufacture. A significant advantage of 3D printing for implant manufacture is that it enables the construction of a complex lattice on these orthopaedic devices. In an acetabular cup, this capability is capitalised on the outer bone-facing region where a layer with a highly porous lattice is printed [53]. Therefore, this type of implant has both a porous and a dense region, where different features and defects exist.

Another improved feature of a 3D-printed acetabular cup which is difficult to attain using traditional methods such as casting is a thinner shell wall to accommodate a larger femoral head and therefore reducing the possibility of dislocation in service.

It is also important to note that whilst 3D printing is quite well-accepted for the production of hip implants in particular, this manufacture method is being applied to implants for other regions of the body for the same advantageous reasons, such as in reconstructive craniomaxillofacial (CMF) implants such as custom plates and rods, for both cosmetic procedures as well as treating traumatic cases [91]. This particular area of the body also requires a high level of symmetry and dynamic designs which can be achieved through a combination of medical imaging of the patient, developing a CAD of the implant, before production via 3D printing (similar to the workflow of a

patient-specific 3D printed acetabular cup). 3D printing enables the customisation and level of complexity required for an intricate area of the body, also where the overall aesthetic and appearance of soft tissue overlying the implant is also imperative to the patient satisfaction [91].

Two prevalent methods for 3D-printed implants are Selective Laser Melting (SLM) and Electron Beam Melting (EBM) [92], as defined by ISO/ASTM. These methods utilise metal powders and powder beds to construct the part layer-by-layer, where thermal energy selectively fuses the powder particles using a laser or electron beam [93]. These methods give rise to new features of the implant both at the surface, such as complex porous layers [93], and in the dense regions where defects may occur if powder particle consolidation is insufficient [94]. These and other features will exhibit different characteristics depending on the 3D-printing method used, alongside the respective printing parameters and particular post-processing methods.

2.5.1 | Current Designs of 3D Printed Acetabular Implants

The first 3D printed acetabular cups became commercially available in 2007 and since their release, the number of designs on the market has steadily grown, and current there are more than twenty designs available for patient use. These designs from different manufacturers are summarised in Table 2.04, where the majority are

Table 2.04: Summary of the commercially available 3D-printed acetabular designs (custom designs are specified) and morphometric parameters of their porous structures

Company*	**Design**	**Porous Structure**	**Porosity (%); pore size (μm)**
Adler Ortho	Agilis, Fixa, Omnia, PolyMax	Tri-Por	65; 700
Corin	Trinity	Porous Layer Unique Structure (PLUS)	50 – 90; 300 – 900
Exactech	Novation Crown	InteGrip	45 – 57; 130 – 390
Implantcast	EcoFit, C-Fit 3D (custom)	EPORE	60; 100 – 500
Kyocera	SQRUM	Tesera Trabecular Technology (TT)	64 ± 6 ; 504 – 640
Lima Corporate	Delta, Delta ONE, Delta Revision, Promade (custom)	Trabecular Titanium (TT)	65; 640
Materialise	aMace (custom)	aMace	70; 720
Medacta	MPact	3D Metal	~75; 600 – 800
Smith+Nephew	Redapt	Conceloc Advanced Porous Titanium	~67; 202 – 934
Stryker	Trident II	Tritanium AMagine	55 – 65; 100 – 700
Zimmer Biomet	G7	OsseoTi	~ 70; 475

*Adler Ortho, 2020; Corin, 2020; Exactech, 2018; Implantcast, 2020b; Kyocera, 2020; Lima Corporate, 2020; Materialise, 2020; Medacta, 2020; Smith-Nephew, 2016; Stryker, 2020; Zimmer Biomet, 2020

appropriate for clinical use, and approximately 800 3D printed acetabular implants were employed in 2018 in the UK[13]. Additionally, it has been reported that an estimated 170,000 off-the-shelf 3D printed acetabular implants produced via EBM were used clinically worldwide by 2017 [95].

The various different 3D printed porous structures constructed on the outer bone-facing side of the acetabular implants are often classified based on their dimensional and morphometric features, despite the end-use application of the implant, in terms of custom or off-the-shelf. As with conventionally manufactured implants and the traditional methods to form the coating, the effectiveness on the fixation of the porous layer is heavily influenced by the geometric characteristics of the complex structure [96]. Therefore, a balance must be reached in order to ensure the mechanical strength of the porous structure is not compromised, but also that a suitable pore size is achieved, and consequently, this leads to different types of porous lattices.

The specifications of these structures vary between manufacturers, but the potential methods to effectively categorise the porous structures found on 3D printed implants have become well established [61,97]. Both regular and irregular lattice structure have been designed and produced by current medical device manufacturers, where both form a porous shape. The design approach for the manufacturers to create a regular lattice structure, to form a network with a periodically repeating unit cell include the utilisation of a CAD software with inspiration drawn from data from a form of medical imaging such as CT of MRI of bone or from modelling these solutions and a mathematical equation can provide assistance in defining the pore shape [83,97]. The design of these structures has been achieved undoubtedly through cycles of ‘trial-and-error’, resulting in the process being termed ‘topology optimisation’, to ensure the structures created have the desired properties and effect, while satisfying pre-determined limitations of the process [83]. It is important to note that the quality and final dimensions of the porous structure will be significantly impacted by the design input but also the real 3D printing process to produce the final part.

Some examples of the different highly porous structures on 3D printed acetabular implants that are currently commercially available include ‘Trabecular Titanium’ (TT, Lima Corporate, San Daniele del Friuli, IT*)* which is the hexagon-shaped structure similar to that of a diamond crystal, and this is an example of a regular, cell-based repeating lattice, in an attempt to mimic the properties of trabecular bone. An example of an irregular, stochastic porous structure is shown by ‘Tritanium’ (Stryker, Mahwah, NJ, US), which is a network of random interconnected pores and struts, irregular in length, pore size and shape. A final example which was developed on the basis of CT data of human bone is ‘OsseoTi’ (Zimmer Biomet, Warsaw, IN, US), which appears irregular but may lie within the spectrum of regular and irregular lattice structures.

2.5.2 | Custom-made Hip Implants

A key advantage of using 3D printing to manufacture acetabular cups, and in particular those for patients undergoing revision surgeries with massive acetabular defects, reduced host bone stock and low-quality bone, is the ability to design and create a patient-specific device fit for the specific defect.

The surgical planning and manufacturing workflow consists of several steps to ensure a high-quality final product for the patient. Pre-operatively, patients would need to undergo medical imaging of the pelvis; in most cases this is computed tomography (CT) scanning. This data is then implemented by the medical device manufacturer to which provides a dedicated engineering design service for precise and accurate assessments of key landmarks including the centre of rotation of the filed hip, examining the morphology of the remaining host bone and subsequent design of the implant and finally the surgical approach for implantation. The

capability of 3D printing is realised in the design and development of the implant, where areas of the defects are identified to be filled with the complex porous titanium, in order to encourage initial fixation and stability, as well as areas for structural titanium and appropriate locations of the screw holes. Once a suitable design has been formulated, this is reviewed by the operating surgeon along with the surgical plans for the procedure prior to the final approval, to provide essential feedback to fine-tune the design and ensure the practicality of implantation of the device. After final approval, the patient-specific implant is constructed using a 3D printing method; either SLM or EBM, integrating dense regions which accommodates the screw holes for fixation, and the areas of porous trabecular titanium to enhance osseointegration. 3D printing enables the construction of these complex architectures versus conventional methods, without the compromise on the mechanical properties. Additionally, 3D printed plastic surgical guides are often provided alongside the custom implant to aid with surgical planning [98].

2.5.3 | Off-the-Shelf Hip Implants

The main advantage when considering off-the-shelf acetabular cups manufactured via 3D printing is the integration of the porous structure in the same step of production as the dense main body of the part. This outer layer is beneficial for osseointegration, however from an engineering perspective, it is very useful that steps post-production including other surface treatments and coatings would no longer be required.

Also, from a clinical performance perspective, the current pre-clinical studies on 3D printed off-the-shelf cups, there have been some promising findings. This included reduced micromotion when compared to conventional cups, and the highly porous outer surface improved the stability of the cup and enabling the micromotion of the

peripheral sockets [99]. A recent study compared three different designs of 3D printed off-the-shelf acetabular cups and examined the bone-facing porous layer. They found that all three cups had differing wall thicknesses, makeup of the porous structure and subsequently different pore sizes, porosities and strut network. And when comparing these cups with the porous structures produced by conventional methods, the pore size and porosity as well as the mechanical properties of the pores and the overall porous layer were significant different [100]. Another study also reported a positive finding in terms of the performance of these implants in vivo; assessment of the 3D printed, and conventional cups revealed that higher percentages of bony attachment and tissue ingrown were observed in the 3D printed cups when compared with the conventional counterparts [99,101].
Additionally, the presence of surface adhered particles was reported, with different particle sizes and frequency across the three designs, due to the different 3D printing techniques used [99]. Therefore, it is important to also consider the defects and limitations of these implants and their medium- and long-term clinical impacts.

2.5.4 | Porous Region

The porous region of a 3D printed implant is often across the bone-facing region to encourage integration with bone and improve initial and long-term implant fixation. In the case of 3D printed acetabular cups this usually applies to the outer backside of the cup as well as flanges where the implant could come into contact with bone.
3D printing allows for the specific design of pore shapes in the porous structure similar to that of bone for enhanced fixation. This layer is made up of a complex design produced specifically to imitate the likeness of pores found in that of trabecular bone, unlike what can be achieved with conventional technologies for this

kind of surface, where the control of the final architecture is limited [53]. Additionally, this manufacture method facilitates matching the structure closely with bone characteristics also in terms of mechanical properties such as ensuring a similar coefficient of friction and modulus of elasticity to reduce issues associated with stress shielding.

This design varies greatly between manufacturers including the level of regularity of the lattice structure, and this can be observed in Figure 2.11 [102]. Some of the major orthopaedics manufacturers and their corresponding off-the-shelf 3D printed acetabular cup designs for revision hip arthroplasty and porous structure technology are shown in Table 2.01 [53].

Therefore, there are several features that are often analysed to characterise the porous layer which include porosity, strut thickness, pore size and strut length, among others. Additionally, it is likely that there are also imperfections present in this region such as surface adhered particles that occur as a result of this manufacture method which can also be observed and characterised.

Figure 2.11: A selection of 3D-printed custom and off-the-shelf acetabular cups, from a range of manufacturers and 3D-printing methods. Certain features of the cups can start to be considered, such as the locations of the porous regions and the different types of porous structures [102].

Porosity

Porosity is defined as the percentage of void spaces over the total volume [100]. When considering medical 3D printed implants, and more specifically orthopaedics, porosity is a feature that helps to characterise the highly porous bone-facing outer layer of an implant, for example, an acetabular cup [53]). This porous region is usually made up of a complex lattice with a regular or irregular structure, to aid and facilitate bone ingrowth [53], and it aims to simulate the porous structure and mechanical properties of human trabecular (or cancellous) bone. This is to prevent any potential challenges in-vivo, including stress shielding, by reducing the stiffness value between the implant and the surrounding bone stock [53,100].

Porosity of human trabecular bone ranges from 50 to 90%, pore sizes in the region of 300-500 and 300-500μm and strut thickness in the order of hundreds of microns [100,103]. Consequently, the level of porosity of the porous layer is designed to assimilate these properties and is dependent on the dimensions of the features used for its construction, such as pore size and strut thickness [104], as indicated in Figure 2.12.

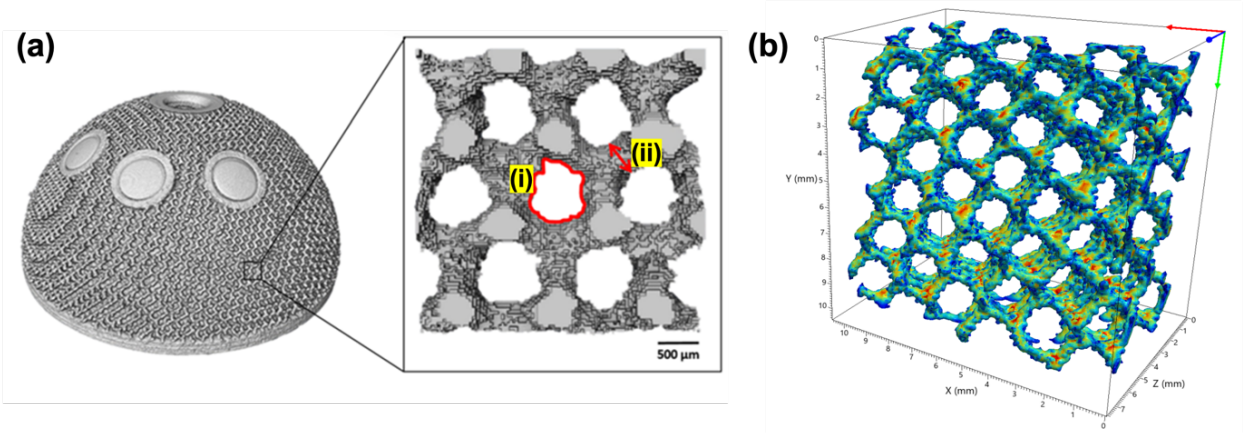

Figure 2.12: (a) A 3D-printed off-the-shelf acetabular cup. An area of the porous layer has been enlarged, displaying its structure. (i) Pore Size and (ii) Strut Thickness are indicated. The diameter of the pore is calculated as the diameter of a circle of equal area to the shape indicated in red. (b) A mesh structure from an AM cup rendered in an analysis software (Simpleware, Synopsys, Exeter, UK), where the colours indicates variability in strut thickness in the porous layer [102].

There are currently many different designs of 3D printed acetabular cups that are commercially available from various manufacturers, and so there are a range of different porous lattice designs that exist. Their aim is to achieve an open-pore structure (lattice or cellular) to mirror that of highly porous trabecular bone, and aid bone ingrowth to reduce the likelihood of loosening of the implant post-implantation [53].

The effectiveness of the fixation of the porous layer is impacted by the geometry that is chosen for its design (hexagonal, cuboidal, cylindrical etc), and this depends on the chosen 3D printing approach and overall design of the implant. When designing the porous layer, a compromise is made to ensure sufficient mechanical strength of the structure, whilst also providing an adequate pore size and porosity for sufficient osseointegration [53]. This therefore leads to several different architectures for the porous structure amongst implant manufacturers. 3D printing enables the design and construction of any kind of porous shape; both regular (repeat unit cells) or irregular (random structure). Repeat unit cells usually have a specific geometry (hexagonal or cuboidal etc.) which is repeated throughout the structure. CAD tools are used together with computed tomography (CT) or magnetic resonance imaging (MRI) and mathematical modelling to design the structure and choose the pore shape based on that of trabecular bone [53]. A variety of porous structures from different manufacturers can be observed in Figure 2.13.

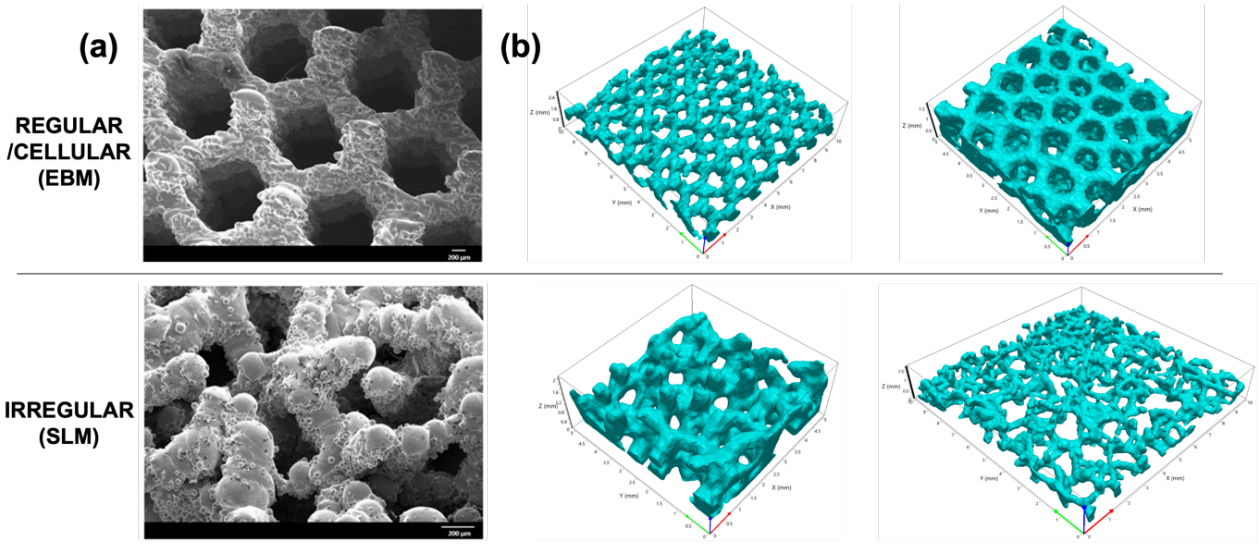

Figure 2.13: (a) SEM Images of a regular or cellular and an irregular 3D-printed porous structure and the corresponding manufacture method (Electron Beam Melting (EBM) and Selective Laser Melting (SLM)). (b) Computer rendered meshes formed using Micro-CT data from AM acetabular cups from four separate manufacturers with varying porous structures. Comparisons between porous structures available from different manufacturers can be made [102].

In other industries including aerospace, the term ‘porosity’ can refer to an unwanted defect in a dense part produced by 3D-printing [105]. In orthopaedics this is similar to what is termed a ‘void’ [106].

Strut thickness

The thickness of the struts is the dimension of the single metal rods that form the framework of the porous layer [104]. This minimum size of this feature is limited by the choice of 3D printing method by the manufacturer and its respective minimum feature size capability. Defining the thickness of the strut is influenced by the thickness of the struts found in trabecular (or cancellous) bone, which is in the range of hundreds of microns [104]. When considering the two main 3D printing techniques for these implants, it has been reported that the minimum feature size for SLM is in the range of 40–200μm, and ~0.5mm for EBM [104], and the capability to alter this aspect can impact the level of complexity and intricacy that can be achieved for the porous layer, which consequently will influence the degree of osseointegration by the

surrounding bone stock. The differences between manufacturers for strut thickness can be observed in Figure 2.13, where the cups have been manufactured by both SLM and EBM, respectively. Also, the difference in the features that can be observed on the internal and external strut surfaces (surface adhered particles) can pose the question if one of these 3D printing methods is more suitable.

Pore size

Pore size, similar to porosity and is a metric that helps characterise the space available for bone ingrowth into the porous region and is measured by calculating the equivalent diameter of the pores in the lattice [100,104]. As with strut thickness, pore size is affected by the choice of manufacture methods, and a larger pore size results in higher porosity of the porous layer. Pore size is a critical parameter for successful bone ingrowth and the dimensions of this feature in 3D printed implants is determined by the pore size found in trabecular (or cancellous) bone, which is in the range of (300-500μm [103]). Pore size in addition to the interconnectivity of these pores jointly directly influence the biological performance of the implant, including initial and long-term adhesion, osteogenic behaviour in the surrounding tissue and ultimately fixation of the implant [100]. This is because pore size fundamentally influences the type of cells that will proliferate within the porous structure.
In the porous structures of currently available implants, pore sizes of ~100-500μm are applied, which is consistent with the range of pore sizes found in trabecular bone and have indicated positive results in recent in vivo studies [100]. 3D printing provides manufacturers with improved control over the design of the porous layer and pore size, which is beneficial, as the optimal pore size of bony ingrowth is yet to be determined [107].

Surface Adhered Particles

Surface adhered particles are a known by-product of the metal 3D printing processes used in orthopaedics, as they utilise a powder-based source feedstock. They are defined as solid metal powder particles that are partially fused to the surface of the as-built component part [53]. Their level of adhesion and the frequency of particles is dependent on the choice of 3D printing method (SLM or EBM) and the respective processing parameters during printing.

The variability of surface adhered particles can be observed in Figure 2.14 which shows the struts of the porous structure of several commercially available implants from multiple manufacturers using different 3D printing methods. Surface adhered particles are relatively common when using powder-based 3D printing methods, and it is possible that these particles can be easily dislodged post implantation [108], raising the question of their impact in the human environment. Along with the printing processing parameters, additional factors also affect the presence of surface adhered particles, including the size of the powder particle and also the size, type and angle of heat source used in the printer [109], which can provide some

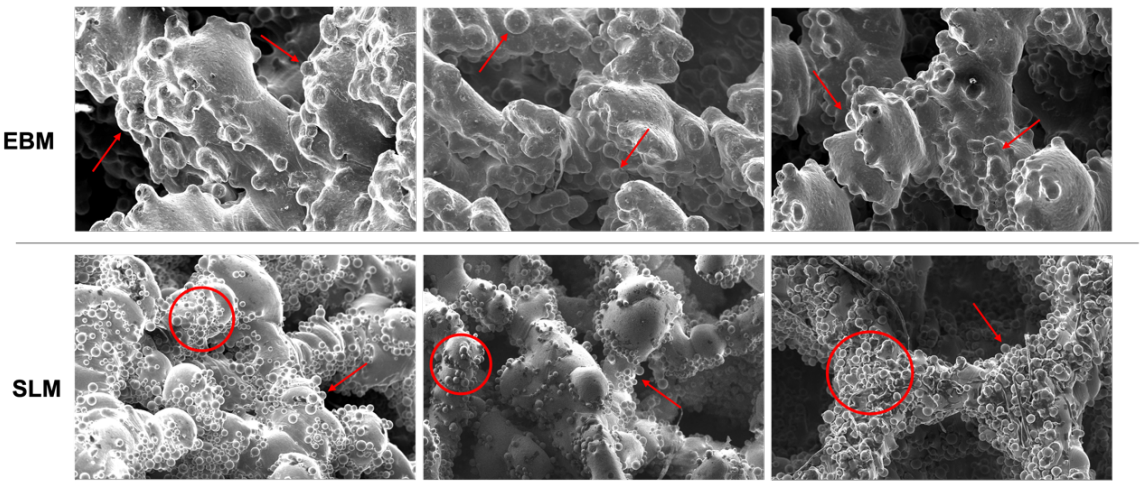

Figure 2.14: A panel of SEM images depicting surface adhered particles (indicated) in the porous layer of 3D-printed acetabular cups, and the variability of the particles with AM method; Electron Beam Melting (EBM) and Selective Laser Melting (SLM). All Images at x200 magnification [102].

explanation for the variability in the appearance of these particles between different manufacturers and implant designs.

It is important to note that surface adhered particles are sometimes confused with unmelted particles, which is a separate defect and potential by-product of 3D printing. These particles differ in that they are, non-melted, free and loose stating powder that has become trapped in the lattice or porous structure and have no adhesion and can often be washed away relatively easily post-production. This is unlike surface adhered particles, which are fixed to the struts of the structure, and require chemical or mechanical methods of post processing for removal. Additionally, it is also possible that some particles have joined together at the fringes of the melt pool during printing, forming an agglomeration, and can be both adhered and loose in the structure.

Surface adhered particles can vary in their appearance and range between more consolidated and hemispherical in shape to more full particles that are just barely attached to the surface of the strut. The level of adherence is dependent on the choice of 3D printing method, the size of the particles in the source powder feedstock and also the printing processing conditions. The range of appearances of the particles can be observed in Figure 2.15.

In a recent study, it has been reported that the presence of surface adhered particles as a result of SLM, has led to increased bacterial growth. The extent of adhesion and existence of bacteria is impacted by the physical and chemical properties of the implant material and is considered a significant challenge in orthopaedic implants. While it has been demonstrated that 3D printed implants with a porous layer can encourage and improve osseointegration, this study examined the effect of the presence of surface adhered particles in the porous structure [110]. It has been

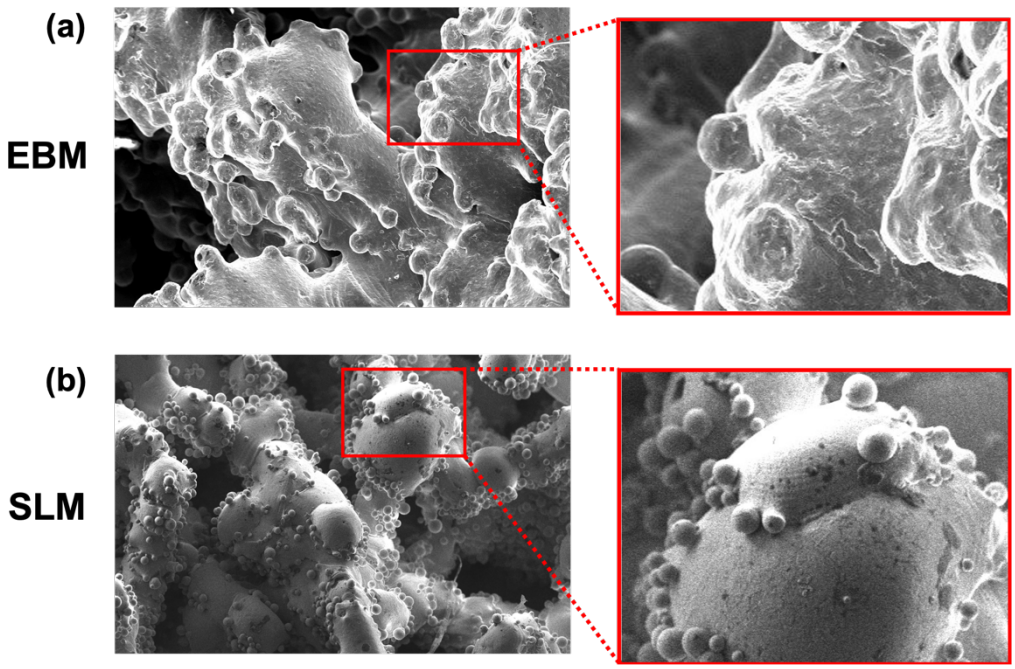

Figure 2.15: Images displaying the extremes of surface adhered powder particles within the porous layer. (a) Almost completely consolidated particles protruding from the strut surface compared with (b) almost completely unmelted particles only just attached to the strut surface. Images at 200x magnification [102].

proposed that a surface with topological properties and dimensions similar to that of bacteria, such as that of a strut in the porous layer of an implant could allow an ideal contact area, resulting in elevated bacterial proliferation and adhesion [111]. Therefore, increased bacterial adhesion was observed in samples with surface adhered particles present, when compared to samples that had been treated to remove them, and the existence of bacteria in turn had an inhibitive effect on the osteogenic activity. The results of this study therefore suggest that surface adhered particles can have a negative effect on overall bone ingrowth into the porous regions of these implants. Additionally, this also introduces that surface adhered particles could potentially encourage inflammation in the periprosthetic tissue surrounding the implant and possibly result in bone resorption and ultimately aseptic loosening and premature failure of the implant. This study concluded that the depth of the porous layer should be optimised to not exceed the point of successful bone ingrowth, as osseointegration must occur in order to prevent implant-related infection [110].

Furthermore, it is possible that this observation could help in identifying the optimal thickness of the porous layer, which is yet to be determined.

The results of this study further highlight the importance of post processing to remove surface adhered particles. However, a homogeneous surface is challenging to achieve via mechanical methods that require ‘line-of-sight’ or heat-treatment method, due to the complexity of the porous layer, and the aim to maintain this layer, versus removal which is the case in several other industries that utilise 3D printing [112,113]. As a result, other methods such as chemical etching or electrochemical polishing have been evaluated for their effectiveness in removing surface adhered particles from within the porous region, as these techniques are able to infiltrate the intricate porous structure via the interconnected pores [114].

Of these methods, chemical etching has demonstrated effectiveness in the removal of surface adhered particles on sample porous structures similar to those found on 3D printed orthopaedic implants (e.g. a stent), in an experimental environment stents) [108,112]. When the length of time of treatment was extended, the number and size of particles removed also increased [108]. Additionally, when this process was combined with electrochemical polishing, it exhibited encouraging results in reducing surface roughness and the presence of surface adhered particles on the surface of the struts in the porous layer [114]. Despite these promising results, it should be noted that care should be taken when applying these techniques, as prolonged treatment times of etching or polishing could reduce the overall strut thickness, and possibly compromise the overall mechanical properties of the porous structure [114].

2.5.5 | Dense Region

Introduction

This region is similar to the features that are described in literature surrounding the topic of 3D printing in other engineering sectors, as the dense region of an implant has similar requirements to 3D components for other components such as aerospace and automotive [115]. This often includes producing a fully dense component via additive manufacturing, with minimal steps for post processing, and comparable mechanical properties to those achieved by traditional manufacture methods [115].

Diameter and wall thickness

Diameter and wall thickness of the implant are indicated in Figure 2.16. The diameter of the acetabular cup is often engraved on the rim, and both of these dimensions can be characterised using Micro-Computed Tomography (Micro-CT) scanning. The wall thickness can also be determined using a Coordinate Measuring Machine (CMM). When comparing to conventional methods, 3D printing enables the design of the implant to correspond more closely to the original biomechanics of the joint for replacement. For both off-the-shelf and custom acetabular cups, this manufacturing technique enables a thinner wall thickness for the same cup diameter of a conventionally made implant, reducing source titanium alloy powder, but more importantly, sparing significant surrounding bone stock whilst accommodating a larger femoral head; and ultimately aligning closely to the original biomechanics of the hip as a result [100].

Despite the biomechanical benefits of a thinner cup wall, a smaller wall thickness could call into question the mechanical integrity of the implant itself, and if deformation or even failure could be more likely.

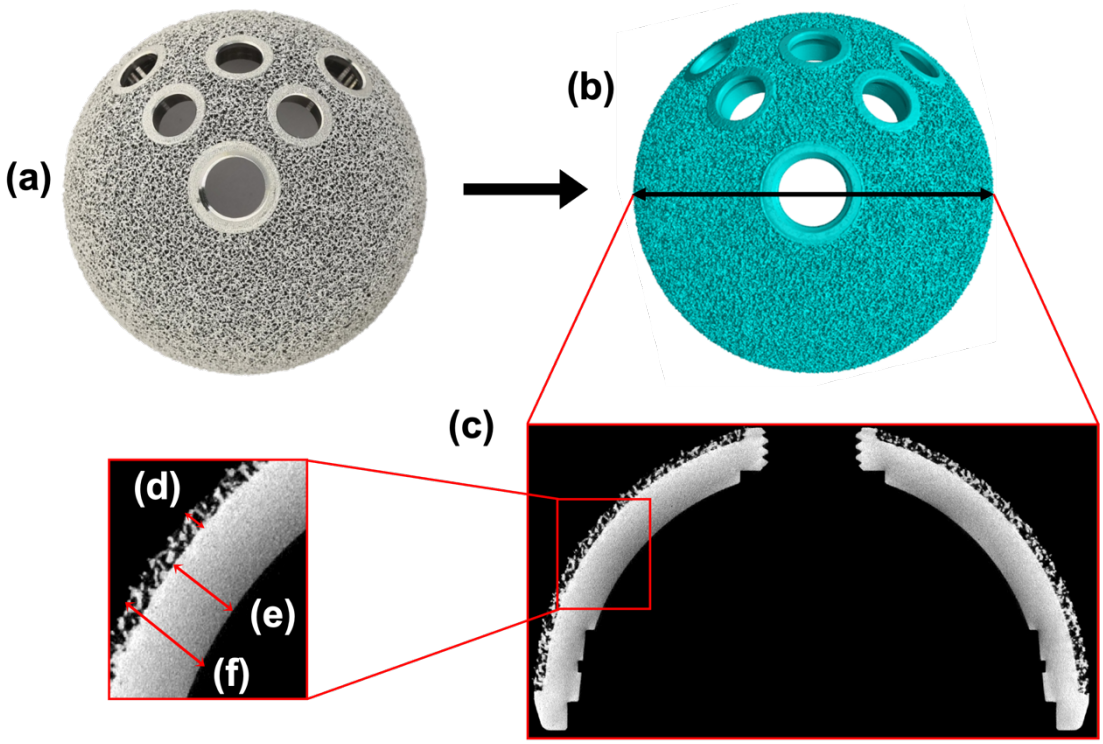

Figure 2.16: A 3D-printed implant (e.g. (a) an acetabular cup). A Micro-CT scan of the implant can assist in determining (b) the diameter of the implant and provide (c) isolated slices of the internal structure for measurement of (d) the thickness of the porous region, (e) the dense region and (f) the total thickness. [102]

Surface Area and Volume

Current literature surrounding morphometric analysis 3D printed acetabular cups has found that the total area of these implants is greater than their conventionally manufactured counterparts [107], and this could be explained by the heightened surface area of the porous regions of these implants. A combined methodology of Micro-CT and software analysis packages such as Simpleware (Synopsys, Exeter, UK) and Vision Graphics (Heidelberg, Germany) have proven useful in determining both of these characteristics. This analysis technique could also provide an insight into the total metal surface area of the implant exposed to patients in vivo, and additionally help evaluate how much metal is used in the final print.

Internal Surface Roundness and Roughness

The roundness and roughness of the internal surface of the cup are important factors to consider as they affect the seating of the liner within the cup [100]. They are influenced by the chosen 3D printing method, which can alter these dimensional and topological features. This variability however is often removed though post-processing such as machining of the internal cup surface, which is carried out to ensure dimensional tolerances and avoid mismatches with the corresponding cup liner. Unsatisfactory seating of the cup liner can lead to adverse effects in vivo, including accelerated wear or potential fracture, and therefore should be prevented [100].

Several metal 3D printing processes involve a layer-by-layer printing approach which leads to inconsistency in the surface roughness, where a larger layer thickness can lead to an uneven curvature of the part. This build error is sometimes referred to as the ‘staircase’ or ‘stair-stepping’ effect, and current literature has found that surfaces printed with some incline or curvature (e.g., the internal surface of an acetabular cup) are more susceptible [116]. Additionally, as previously discussed, a poor surface finish due to residual powder remaining on the surface of the part (surface adhered particles) is inherent to powder-based 3D printing methods, and in most cases both types of build error are rectified via post-processing [117].

High-quality 3D printed components have a surface roughness specified to be <1μm [118]. This is to ensure sufficient contact area between the cup and the liner, which if reduced can lead to accelerated mechanical wear and corrosion [100]. Roundness of the internal surface of a 3D printed acetabular cup can be characterised using a

Coordinate Measuring Machine (CMM), and roughness is evaluated using a Surface Profilometer (Figure 2.17).

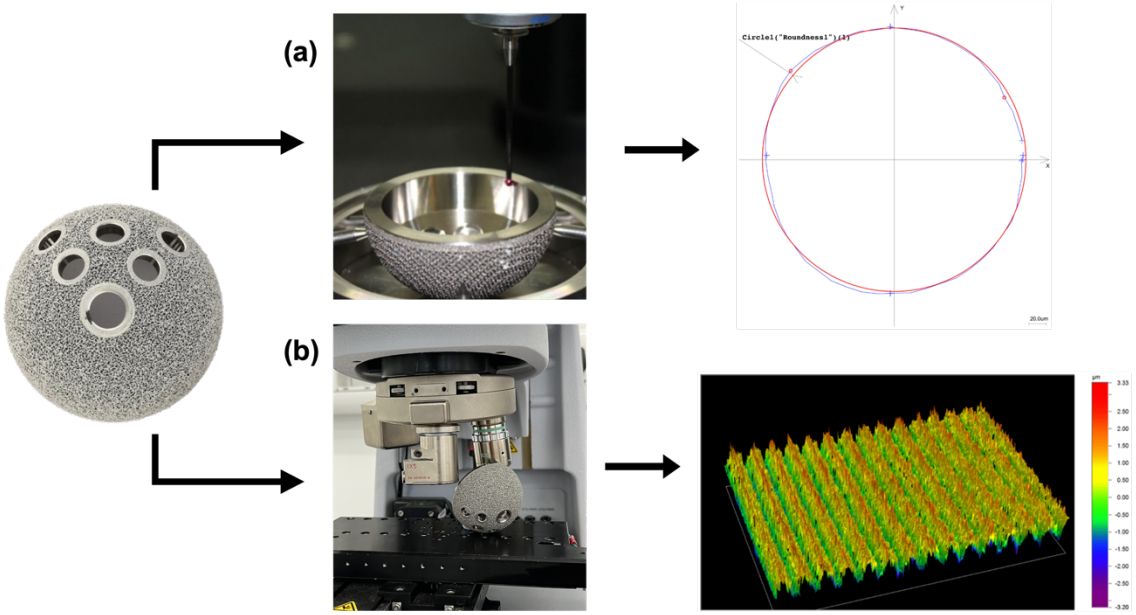

Figure 2.17: (a) Obtaining a roundness measurement using a Coordinate Measuring Machine (CMM). (b) Obtaining a measurement of surface roughness using a Surface Profilometer. [102]

Voids

A key defect that can be found in the dense region of an implant are structural voids. Examples of this defect can be observed in Figure 2.18 and are a negative by-product of metal 3D printing of the dense region, when comparing to conventional manufacture methods. The voids can act as stress concentration sites and therefore compromise the mechanical integrity and fatigue properties of the part [119]. A recent study found that voids tend to occur in areas where the implant transitioned between design features, such as at a main body-flange junction, highlighting a variability in the print quality in these regions [106]. In other industries (e.g. aerospace), this same

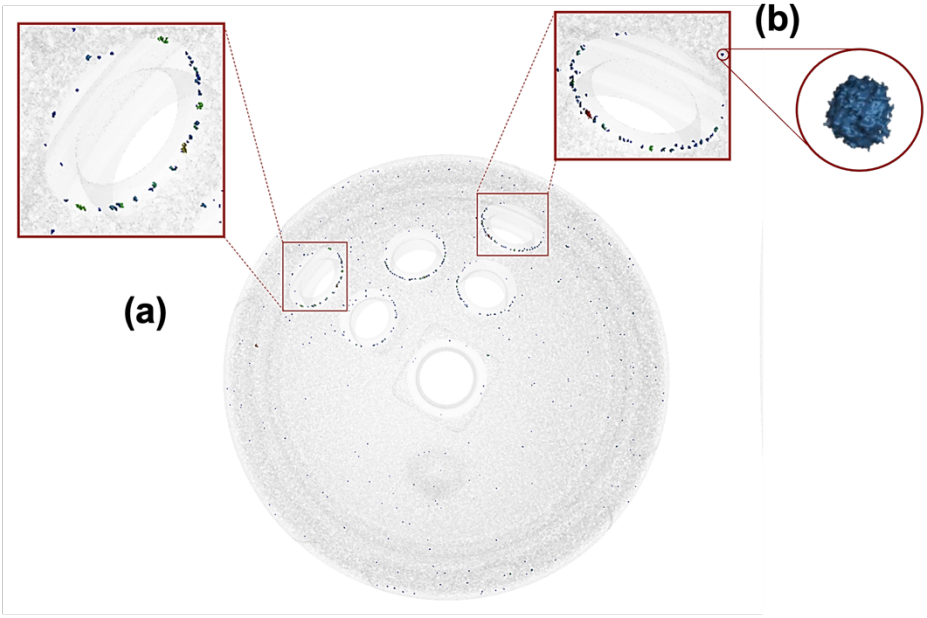

Figure 2.18: (a) Image generated from Micro-CT data to show voids in the dense region of a 3D-printed acetabular cup. From these images, void location and frequency can be analysed. This will be followed by (b) void size and shape evaluation [102].

defect has been referred to as an internal ‘pore’ or ‘porosity’ instead of a void [120], as well as a ‘structural cavity’ [121].

Voids are able to form during the 3D printing of the specified part. They can arise due to poor-quality source powder feedstock, unsatisfactory processing conditions, or when gas in the build chamber becomes trapped in the melt pool, resulting in voids that are spherical in nature [118,121]. Voids that are more irregular and elongated in shape can occur when there is insufficient energy to fully consolidate the powder particles (lack of fusion) [53]. Furthermore, where the combination of processing parameters generates excessive energy to consolidate the particles, a keyholing defect can occur (material vaporisation), resulting in near-spherical voids in the final dense part [53].

Voids can have a significant effect on the mechanical properties of the 3D printed component and there are several factors that contribute to their level of impact. They concentrate stress under loading, potentially leading to early failure of the part,

particularly under fatigue loading conditions [120]. The location, size and shape of the void, in decreasing order of importance, can influence the fatigue life of the respective 3D printed part [106].

Location of the void is the most significant factor when considering crack initiation, and a recent study found that the voids located <0.4mm near the surface can act as crack initiation sites. The size of the void is the second-most influential factor where, unsurprisingly, a larger void (>0.5mm) can increase the risk of fracture and reduce the fatigue properties of the 3D printed component. Thirdly, the shape, or more specifically the sphericity of the void impacts the properties of the part, where more irregular-shaped voids can act more effectively as stress concentrators, altering the mechanical properties, compared to smaller and more spherical voids [106].

Therefore, large and irregularly shaped voids, that are close to the surface of the part are most-concerning, additionally when under cyclic loading conditions that exceed the fatigue limit of the implant [106]. Components for aerospace often experience loading of this nature, which forms the basis of many studies into fatigue of 3D printed parts. In biomedical applications, it is likely a lower level of cyclic loading is experienced, which could provide an explanation for the absence of fracture in 3D printed implants, despite the discovery of voids in the dense regions [106]. It should be noted that in some cases, that voids can become interconnected, forming a more harmful defect, with potentially detrimental effects on the mechanical properties of the implant, particularly where the structural integrity of the implant is important (e.g. at the body-flange junction).

Therefore understandably, manufacturers undertake measures to prevent the formation of voids in the final part, such as optimising the processing parameters [119]. Post-processing is also employed in other industries in attempts to close up

voids, such as heat treatment and Hot Isostatic Pressing (HIP) [122].HIP has demonstrated that it is effective in decreasing the size of voids and help parts manufactured via SLM reach strengths similar to that of conventionally processed titanium alloys [120].

2.5.6 | Risks and Limitations

With the novelty of 3D printing comes potential for clinical and economic gains, but it is important to acknowledge the unknown risks and limitations associated with this particular manufacture method on a mass scale for implants in load-bearing applications. 3D printing can be optimised to manufacture parts with high dimensional accuracy, improved surface roughness and minimised residual stresses, through the optimisation of parameters, correct feedstock and a vacuum or inert gas-filled chamber. However, despite taking these measures, it is still possible for defects to develop during the printing process and remain in the final part. This includes some common defects as discussed; voids in the dense region that can occur due to a variety of reasons, and surface adhered particles which vary based on the type of 3D printing method used. Post-processing steps are often employed to resolve some of these issues, but these techniques still require development and optimisation to be more effective.

Therefore, further studies are required to investigate the long-term impacts of these defects and also on the optimisation of post-processing methods to manage their effects.

2.5.7 | Methods of Analysis

Introduction

Several analysis techniques have been investigated for analysing the features of 3D printed implants. They are chosen based on the type, size and location of the feature

of the implant for evaluation. However, an ongoing challenge with certain techniques is the inability to sufficiently characterise the feature due to issues relating to 'line-of-sight', for example when using SEM or CMM. This was addressed by Carter et al. [123], where limitations of these methods were identified, including the failure to quantify regions on the surface of a 3D printed part that are obscured by foreground overhangs and surface adhered particles. This is specifically relevant to 3D printed orthopaedic implants due to the complexity of the porous lattices, which requires a technique that is able to overcome 'line-of-sight' and analyse the topology of both the internal and external strut surfaces, as well as any other defects and features. This review has highlighted the kinds of features that require evaluation and the requirements of suitable analysis methods for their characterisation.

Scanning Electron Microscopy (SEM)

Scanning Electron Microscopy (SEM) has been used in several studies to characterise the porous structure found on 3D printed orthopaedic implants and the surfaces of the struts within these structures [124,125]. SEM provides a suitable resolution to visualise the kinds of features in these structures as shown in Figure 2.14. The partially adhered particles can be adequately observed, identified and their dimensions and frequency can be measure. The variability in the presence and appearance of the particles between different manufacturers can also be compared thoroughly via this analysis method.

However, due to the nature of this structure, the foreground features (struts) obstruct some of the background surface, therefore leading to the omission of identifying certain particles. This specific analysis method suffers from the challenge of 'line-of-sight' where observation can only be achieved in the direct line of sight from the

detector, which could be subject to obstruction and/or contamination, altering the evaluation of the sample. A technique to reduce the impact this can have on observations and gathering data is to take many images of the specific from different angles and approaches. However, utilising a different method that could provide a suitable resolution to evaluate characteristics of this scale would be most beneficial.

Micro-computed Tomography (Micro-CT)

Micro-CT has demonstrated promise as a technique that could overcome the challenge of 'line-of-sight' when analysing these implants. It has been found to be reliable when characterising both the dense and porous regions of orthopaedic implants in several studies, and it has been able to analyse features that would be difficult to observe via alternative methods such as SEM, whilst also preventing the need for destructive testing [126].

Several ways of characterising pores in the porous structure have been discussed in previous literature, depending on the regularity of the structure and the size of the pores. A method involving modelling a sphere of the largest diameter in the pore of interest is recommended when characterising pores in regular lattice structures [127] (Figure 2.19). This method is then applied to several pores (~8-10) in the porous structure and across several regions, to determine and observe the extent of variability in the pore sizes between different regions of the porous layer. A mean can then be calculated from the measurements collected, and this value (or range of values) is often the measure for pore size that is quoted by manufacturers [128,129]. It should be made clear that while this method is suitable for pores in a porous structure with a regular lattice, a suitable method to examine and characterise the pores in irregular structures is yet to be determined.

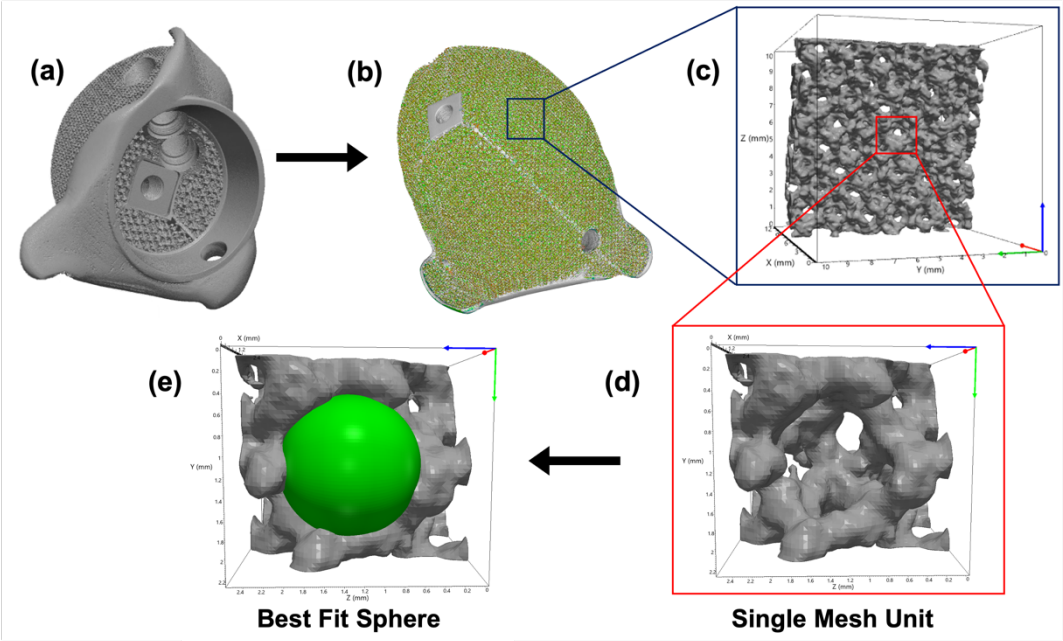

Figure 2.19: (a) A render of a custom 3D-printed acetabular cup created using Micro-CT data and imported into an analysis software (Simpleware, Synopsys, Exeter, UK). From this data, (b) the porous layer is examined and isolated, and (c) a mesh model of the structure is generated. (d) A single mesh unit can then be extracted, followed by (e) best fit modelling with a sphere, to assist in calculating the porosity of the porous layer. [102]

2.6 | Clinical Outcomes of 3D Printed Acetabular Implants

Longevity is another key aspect of these implants, and currently 3D printed acetabular cups are exhibiting positive results in vivo. Many 3D printed acetabular cups with off-the-shelf designs, including both the Stryker Trident II and the Lima Delta TT revision cups have been successfully applied for a number of years, and have an ODEP (Orthopaedic Data Evaluation Panel) Rating range of 3A-10A* [130]. The ‘A’ indicates high strength evidence of the implant collected over a number of years (3-10), with the star denoting a <5% revision rate at 10 years [131]. As the use of 3D printed implants in orthopaedics becomes more prevalent, increased clinical monitoring and data surrounding their longevity and positive clinical performance is required.

Therefore, ongoing evaluation of both unused and retrieved implants, alongside long-term surveillance of implanted devices, will ensure an up-to-date understanding of 3D-printing in orthopaedics.

In terms of the longevity of custom 3D printed acetabular cups, a recent study reported a positive performance on devices constructed via EBM with areas of porous trabecular titanium, where there was a cumulative survival rate of 100% on the 25 implants studied and monitored, indicating these implants are a good option for the treatments of these kinds of pelvic defects [98].

Whilst there is promising data currently on these implants, more studies on the long-term clinical outcomes would be beneficial and could even potentially resolve the question if SLM or EBM should be recommended for the manufacture of 3D printed orthopaedic implants going forward, from a clinical safety perspective.
Studies on retrieved implants would also be useful, where features such as the depth of bone ingrowth into the porous layer, the total bone contact area and the type of bone stock could be examined, and also, any wear or reduction in the thickness of the porous layer as well as other features may be of interest, as a result of the contact in vivo. Another feature that could be monitored is the presence of surface adhered particles in the porous region and their effect on bone ingrowth and if they contributed to the reason for revision of the implant (e.g. infection). Additionally, the techniques by which these features could be characterised most effectively, such as Micro-ST or SEM, must be evaluated.

2.7 | Regulations and Standards for 3D Printed Medical Devices

International medical regulatory bodies, including the U.S. Food and Drug Administration (FDA) [132], and Medicines and Healthcare products Regulatory Agency (MHRA) [133], have established and identified which ISO and ASTM standards should be followed as guidance by manufacturers when constructing 3D printed implants and instruments [50,134–137]. With the novelty of 3D printing and

the use of metal powder as the source material, there is a clear knowledge-gap in the applicable regulation, which is apparent in the guidance that is currently provided to manufacturers. An example of this are the recommendations for manufacturing and testing of 3D printed parts, regardless of the material that is being printed (metal or plastic) and type of device (e.g. surgical guide or implant) [138]. Additionally, when considering the post-processing of these parts, the suggested techniques are often unsuitable for the complexity of the porous layer created using SLM or EBM and lack the necessary detail to correctly guide manufacturers during production.

The Technical Consideration for AM Medical Devices was published in 2017 by the FDA and is the most recent guidance in this subject area. It states that ‘it is anticipated that AM devices will generally follow the same regulatory requirements and submission expectations as the classification and/or regulation to which non-AM device of the same type is subject’ [138]. However, in the 7 years since its publication, there have not been any significant revisions to this advice.

Similarly, EU Medical Device Regulations (MDR) has also been criticised for its lack of conciseness and clarity in the guidance provided. The EU MDR conducted two surveys of employees within medical device manufacturers in Germany before and after changes were made to guidance relating to 3D printing in medical devices (2021 and 2023, respectively) [139]. The results of this investigation highlighted that the participants’ knowledge of the MDR changes had not improved, and also that several of the companies included in the survey did not consider these changes as an improvement, and that the over-administration is resulting in the reduction of product portfolios and ultimately withdrawal of devices from the EU market [140]. In the future, it appears that this approach to MDR could lead to stunted innovation and competition within medical devices.

From this evidence, it is clear that the current guidance remains unsuitable and requires sufficient revision to include the different commercial-available 3D printed devices and processes used. In an effort to reduce this knowledge-gap in the regulation, the ASTM F42 Committee meetings are held bi-annually to discuss relevant improvements in Additive Manufacturing (AM) Technologies and update existing standards and develop new advice [141].

3D printing as a manufacturing process is also problematic from a standards and regulatory point of view because it involves the flexibility to adapt the design of an implant for patient customisation and increase complexity. This therefore means that manufacturers are able to include relatively small design changes for print, which complicates managing this process for regulators, and so often designs for customised 3D printed implants must be submitted for approval on a case-by-case basis before production. On the other hand, conventional methods of implant manufacture, such as casting of implants, are well-accepted and considered reliable while providing repeatability of the quality of the part and also consistency between designs and devices, allowing for relatively uncomplicated regulation. This is a significant advantage of traditional manufacture methods compared to 3D printing and is appreciated by regulatory bodies [100].

2.8 | Summary and Conclusion

3D-printing in orthopaedics will continue to grow with the development of off-the-shelf as well as custom orthopaedic implants. The ability to vary implant design for patient specificity and to construct intricate surface geometries, both of which are challenging to achieve via conventional methods [53], make this process desirable. However, with the novelty of 3D-printing, there lacks the data to evaluate the long-term clinical impact of these implants. It is important to characterise the features of these components as

they are for patient use, and that there are no clear guidelines or knowledge on what the optimal designs of the implants. This inevitably has led to the significant variability among manufacturers in the designs of the porous structures, and these differences should be characterised in order to evaluate and understand their long-term impacts when future clinical data can be generated and analysed. These investigations could also discuss the impact of defects of these manufacture methods such as the surface adhered particles, and pose the question if SLM or EBM is more suitable for manufacturing 3D-printed implants and should this be recommended to manufacturers from a clinical safety perspective.

With the growing uptake of this manufacture method, it is necessary to consider the features of retrieved 3D-printed implants. Going forward, dedicated investigations into retrieved implants and observing the impact of surface adhered particles could also provide an explanation for elevated levels of blood titanium in patients with 3D printed acetabular cups when compared to those with conventionally manufactured implants [142,143]. Further studies could include monitoring levels of blood titanium and other elements post implantation to assist in monitoring the performance and condition of the implant in vivo, and if elevated metal ion levels could indicate potential particle breakages, or advanced diffusion due to a higher implant surface area, and any associated risks to patient and clinical safety.

Additionally, given the challenges with certain analysis techniques, evaluation of which analysis methods are most appropriate for each feature requires investigation. Therefore, continued examination of both unused and retrieved implants, alongside long-term surveillance of implanted devices, will ensure an up-to-date understanding of 3D-printing in orthopaedics.

2.9 | Aims and Objectives of this Thesis

Several gaps in the literature have been highlighted, including the incomplete understanding around the features of the complex porous structures on 3D printed implants, and their longer-term clinical impacts. The aim of this report is to investigate the influence of the manufacture method on the physical features of 3D printed implants, with a particular focus on the complex porous structures, using the example of 3D printed final production custom and off-the-shelf acetabular cups produced by several manufacturers.

Analysis was achieved through the utilisation of Micro CT combined with the Synopsys Simpleware software to evaluate the dimensions of struts within the porous regions and the variability in porosity levels among current designs of the porous lattices from different manufacturers. The second study built on this through the examination of the surface topology and morphology of the porous structures, including the characterisation of surface adhered particles and how their presence differs based on the manufacture method. This was achieved through imaging using SEM followed by analysis in ImageJ. These studies are among the first of their kind to present both engineers and surgeons with an improved understanding of the types of structures that 3D printing has enabled and also an awareness for what features exist in implants that are currently being used in patients. Furthermore, these studies could present regulatory bodies with additional information with which to revise and develop existing and new standards and guidance to manufacturers and potentially suggest clearer guidelines in the approach to designing and printing the porous layer. The clinical relevance of the results of these studies and the uncertain guidelines were also then discussed, and further ways of monitoring the impacts of the features studied have been suggested for future investigations.

3 | Modelling Analysis of 3D Printed Orthopaedic Implants

3.1 | Background

3D printing is being increasingly employed in orthopaedics for the manufacture of titanium hip, spine and knee implants. Acetabular cups are a popular implant produced using this method, and a key advantage so far involves enabling patient-specific implants for treatment of large and complex acetabular defects, as well as off-the-shelf designs. The main clinical rationale of this technique is providing enhanced bony fixation when comparing to conventionally manufactured implants. 3D printing promotes improved design control enabling manufactures to produce highly porous lattices with a view to enhancing the compatibility of the implant surface with trabecular bone. This is particularly significant given that aseptic loosening is one of the most common reasons for revision in Total Hip Arthroplasty (THA).

Currently, there are no standards to guide or regulate the type and design of the porous structure on the outside of 3D printed custom or off-the-shelf implants. Consequently, manufacturers have different approaches to the designs of their implants including varying factors such as 3D printing method, extent of regularity of the structure, the overall porosity and the dimensional properties of the struts of the lattice. It is important that these different approaches are investigated and understood to inform the post-market surveillance of these devices and aid the determination of which strategy achieves optimal osseointegration.

Previous studies have looked to characterise features of the dense region of 3D printed acetabular cups using Micro-Computed Tomography (Micro-CT), including structural defects such as voids and cavities, and broadly the characteristics of the porous structure. This study aims to explore and analyse the differences between the

approach of several different manufacturers to printing the porous structure and the variability in the print for a single porous structure design of off-the-shelf acetabular cup. A novel aspect of this study includes the development of a methodology using a software traditionally applied to medical imaging for analysis of Micro-CT scans of the porous layer of 3D printed cups.

3.2 | Aims and Objectives

The aim of this chapter was to evaluate how the manufacture method influences the final properties and architecture in the porous layer. An additional aim was to evaluate how the manufacture method affects the variability in the final product and also the effect of the component size on the resulting porous structure (i.e. with the change in size of the implant of the same initial manufacturer design). The variation in porous structure within the same off-the-shelf implant design was therefore explored.

Our objectives were to:

1) Scan the porous structures of the 3D printed custom and off-the-shelf acetabular implants using Micro-Computed Tomography (Micro-CT).
2) Utilise a medical imaging analysis software (Simpleware) in a new context to analyse the features within different 3D printing methods and 3D printed implant designs.
3) Compare between manufacturers, lattice designs, 3D printing method and within the same off-the-shelf implant design.

3.3 | Study Design

The study design is summarised in Figure 3.00. Twelve brand new, unused 3D printed custom acetabular cups of 6 different designs from 6 manufacturers, were analysed (Figure 3.01). Additionally, six brand new, unused 3D printed off-the-shelf acetabular cups from a single manufacturer were also scanned and characterised (Figure 3.02). The sizes and quantities of the off-the-shelf cups were 3x 54mm

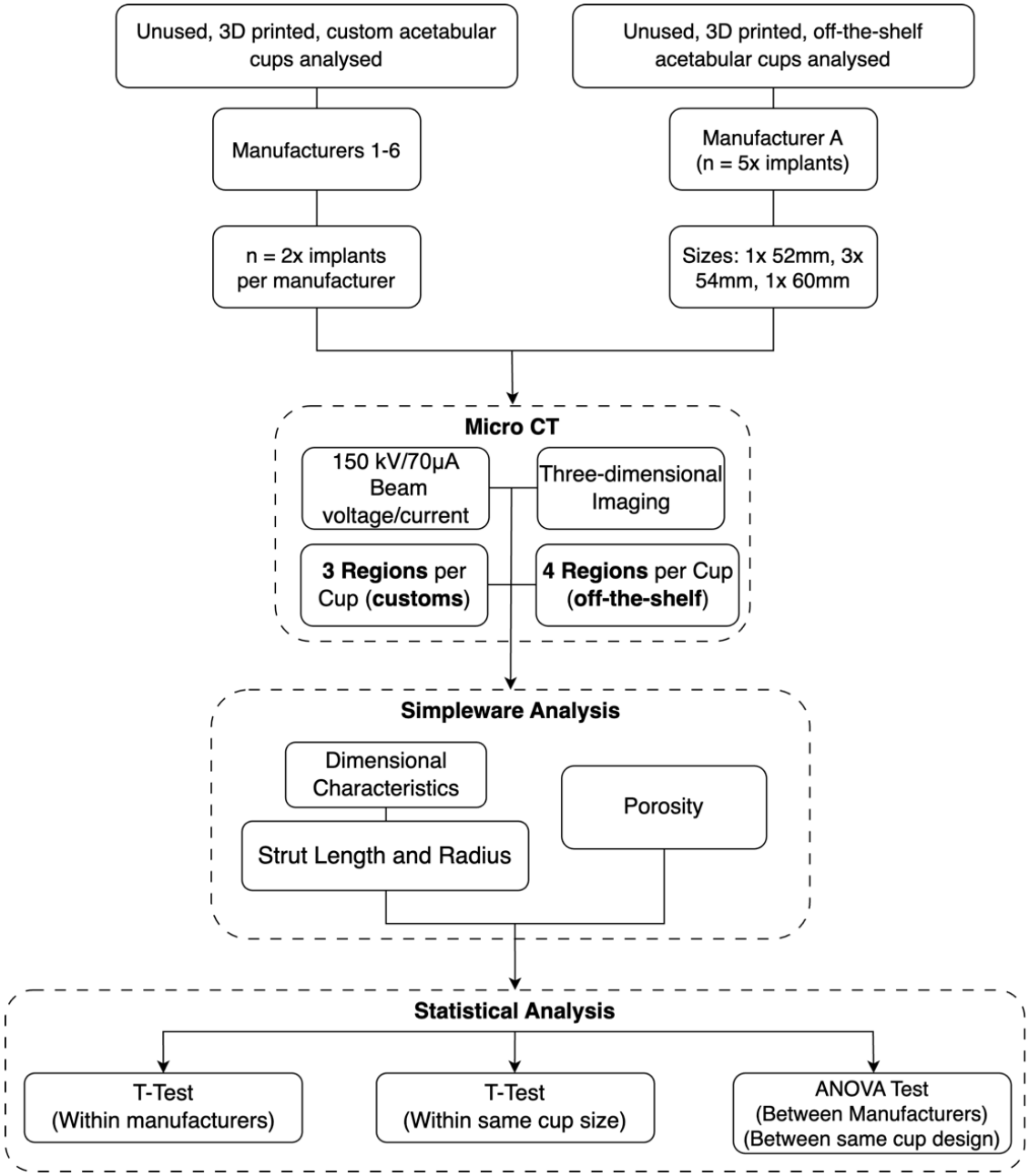

Figure 3.00: The study design showing the analysis steps that were performed on unused, 3D-printed, custom and off-the-shelf implants that imaged using micro-computed tomography, where the dimensional features and porosity were determined by analysis in Simpleware, followed by suitable statistical analysis.

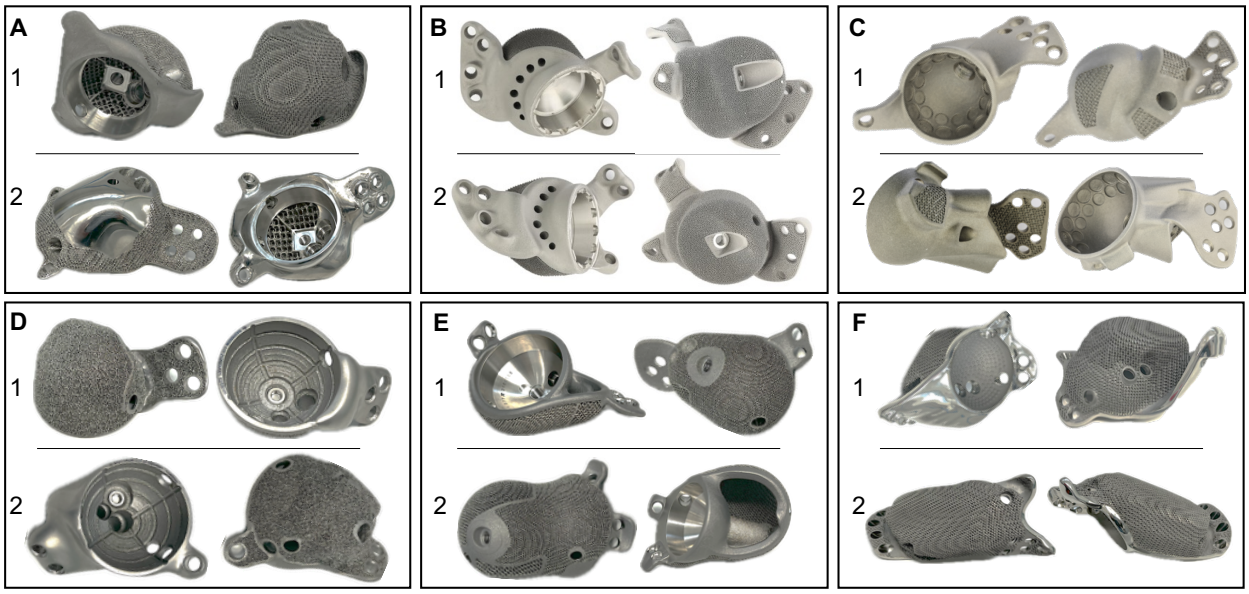

Figure 3.01: Macroscopic images of the twelve custom acetabular cups examined in this study, 3D printed by six manufacturers. For each cup, two different views are presented.

diameter cups (S1-3), 1x 52mm diameter cup (S4) and 1x 60mm diameter cup (S5) (Figure 3.02).

3.4 | Materials and Methodology

The Micro-CT scans of all implants examined in this study had been obtained previously for a past investigation [107]. This study looked to build on this established methodology and capture additional useful data from the scans of these implantsby utilising Simpleware for analysis. Simpleware, which has traditionally been used to analyse medical imaging such as patient CT scans, was utilised in this case to interrogate the porous structure of 3D printed acetabular cups.

3.4.1 | Micro-Computed Tomography

All 3D-printed orthopaedic cups in this study were scanned using a micro-CT scanner (XTH 225, Nikon Metrology, UK) equipped with a Tungsten target as an X-ray source, where the beam voltage and current were set to 150kv and 70μA, respectively, to obtain high-resolution three-dimensional imaging of the implants (Figure 3.03). All cups were mounted as close to the beam source as possible whilst

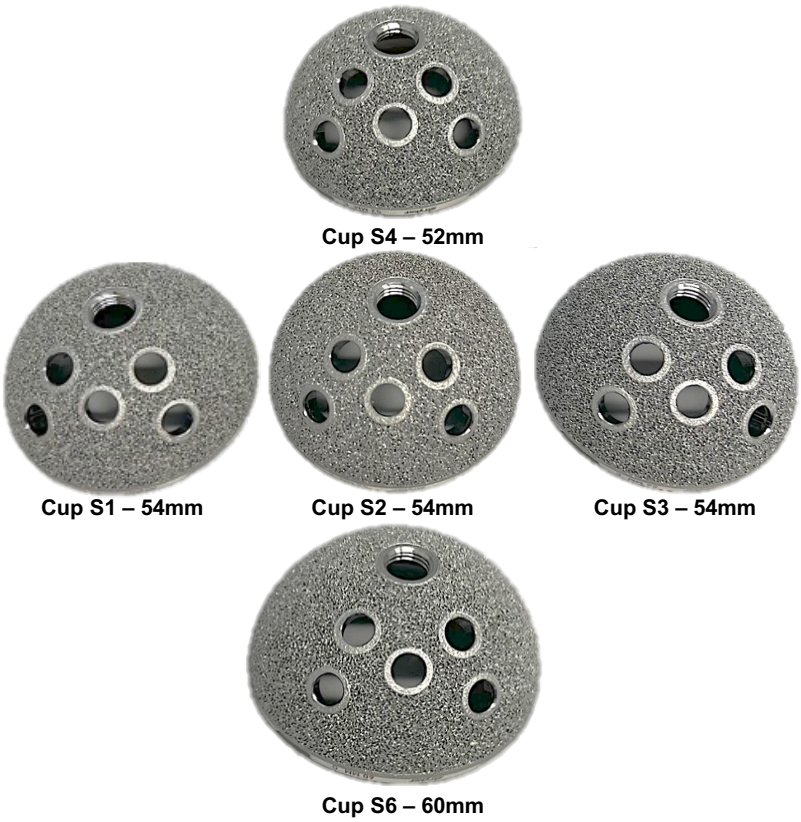

Figure 3.02: Macroscopic images of the porous backside of six off-the-shelf acetabular cups examined in this study, 3D printed by one manufacturer.

still ensuring the whole component was in the field of view. A total of 3177 frames were captured at 0.11° increments, set to an exposure of 100ms. A 1mm thick copper filter was positioned in front of the beam source to prevent the effects of beam hardening during scanning of the implants.

The initial two-dimensional projection images captured during scanning were then imported into CT Pro 3D software (Nikon Metrology, UK), for reconstruction of the 3D image using a filtered back-projection algorithm. Numerical filtering (second-order polynomial correction) was also incorporated to further minimise the effects of beam hardening that may have occurred.

3.4.2 | Simpleware Analysis

The filtered and corrected micro-CT data of the implants were imported into the analysis software package Simpleware (ScanIP Medical Version 2022.3; Synopsys

Inc.) in order to analyse and characterise the porous structures of each implant and quantify the following parameters.

(a) Length of the struts

(b) Radius of the struts

(c) Porosity of the porous layer.

These measurements were chosen for a range of dimensional features for comparison between the different manufacturer designs of the porous structures. Additionally, these particular measurements allowed us to evaluate how Simpleware can be useful in the analysis of these kinds of characteristics on non-clinical imaging. The measurements for these parameters were captured at 3 locations within the main body of the 3D-printed custom acetabular cups (Figure 3.04), and 4 locations on the backside of the off-the-shelf acetabular cups (Figure 3.05).

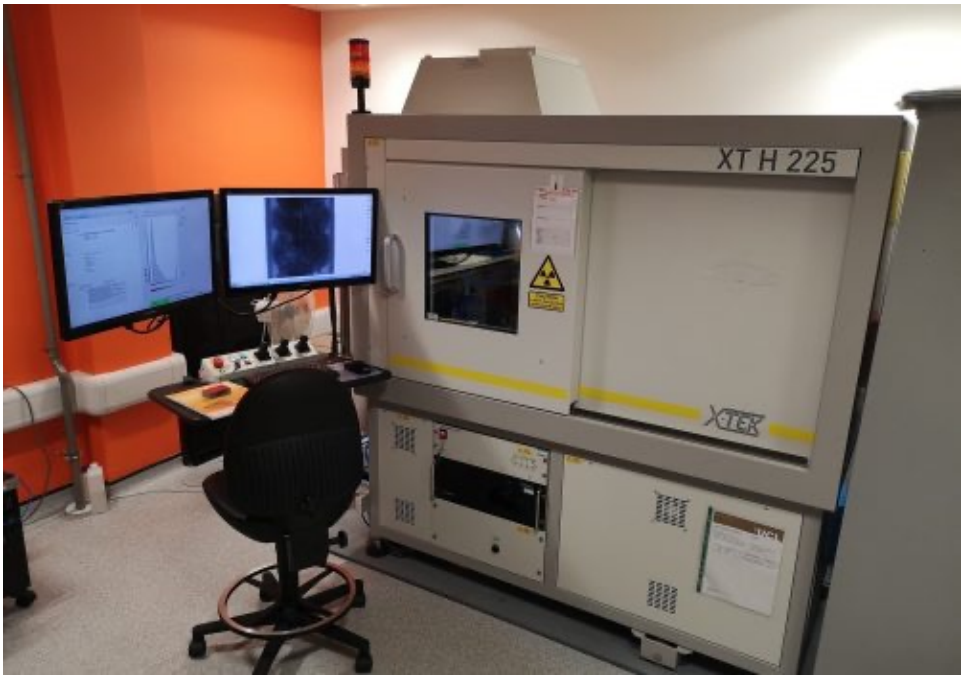

Figure 3.03: An image of the Micro-CT scanner that was used to obtain the raw data scans of the implants analysed in this study.

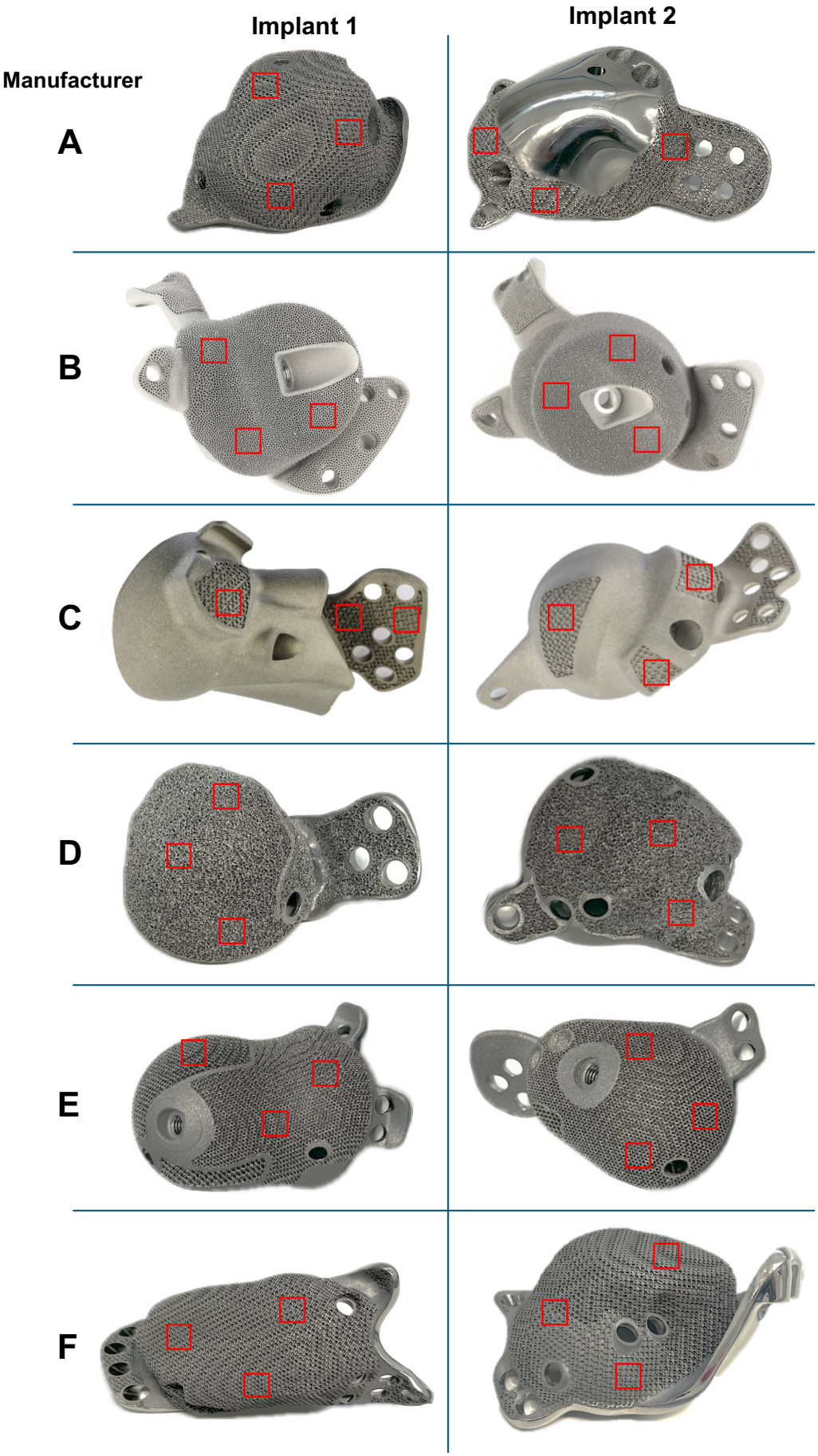

Figure 3.04: The approximate regions at which the porous layer was sectioned for samples on the custom 3D printed acetabular cups. Three main body samples were taken for each cup.

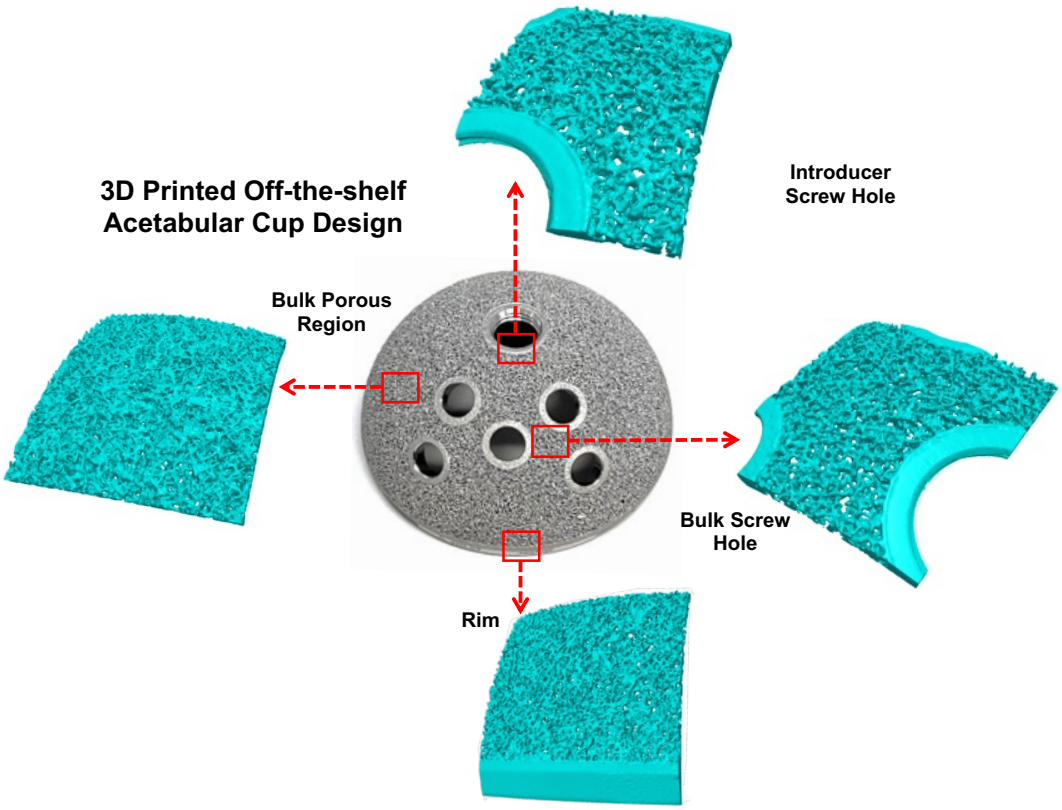

Figure 3.05: The locations at which the porous layer was sectioned for samples on the off-the-shelf design that was examined in this study. These same regions were applied to take samples for every off-the-shelf cup.

Simpleware evaluated length as the distance between two node centres, where a node was determined as the junction of two struts, and radius was calculated through built-in modelling of the cross-section of the struts as a circle. A detailed methodology to outline the steps and specific tools utilised in Simpleware to obtain these measurements can be found in Appendix I (A).

3.5 | Results

The data in this study was generated by utilising Simpleware and consist of four parameters to investigate the struts of the porous structure: Length, Radius and Porosity. These parameters were used to compare between manufacturers, design of the porous structure and within the same manufacturer. The inter-manufacturer differences were analysed to a higher degree using the same parameters within the

same implant design for the off-the-shelf 3D printed acetabular cups that were investigated.

Customs: Length

The range of the median strut lengths for the six manufacturers vary between 0.248 and 1.707 mm. The spread of the data is similar for all implants except manufacturers C and E where the range is approximately two times more compared to the other implants (Figure 3.06). This could suggest longer struts were found on the cups from manufacturers C and E when comparing to manufacturers A, B, D and F. The shortest struts were found on the cups from manufacturer B and the longest from manufacturer C.

Strut lengths in A and D are similar, and C and E have a large spread of data. Additionally, C and F have larger IQR's (Figure 3.06). The boxplot shows the

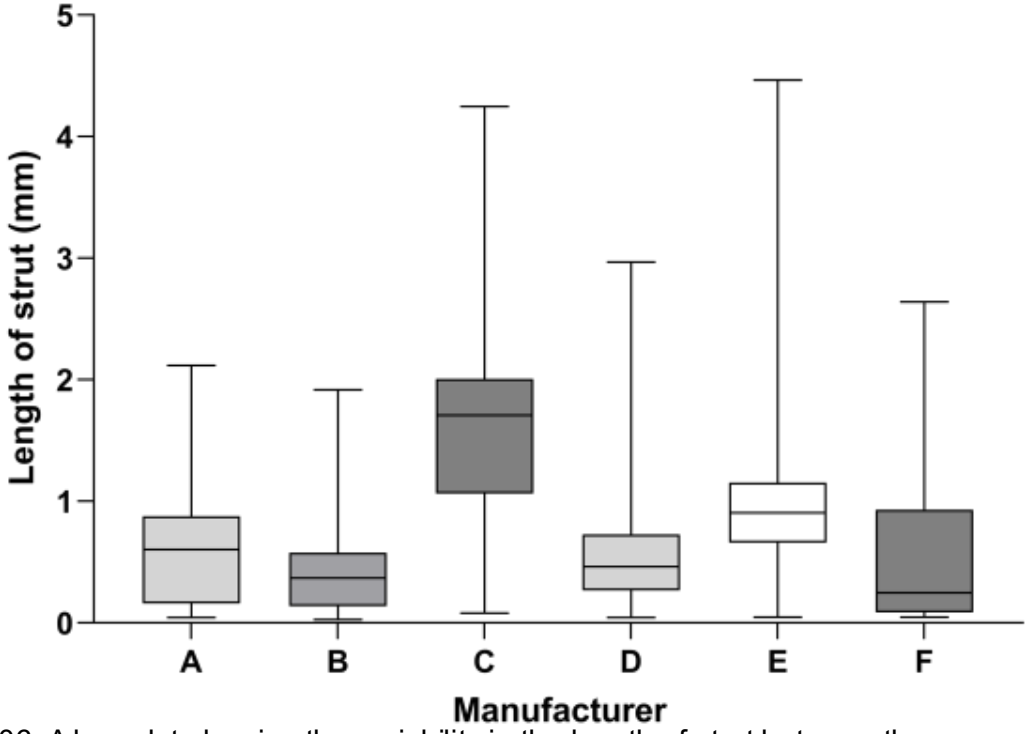

Figure 3.06: A box plot showing the variability in the length of strut between the cups produced by the six different manufacturers.

variability in length of the struts between the cups from different manufacturers. A Kruskal-Wallis test showed there to be a significant variability between the six manufacturers in the length of the struts ($p<0.0001$).

From Table 3.01, it can be observed that there was a significant variability in the strut length between the different manufacturers, except between manufacturers A and D, where the comparison was not statistically significant. This can suggest that there is no standard that is currently followed for strut length in the design stage of producing these lattices. Additionally, there is a vast variability in the designs of these porous structures which can even be observed visually at the macroscopic level in Figure 3.04. These manufacturers use a range of irregular and regular lattice designs and two different types of 3D printing method, and the significant variability suggests these could be a factor in having statistically different strut lengths.

Table 3.01: The comparisons between each of the manufacturers for this particular parameter, where statistically significant p-values are indicated in italics.

	Significant?	***p-value***
A vs. B	*Yes*	*<0.0001*
A vs. C	*Yes*	*<0.0001*
A vs. D	No	>0.9999
A vs. E	*Yes*	*<0.0001*
A vs. F	*Yes*	*<0.0001*
B vs. C	*Yes*	*<0.0001*
B vs. D	*Yes*	*<0.0001*
B vs. E	*Yes*	*<0.0001*
B vs. F	*Yes*	*<0.0001*
C vs. D	*Yes*	*<0.0001*
C vs. E	*Yes*	*<0.0001*
C vs. F	*Yes*	*<0.0001*
D vs. E	*Yes*	*<0.0001*
D vs. F	*Yes*	*<0.0001*
E vs. F	*Yes*	*<0.0001*

Customs: Radius

The range of the median strut radii for the six manufacturers vary between 0.1296 and 0.2649 mm. The spread of the data in is similar for manufacturers A, E and F, with a smaller spread of data for manufacturers B and D, and a larger spread for manufacturer C (Figure 3.07). This could suggest some struts with a larger radius were found on the cups from manufacturer C when comparing to the remainder of the manufacturers (thicker struts). The struts with the smallest radii were found on the cups from manufacturers B and D (smallest medians), and the largest from manufacturer A (largest median).

The spread and IQR's is comparable for manufacturers A, E and F, where it is smaller for manufacturers B and D, and much larger for manufacturer C (Figure 3.07). The boxplot shows the variability in radii of the struts between the cups from

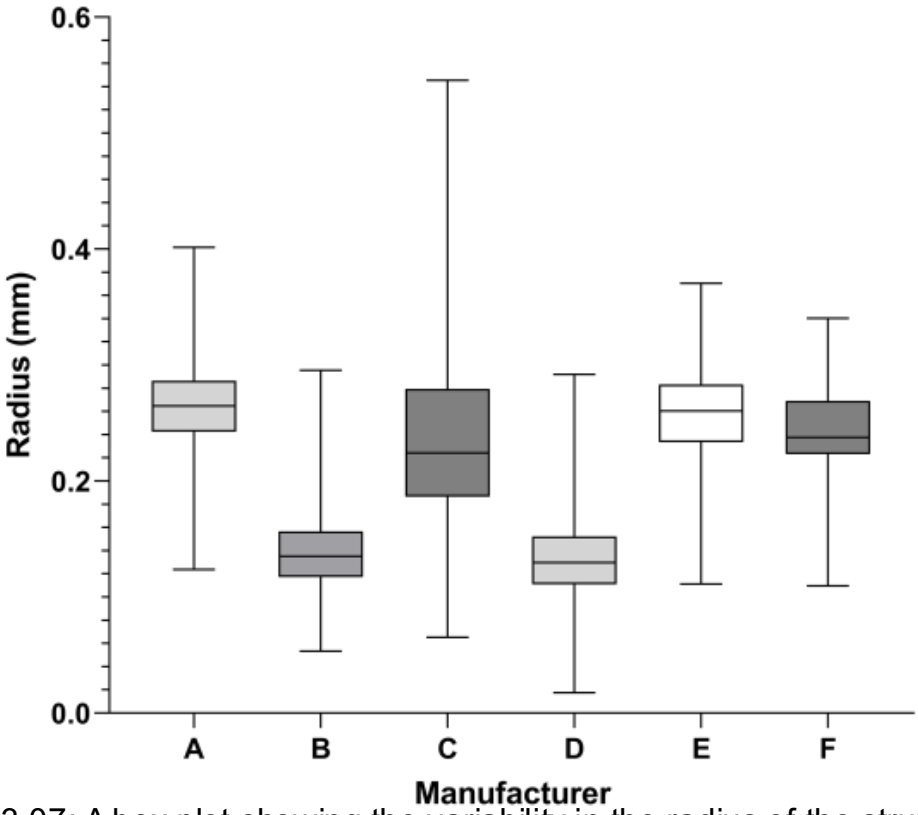

Figure 3.07: A box plot showing the variability in the radius of the struts between the cups produced by the six different manufacturers.

different manufacturers. A Kruskal-Wallis test showed there to be a significant variability between the six manufacturers in the radii of the struts ($p<0.0001$). From Table 3.02, it can be observed that there was a significant variability in the radii of the struts between the different manufacturers, except between manufacturers A and E ($p>0.9999$) and manufacturers B and D ($p>0.9999$). This could be again due to the variation in lattice structure design between the different manufacturers, but perhaps more importantly between the different manufacture methods used by each manufacturer. This is because SLM is capable of producing a smaller minimum feature size than EBM, which could result in finer struts if this is what is designed and printed by the manufacturer, resulting in a smaller strut radius for those manufactured via SLM and larger via EBM.

Table 3.02: The comparisons between each of the manufacturers for this particular parameter, where statistically significant p-values are indicated in italics.

	Significant?	***p-value***
A vs. B	*Yes*	*<0.0001*
A vs. C	*Yes*	*<0.0001*
A vs. D	*Yes*	*<0.0001*
A vs. E	No	>0.9999
A vs. F	*Yes*	*<0.0001*
B vs. C	*Yes*	*<0.0001*
B vs. D	No	>0.9999
B vs. E	*Yes*	*<0.0001*
B vs. F	*Yes*	*<0.0001*
C vs. D	*Yes*	*<0.0001*
C vs. E	*Yes*	*<0.0001*
C vs. F	No	0.0628
D vs. E	*Yes*	*<0.0001*
D vs. F	*Yes*	*<0.0001*
E vs. F	*Yes*	*0.0165*

Customs: Porosity

The range of the median porosities for the six manufacturers vary between 48.73 and 81.84%. The spread of the data is different for all manufacturers, with a range of different levels of porosity (Figure 3.08). The manufacturer with lowest porosity was found on the cups from manufacturer A, and the highest porosity found for the porous structures from manufacturers C and D (largest median). The impact of the radii of the struts could be considered when understanding these results.

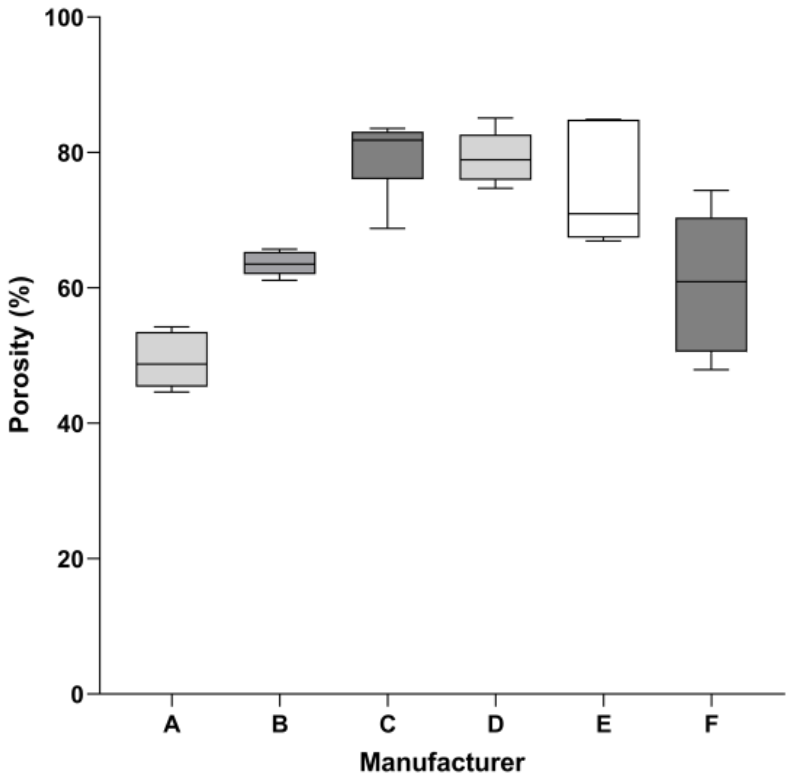

Figure 3.08: A box plot showing the variability in the porosity of the porous structures between the cups produced by the six different manufacturers.

Manufacturers E and F have a larger IQR than other manufacturers, and manufacturer A had a significantly lower porosity than other manufacturers (Figure 3.08). The boxplot shows the variability in porosity of the porous structure between the cups from different manufacturers. A Kruskal-Wallis test showed there to be a significant variability between the six manufacturers in the porosity of the porous structures ($p<0.0001$).

From Table 3.03, it can be observed that there was no significant variability in the porosity of the porous structures between the different manufacturers, except between manufacturers A and C (p=0.0013), A and D (p=0.0013), and A and E (p=0.0184). This can suggest that the porosities of the manufacturers are not statistically different when compared with each other, except for manufacturer A, and that the standards that manufacturers follow for this design feature should be considered. Porosity is a feature of the porous layer where the optimal value is yet to be determined by the industry and recommended by the corresponding regulations. Therefore, this gives rise to the range of porosities that have been observed in this study, where all manufacturers have taken a different approach to the design and features of the porous layer. The understanding surrounding optimal porosity can be improved through further studies, which are more clinical in nature, investigating bone ingrowth into different types of porous structures on acetabular cups, where also the optimal depth of the porous layer could also be considered and discussed.

Table 3.03: The comparisons between each of the manufacturers for this particular parameter, where statistically significant p-values are indicated in italics.

	Significant?	***p-value***
A vs. B	No	>0.9999
A vs. C	*Yes*	*0.0013*
A vs. D	*Yes*	*0.0013*
A vs. E	*Yes*	*0.0184*
A vs. F	No	>0.9999
B vs. C	No	0.1386
B vs. D	No	0.1386
B vs. E	No	0.8267
B vs. F	No	>0.9999
C vs. D	No	>0.9999
C vs. E	No	>0.9999
C vs. F	No	0.1898
D vs. E	No	>0.9999
D vs. F	No	0.1898
E vs. F	No	>0.9999

Customs: Inter-manufacturer comparison

Table 3.04 presents the data of the inter-manufacturer comparisons, to investigate if there is a statistical significance for these parameters of the struts of the porous structures (length and radius), between cups from the same manufacturer. Figure 3.09 shows a panel of graphs for length and radius.

For length, was a significant variability in the length of the struts within cups from the same manufacturer for manufacturers A, B, E and F, and no statistical significance for cups from manufacturer C and D. The type of structure (regular or irregular) should be considered as for irregular structures it would be expected that is will not be a consistent feature across the porous layer, but for a structure that was more regular in nature we would expect to see more consistent measurements. These results can suggest that strut length is not a consistent feature across most of these manufacturers.

For radius, there was no significant variability within cups from the same manufacturer for all manufacturers. This suggests that these features are consistent across different cups from the same manufacturer, and so the consistency of the 3D

Table 3.04: The comparisons between the cups within the same manufacturer for length and radius, where statistically significant p-values are indicated in italics.

	Length		**Radius**	
	Significant	***p-value***	***Significant?***	***p-value***
A1 vs A2	*Yes*	*<0.0001*	No	>0.9999
B1 vs B2	*Yes*	*<0.0001*	No	>0.9999
C1 vs C2	No	>0.9999	No	>0.9999
D1 vs D2	No	0.6446	No	>0.9999
E1 vs E2	*Yes*	*0.0502*	No	>0.9999
F1 vs F2	*Yes*	*<0.0001*	No	>0.9999

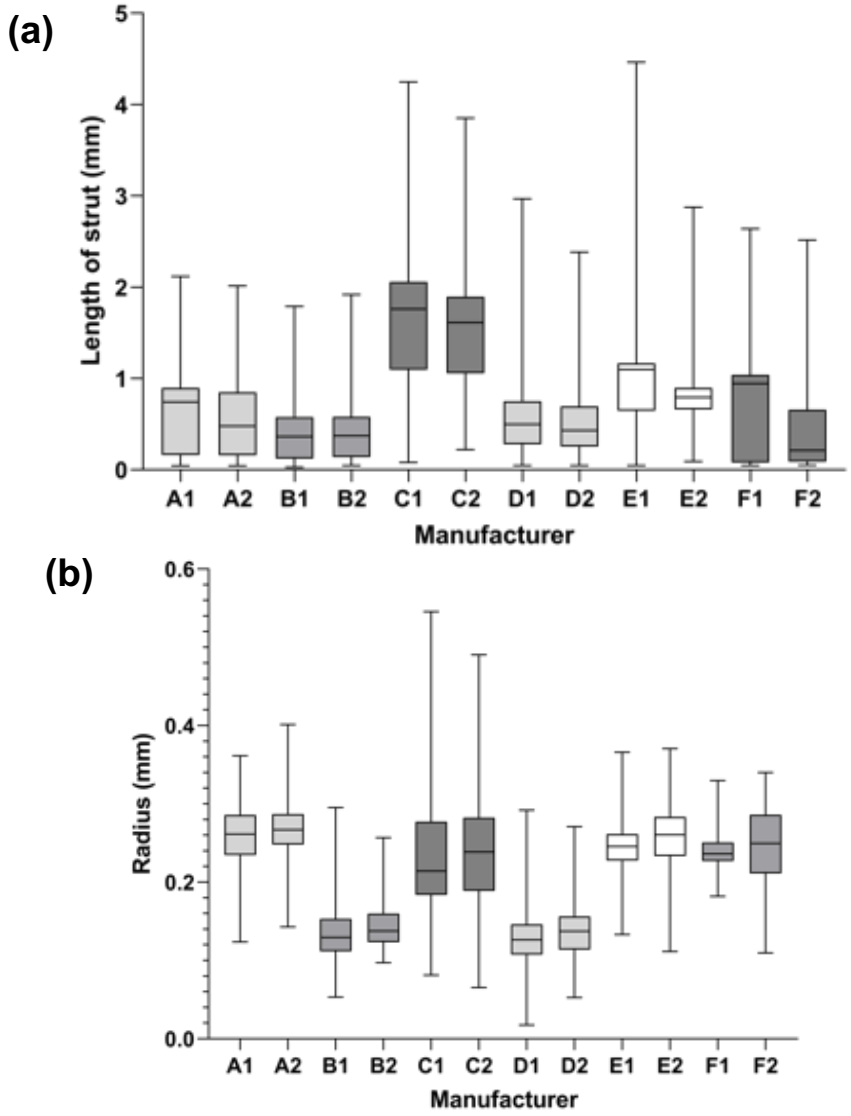

Figure 3.09: Box plots showing the variability of the features of the porous structure within the same manufacturer for the six different manufacturers.

printing method in the production of these implants can be considered, as previously discussed.

Off-the-Shelf: Length

The range of the median strut lengths for the six manufacturers vary between 0.1576 and 0.2105 mm. The spread of the data is very similar for all cups (Figure 3.10). This could suggest that visually this manufacturer is achieving the same length of

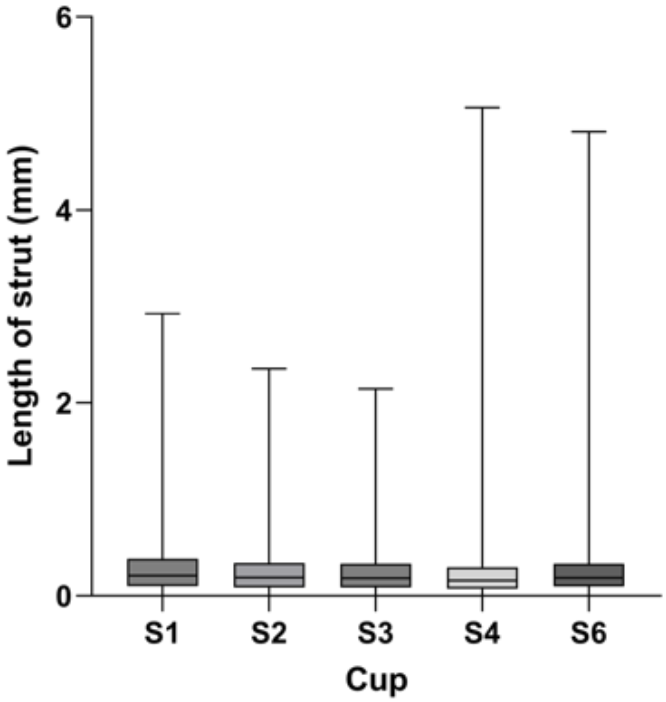

Figure 3.10: A box plot showing the variability in the length of the struts between the cups of the same design and different sizes produced by the same manufacturer.

strut for all cups. This is a reassuring observation as these are cups of the same design from the same manufacturer.

All cups have a similar IQR and median (Figure 3.10). The boxplot shows the variability in the spread of the data for the length of the struts of the porous structure between the cups. A Kruskal-Wallis test showed there to be a significant variability between the six cups in the length of the struts ($p<0.0001$).

From Table 3.05, it can be observed that there was a significant variability in the length of the struts between the cups, except between cups S2 and S3 ($p=0.1123$), where the comparison was not statistically significant. This is still reassuring as S2 and S3 are the same size of cup.

A very similar spread in the data (interquartile ranges) indicate that there is some consistency in the strut length across this cup and therefore this design despite the

Table 3.05: The comparisons between each of the cups for this particular parameter, where statistically significant p-values are indicated in italics.

	Significant?	***p-value***
S1 vs. S2	*Yes*	*<0.0001*
S1 vs. S3	*Yes*	*<0.0001*
S1 vs. S4	*Yes*	*<0.0001*
S1 vs. S6	*Yes*	*<0.0001*
S2 vs. S3	No	0.1123
S2 vs. S4	*Yes*	*<0.0001*
S2 vs. S6	*Yes*	*<0.0001*
S3 vs. S4	*Yes*	*<0.0001*
S3 vs. S6	*Yes*	*<0.0001*
S4 vs. S6	*Yes*	*<0.0001*

different sizes of cup. This is despite the irregular design of this particular porous structure, which can also be observed macroscopically in Figures 3.02 and 3.05.

Off-the-Shelf: Radius

The range of the median strut radii for the six manufacturers vary between 0.08725 and 0.09972 mm. The spread of the data is similar for all cups (Figure 3.11). This is a

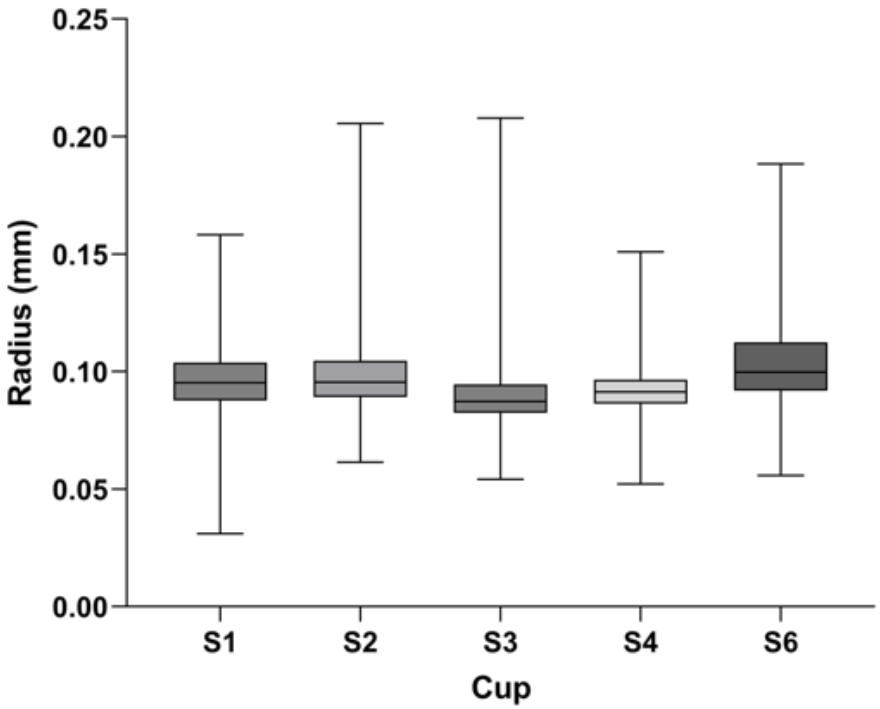

Figure 3.11: A box plot showing the variability in the radius of the struts between the cups of the same design and different sizes produced by the same manufacturer.

reassuring observation as these are cups of the same design from the same manufacturer.

All cups have a similar IQR and median (Figure 3.11). The boxplot shows the variability in the spread of the data for the radius of the struts of the porous structure between the cups. A Kruskal-Wallis test showed there to be a significant variability between the six cups in the radius of the struts ($p<0.0001$). This was a similar observation made for strut radius.

From Table 3.06, it can be observed that there was a significant variability in the length of the struts between the cups, except between cups S1 and S2 ($p>0.999$), where the comparison was not statistically significant. This is still reassuring as S1 and S2 are the same size of cup and so we would expect this result.
Similarly, the close spread of interquartile ranges of the radii of the struts indicate that there is some consistency across the cups of the same porous structure design, despite the statistical significance between many of the cups. This could be explained by the scale used to measure this metric rather than looking at the values in isolation, as macroscopically, they are similar.

Table 3.06: The comparisons between each of the cups for this particular parameter, where statistically significant p-values are indicated in italics.

	Significant?	***p-value***
S1 vs. S2	No	>0.9999
S1 vs. S3	*Yes*	*<0.0001*
S1 vs. S4	*Yes*	*<0.0001*
S1 vs. S6	*Yes*	*<0.0001*
S2 vs. S3	*Yes*	*<0.0001*
S2 vs. S4	*Yes*	*<0.0001*
S2 vs. S6	*Yes*	*0.0007*
S3 vs. S4	*Yes*	*0.0078*
S3 vs. S6	*Yes*	*<0.0001*
S4 vs. S6	*Yes*	*<0.0001*

Off-the-Shelf: Porosity

The range of the median porosities for the six manufacturers vary between 54.30% and 61.85%. The spread of the data is similar for most of the cups (Figure 3.12). This is a reassuring observation as these are cups of the same design from the same manufacturer. However, a higher level of porosity was observed for cup S3.

Cups S1, S2, S4 and S6 have similar medians, which is much higher for S3. The boxplot shows the variability in the spread of the data for the porosity of the porous structure between the cups. A Kruskal-Wallis test showed there to be a significant variability between the six cups in the porosity of the struts ($p<0.0001$).

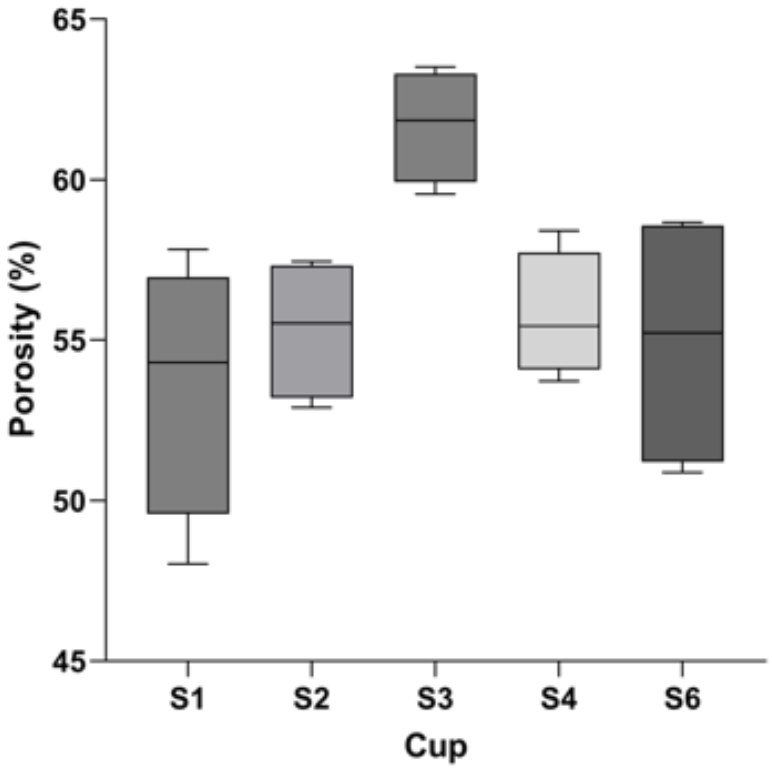

Figure 3.12: A box plot showing the variability in the porosity of the porous structures between the cups of the same design and different sizes produced by the same manufacturer.

From Table 3.07, it can be observed that there was no significant porosity of the porous layer between any of the cups. This is a reassuring observation as all cups are from the same manufacturer and the same off-the-shelf design.

Despite the visual variability observed in Figure 3.12, it is clear through statistical testing that these values are statistically similar and that there is consistency across the level of porosity across the six cups from the same manufacturer and acetabular cups design. This is also important as despite a largely irregular design of the porous structure that this manufacturer has opted for, they have been able to achieve similar porosity vallues across cups of different sizes. In further studes, it can therefore be studied how the porous structure is effectuvely scaled up and down between cup sizes and how the manufacturer can achieve consistency across prints and different cup sizes.

Table 3.07: The comparisons between each of the cups for this particular parameter, where there were no statistically significant p-values.

	Significant?	***p-value***
S1 vs. S2	No	>0.9999
S1 vs. S3	No	0.0716
S1 vs. S4	No	>0.9999
S1 vs. S6	No	>0.9999
S2 vs. S3	No	0.1428
S2 vs. S4	No	>0.9999
S2 vs. S6	No	>0.9999
S3 vs. S4	No	0.3647
S3 vs. S6	No	0.1977
S4 vs. S6	No	>0.9999

3.6 | Discussion

This is the first study to characterise the features of the porous structures on 3D printed custom and off-the-shelf acetabular cups using Micro-CT data and Simpleware for analysis. The porous structures produced by different manufacturers were compared using their dimensional features and porosities and a single off-the-shelf design was interrogated for consistency and repeatability of the print of different sizes of the same implant.

3.6.1 | Custom Implant porous structures

The medians of the length of the struts spread from 0.25 mm up to as high as 1.7 mm, and this is a considerable difference between the smallest and largest medians for the length of the struts found across the six manufacturers. Additionally in Figure 3.06, Manufacturers B, D and E have smaller interquartile ranges whereas for Manufacturers A, C and F, this range is much larger, and when comparing between all manufacturers, the comparisons of the measurements for length are all statistically significant, except for the comparison between Manufacturer A and D, which was not significant.

This can be due to the different porous structure designs, where among the 6 manufacturers investigated in this study a range of regular and irregular structures were analysed. Therefore, from the perspective of porous structures, length is likely dependent on the manufacturer, and in this study, this was different for all manufacturers.

The medians of the radii spread from 0.13 mm to 0.26 mm, and this is a considerable difference between the smallest and largest radii of the struts for the six manufacturers. Additionally in Figure 3.07, the variability in the radius can be

observed for the six manufacturers, where B and D have smaller interquartile ranges and comparatively Manufacturer C has a much larger spread of data. However, in this figure the remaining Manufacturers A, B, D, E and F all have comparable interquartile ranges. Also, the comparisons between the manufacturers were all statistically significant except for the comparison between Manufacturer A and E, Manufacturer B and D and Manufacturer C and R, and these results emphasise a similar message as radius, where these parameters are not significantly similar enough to each other that they are unlikely to have been guided via a clear regulation or standard.

The medians of the porosities spread from 49% to 82%, and this is a very considerable difference between the smallest and largest porosity of the porous structure for the six manufacturers. Additionally in Figure 3.08, the clear variability in the porosity can be observed for the six manufacturers, where visually, there is a significant variation in the porosities. However, when looking at the comparisons between the manufacturers, all were not statistically significant, except for Manufacturers A and D and Manufacturers A and E. This is reassuring as while the medians seem disparate and this can be observed on the box plot, statistically the manufacturers are achieving largely similar porosities, despite different porous structure designs and strut characteristics.
Going forward, these porosities should be considered from a clinical performance perspective as well as their statistical differences, where does this range in porosities across manufacturers also correspond to a range of different behaviours in vivo.

Inter manufacturer

From Figure 3.09, visually it is clear that within each manufacturer there is consistency across length and radius, in terms of interquartile ranges and medians. Additionally, from the comparisons across parameters in Table 3.04, the only statistically significant comparisons were for length within the implants from Manufacturer A, B, E and F. However, when looking at Figure 3.09 for these manufacturers, there are still similarities in their interquartile ranges and the spread of data. The medians between the cups within the same manufacturer that had significant differences for length (Manufacturer A, B, E and F) were; A1 vs A2 had median lengths 0.741 mm vs 0.4777 mm, B1 vs B2 had median lengths 0.3643 mm vs 0.3705 mm, E1 vs E2 had median lengths1.099 mm vs 0.7927 mm, F1 vs F2 had median lengths 0.9430 mm vs 0.2118 mm.

When looking at Figure 3.09, it is reassuring that between the designs from the same manufacturers that they appear to be quite consistent within their prints, even when these are custom made implants. This suggests that each manufacturer have their own design ethos and approach when printing their implants which is fairly consistent. Despite the patient-specific nature of these implants, it is clear that all manufacturers in this study have a set design approach to the porous structure, and there for as of yet do not also tailor the porous structure specifically for the patient in terms of their particular bone stock and structure. This could be considered in the future, but there are some apparent limitations when producing this type of implant which include higher costs and increased timescales.

3.6.2 | Intra off-the-shelf cup porous structures

The box plots in Figures 3.10 and 3.11 demonstrate the variability of length and radius which were measured for the struts in this study. From these figures, it is clear that all cups for these parameters appear consistent, in terms of medians and

interquartile ranges. This is very reassuring as these are cups of the same design from the same manufacturer. Cup S6 had a larger interquartile range than the cups of other sizes for radius, and this could be due to the larger cup size leading to a design using thicker struts in the porous structure. Looking at Tables 3.05 and 3.06, all comparisons across length and radius were statistically significant, except for S2 vs S3 for length and S1 vs S2 for radius, and these exceptions are reassuring as S1, S2 and S3 as well as being the same design and manufacturer, are also cups of the same size. The statistical significance of the other comparisons is likely due to the millimetre and micron scale of the metrics involved in this study, and when comparing in perspective across the cups, they are sufficiently similar across these parameters.

However, the important consideration to note of these characteristics is their effect on the overall porosity of the porous structures of these implants, which we would expect to be in agreement, given these are implants of the same design.

The box plot in Figure 3.12 demonstrates the variability in the porosity between these cups, where visually there is a difference between the interquartile ranges, but the medians appear relatively consistent. When looking at Figure 3.12, the medians are consistent, but cup S3 has a higher median than for the other implants. However, when considering the comparisons between the cups in Table 3.07, no comparisons were statistically significant, indicating that the porosity for all cups was consistent and relatively similar to each other. This is another reassuring observation given all cups are of the same design and manufacturer.

When considering the higher median seen for cup S3, this could be due to a variability in the print of the implant given that these cups have an irregular porous

structure design, which in turn may be more difficult to control in terms of consistency of porosity. However, it is important to note that this level of porosity was not statistically significant when comparing with the other cups, and the characteristics of the struts also remained consistent. The spread of this data is 6 percentage points between the smallest and highest porosity of the cups, which in perspective is a small difference and statistically insignificant relative to the other medians.

3.6.3 | Previous literature and Analysis Methods

This study is one of the first to utilise Simpleware on raw micro-CT data of a non-clinical nature to analyse and characterise the features of the porous structure of 3D printed implants. Previous literature has explored these implants using combinations of micro-CT and other software programs and analysed features including in the dense and porous regions of both 3D printed custom and off-the-shelf acetabular cups. Papers surrounding this subject include characterising the design of the porous structure on 3D printed off-the-shelf acetabular cups, as well as the application of other analysis methods to assess the suitability of micro-CT as a characterisation technique in the context of 3D printed implants [126]. It was concluded that micro-CT was a reliable investigation method for 3D printed orthopaedic cups for the characterisation of dimensional features in both the dense and porous regions. This is further demonstrated in this study where micro-CT has allowed the measurement of several important characteristics of the porous structures of these implants.

The custom implants analysed in this study have been investigated previously using micro-CT to identify and characterise voids present in their dense regions [106].

Micro-CT allows a sufficiently high resolution to capture these defects within the dense region, and by the same token, makes it a suitable method to capture the struts of the porous structures of these implants, which are of a comparable scale, and enable their characterisation. Additionally, this paper characterised the defects found in and around the flange regions of the implants, which could be included in future studies of the porous structures. In any case, the results of our study complement the findings of this paper and give a more complete perspective of these implants, with the features of both the dense and porous regions having been analysed in depth.

In terms of the characterisation of off-the-shelf 3D printed acetabular cups, these have been characterised in previous literature using alternative analysis techniques and metrics, and comparisons have been made between competing commercially available designs [100], as well as with conventionally manufactured cups [104,144]. This included characterisation via Scanning Electron Microscopy (SEM) and Coordinated Measuring Machine (CMM), and also micro-CT to quantify different characteristics of these implants such as the thickness of the porous and dense regions, roundness of the inner surface and different parameters in surface topography analysis [100]. The novelty of this study is the comparison of the porous structures of 3D printed off-the-shelf acetabular cups from the same manufacturer and of the same design, and where three cups from this sample set are also the same size. Acetabular cups are sized using their inner cup diameter measurements, where in this study we had 3x 54mm cups, indicating an inner cup diameter of 54mm, as well as 1x 52mm cup and 1x 60mm cup. This allows the interrogation of aspects such as consistency of the design, approach to 3D printing and production of these implants in a way that has not been investigated previously. The

manufacturer of the implants examined in this study has also opted for an inherently irregular porous structure in their approach to encourage bone ingrowth post-implantation. From the results of this study, despite the intentionally irregular nature of the design of the porous structure itself, the characteristics of the struts remain notably consistent where despite the statistical differences in the radii of the struts between the six cups, visually and numerically in Figures 3.26-3.28 and Tables 3.14, 3.16 and 3.18 respectively, these values are comparable and indicate consistency and a set approach by the manufacturer. This is emphasised by the measurements for porosity where despite some variability in the values, the comparisons between the cups were not statistically significant, indicating the manufacturer is achieving overall consistency in this more indicative metric of the porous structure, despite any differences at the strut-level.

This study has highlighted the applicability of Simpleware for analysis and in a non-clinical context with the micro-CT data of these implants. We were able to determine and obtain dimensional measurements of the struts of the porous struts effectively, precisely, reliably and efficiently with this software, as well as determine respective volumes of different samples to calculate values for porosity. Enabling this type of analysis as a research tool is particularly useful in context of these implants and their porous structures due to the IP protection of the manufacturers' designs. This methodology and the resulting data therefore help in our overall understanding of 3D printed implants. They also demonstrate the practicability of micro-CT and Simpleware for the potential use in manufacturers' additive manufacturing workflows and quality checking of the final products.

3.6.4 | Clinical Relevance

In previous literature, it has been discussed that 3D printed implants with a porous bone-facing layer have exhibited a higher degree of osseointegration comparatively with the conventional counterpart [101]. The most common reason for revision in conventionally manufactured implants is aseptic loosening. 3D printed implants aim to prevent this through improved bony fixation through an increased coefficient of friction between the bone and implant, providing an increased initial stability, and a porous structure designed to complement that of the surrounding bone tissue. This study compared retrieved conventionally manufactured and 3D printed off-the-shelf acetabular cups and found that osseointegration into the porous layer of the 3D printed cups was deeper and predominantly more uniform than the porous layer on the conventional cups [104]. Overall, this study found a higher percentage of bone occupying the available porous space in the 3D printed cups versus conventionally manufactured cups.

Porosity and the features of the porous region are important in the interaction between the implant and bone tissue and are directly linked to the mechanical and biological performance of the implant in vivo. The intention of the porous structure is to improve fixation and stability of the implant with the increased mechanical bony fixation integrated into the structure. It has also been discussed that 3D printed implants demonstrate morphometric values for features of the porous region similar to that of trabecular bone, and preliminary findings suggest that this is the type of bone that has grown into the porous structures of retrieved 3D printed implants [104]. While not directly characterised in this study, the consideration of pore size is heavily debated, where recent studies and investigations involving animals have indicated that sufficient bone infiltration can occur in the range of 100–500 μm, however the

optimal pore size and complementing porous structure design are yet to be determined and remains a controversial subject in the literature. It requires further studies on retrieved 3D printed implants of several designs of porous structures as well as comparison with conventional designs to determine if this manufacture method provides comparable or enhanced bony fixation.

While there are animal studies and preliminary investigations surrounding the performance of these implants in vivo, this is a relatively underexplored subject area and lacks sufficient clinical data to support the initial positive observations, which have also been observed in the registry data. It requires further analysis to understand how the design of the porous structure in terms of regularity, strut and pore size as well as the depth of this layer affect the initial and long-term osseointegration of these implants. Where this study characterises, the porous structures based on their morphometric and dimensional features, this research area would now benefit from a study investigating the levels of bony fixation between different manufacturers and therefore porous structure designs. Additionally, the risk of infection from these new designs of implant must be investigated. Realistically, the tangible indication of how these implants perform in the patient compared to the tenured conventionally manufactured acetabular cups will become clear when the current implanted 3D printed cups reach ~10-15 years of service and increase the quantity of informed clinical data. Additionally, then if or when these implants are removed and the reasons for revision can also be considered.

3.6.6 | Application to Industry and Regulation

This new methodology has highlighted the usefulness of micro-CT for computational analysis from a research perspective in capturing the dimensional features of 3D

printed implants, down to the strut-level of their porous structures. Alongside a computational software such as Simpleware for examination, it raises the question if micro-CT could be applicable to industry in the case of regulatory assurance. Scanning of these implants could become a step along the standard production workflow and form part of manufacturers' quality clearance processes, inspect for defects, imperfections and dimensional tolerances to a high resolution, including within the porous structures of the implants. Despite the potential value of this step in the implant production workflow, limitations to adding this step could include increased timelines for manufacturers and higher costs associated with the operation and maintenance of micro-CT.

3.6.7 | Limitations

We acknowledge the limitations of this study. While both custom and off-the-shelf 3D printed cups from a range of manufacturers were captured in this study, including those commercially available and distributed by several of the largest manufacturers, future studies would benefit from analysing more implant designs, as well as larger sample sizes from each manufacturer and different sizes of cups, to evaluate the variability and consistency between prints and post-processing for each manufacturer. Additionally, the investigation techniques used in this study, while providing an insight could be utilised further and other tools used to improve the characterisation of the porous layer.

Also going forward, the methodology used in this study could be strengthened to further validate the combination of using Micro-CT and Simpleware for characterisation of these complex porous structures.

3.7 | Conclusion

This was one of the first studies to use Simpleware to take measurements and characterise features on raw micro-CT data from a non-clinical context. Additionally, both custom and off-the-shelf acetabular cups were examined using this novel methodology.

There was considerable statistical significance between the manufacturers of the custom cups for the dimensional metrics measured for the struts of the porous structures in this study, with less difference between them for porosity indicating that the approach of all manufacturers is to achieve a comparable value for this important feature. When comparing between the cups within the same manufacturer, from a porosity perspective, consistency can also be observed, demonstrating some extent of repeatability of the structures from the respective manufacturers in their 3D printing processes.

Comparison within the same manufacturer and design of the off-the-shelf 3D printed cups also indicated similarities for the measurements of the struts and this was further highlighted in the consistency of the values for porosity between the cups.

This study demonstrated the applicability of micro-CT and Simpleware for this kind of analysis as a research tool. Going forward, this tool could be utilised to perform Statistical Shape Modelling (SSM) analysis to examine the consistency of the unit cells of regular porous structures or the extent of irregularity of the irregular designs.

4 | Analysis of the Porous Region of 3D Printed Implants

4.1 | Background

Acetabular cups are among the most used 3D printed orthopaedic implants due to advantages including thinner shell walls for larger femoral heads and greater control over the design of the bone-facing porous structure when compared with conventionally manufactured cups [79]. With the rapid uptake of 3D printing for the manufacture of orthopaedic implants, it is important that the limitations and potential risks of this method are better understood.

Selective Laser Melting (SLM) and Electron Beam Melting (EBM) are the primary methods of 3D printing used in orthopaedics. Both utilise a high-energy beam to fuse metal powder layer-by-layer to construct the desired part, but they have technological differences. A significant challenge of this manufacture method is that, during printing, some source titanium powder does not fully fuse with the component. Therefore, clusters of surface adhered particles remain within the part immediately after printing. Surface adhered particles are a known consequence of 3D printing and occur due to large thermal gradients causing adhesion of surrounding particles [100]. All manufacturers therefore complete post-processing cleaning, a vital step in 3D printing workflows, in an effort to remove the non-fused particles, however there is no standard to regulate or guide these processes.

Their occurrence is not completely understood on 3D printed implants. There is evidence that surface adhered particles exist within the porous structures of acetabular shells, but their extent across different manufacturers is not known [124]. It is possible these particles may trigger adverse biological effects [145], potentially

hindering osteointegration [146]. Additionally, the phenomenon of third body production may occur leading to accelerated overall implant wear, potentially causing premature failure of the implant [147].

The presence of these particles on custom 3D printed acetabular cups has been investigated previously and evidence of surface adhered particles was presented across several manufacturers, suggesting post-processing cleaning has not been refined [124]. The aim of this study is to characterise these particles and further develop and validate the methodology to do so and compare to existing studies.

4.2 | Aims and Objectives

The primary aim of this chapter was to evaluate the influence of the manufacture method on the presence of surface adhered particles on the porous structures of commonly used 3D printed off-the-shelf acetabular cups. The secondary aim was to understand the impact of the choice of manufacture method (SLM or EBM) on the size and frequency of surface adhered particles in the porous structures of these implants.

The objectives were to:

1) Image the porous structures of 3D printed off-the-shelf acetabular cups using Scanning Electron Microscopy (SEM).
2) Understand the relationship between the presence of the particles and the factors relating to the extent of their presence.
3) Compare this with previous findings on custom 3D printed acetabular cups.

4.3 | Study Design

Nine final production 3D printed off-the-shelf acetabular of 5 different designs from 5 manufacturers were analysed (Figure 4.01 [125]).

It should be highlighted that the workflow of this study is one of the first to investigate the characterisation of surface adhered particles on 3D printed implants, when considering previous literature.

Figure 4.01: The study design showing the analysis steps that were performed on unused, 3D-printed, off-the-shelf implants that were obtained and imaged using backscattered electron radiation scanning electron microscopy, where the particle diameter and particles per mm^2 were calculated using ImageJ, followed by suitable statistical analysis [125].

4.4 | Materials and Methodology

4.4.1 Materials

We obtained at our centre nine brand new, unused, final-production 3D printed off-the-shelf acetabular cups printed by five different major orthopaedics manufacturers (Figure 4.02). These designs are some of the most popular for worldwide clinical use and were chosen for use in this study as a result. The cups in this study were manufactured by BBraun, Stryker, Implantcast, Medacta and Zimmer Biomet. They

Figure 4.02: Macroscopic images of the front and back of the different designs of 3D printed off-the-shelf acetabular cup examined in this study.

feature a spectrum of lattice types and exhibit the two 3D printing methods used in orthopaedics: Selective Laser Melting (SLM) and Electron Beam Melting (EBM).

Three brands in this study were printed using SLM and two using EBM, and identifiers consisting of Cup_1A, Cup_1B etc., were assigned to each implant.

4.4.2 Scanning Electron Microscopy (SEM)

Scanning Electron Microscopy (SEM) of the porous structures of the 3D printed acetabular cups using a Carl Zeiss Scanning Electron Microscope (Carl Zeiss Ltd, Cambridge, UK). All analysis was performed using backscattered electron imaging (BSE), at an electron high tension (EHT) of 20kv and probe current of 2.0nA (Figure 4.03).

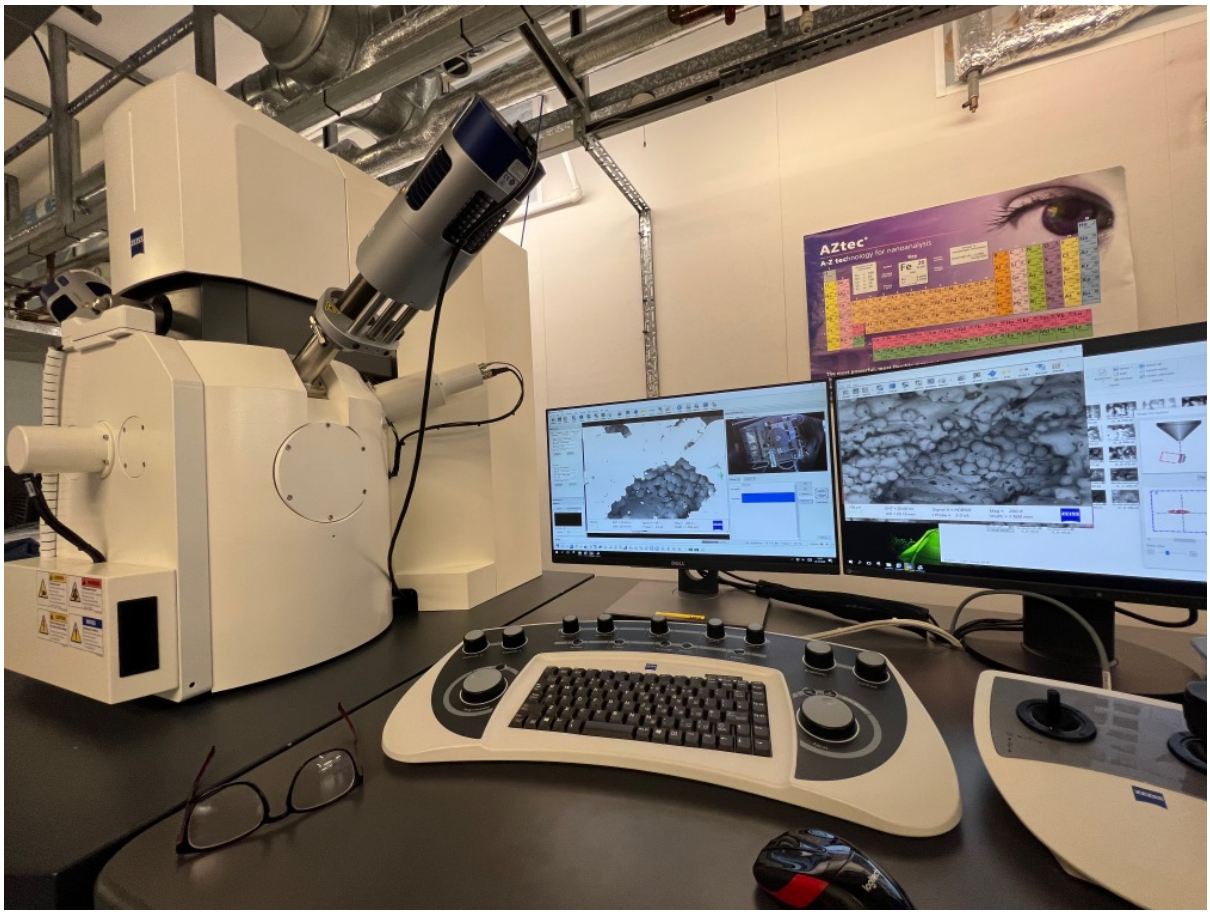

Figure 4.03: The SEM used in this study (Carl Zeiss Scanning Electron Microscope), and the corresponding set up to observe and capture the SEM images on the specific software.

SEM is a common reliable analysis method, and the SEM used in this study was calibrated such that for each image captured, a corresponding scale bar was generated. This was also useful when the images were uploaded into ImageJ for particle characterisation. Each image was calibrated to this scale bar prior to taking any measurements of the particles (see Appendix II).

Each cup was mounted on a circular plate and fastened through the introducer screwhole using a screw and washer to secure it to the circular plate. This plate with the mounted implant was then fixated in the internal chamber to the viewing plate using another screw (Figure 4.04). This was enabled as the internal viewing chamber of this particular SEM (Carl Zeiss EVO 25) can accommodate this size of specimen (420 mm in diameter by 330 mm tall). Additionally, once the implant was mounted inside the SEM, and the SEM was vacuumed down, the internal viewing plate where the implant was mounted was able to rotate and move in 3D dimensions

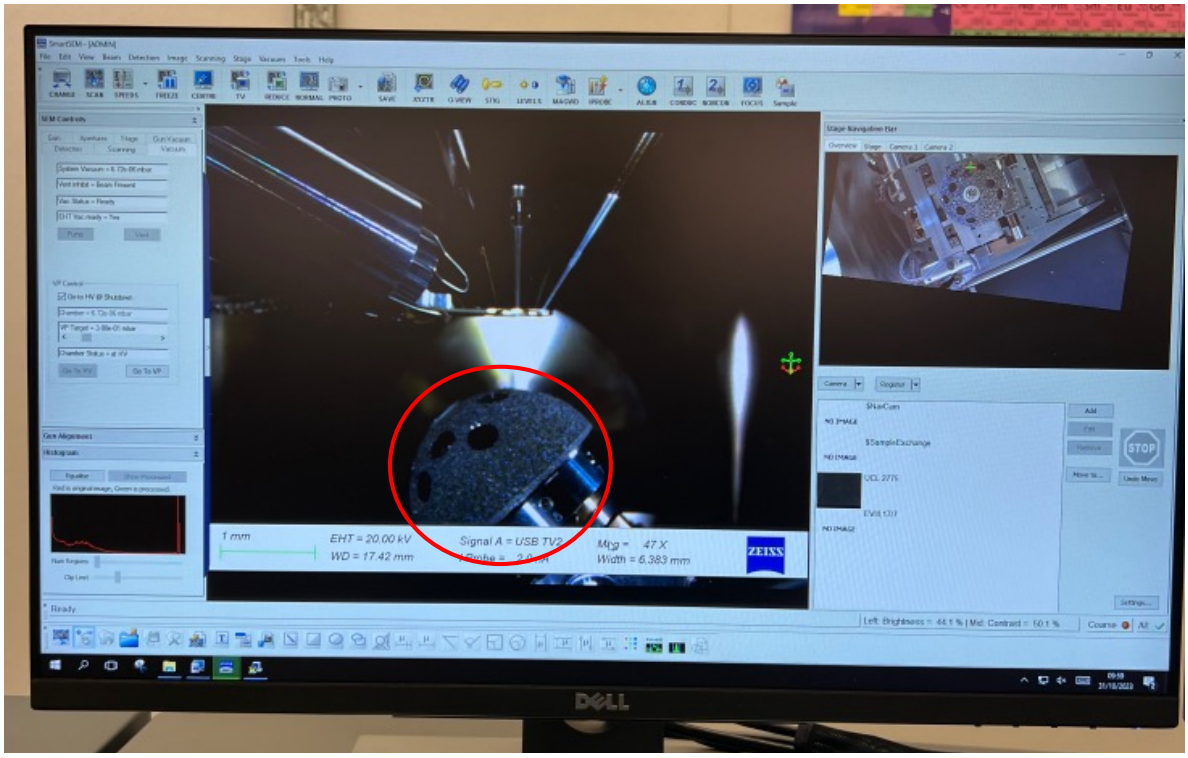

Figure 4.04: This is an image of the sample mounted inside SEM machine, via a camera to view inside the chamber. The cup is circled and mounted on a rotating and movable plate for sufficient observation and imaging.

and could be viewed via internal cameras and instantaneous electron imaging for convenient and versatile scanning of the porous lattice.

Backscattered electron imaging (BSE) was also chosen instead of the more conventional secondary electron imaging (SE) as the struts and surface adhered particles could be observed more clearly with this mode of imaging.

4 strut regions across the backside of these acetabular cups were identified for imaging (Figure 4.05):

1. At the introducer screwhole
2. Around a screwhole within the bulk porous region
3. The bulk porous region
4. At the rim of the acetabular cup.

These regions were selected for a sufficient representation of the porous backside of the cups. The regions selected were also based upon landmarks within the porous region (screwholes etc), for ease of imaging when the implant was with the Scanning Electron Microscope, and also for consistency when imaging across implants from different manufacturers and for sufficient comparisons across the designs.
These regions are illustrated in Figure 4.05 [125]. At each cup location, the first image was captured with the initial surface level in focus, followed by the subsurface level. This was achieved by adjusting the depth-of-field view to alter the focus on struts visible by line of sight below the outermost surface layer. Both the surface and subsurface were imaged for the identification and quantification of particles so the comparison could be made if there was a difference in the presence of particles at these two levels and bring into question different manufacturers' approaches to

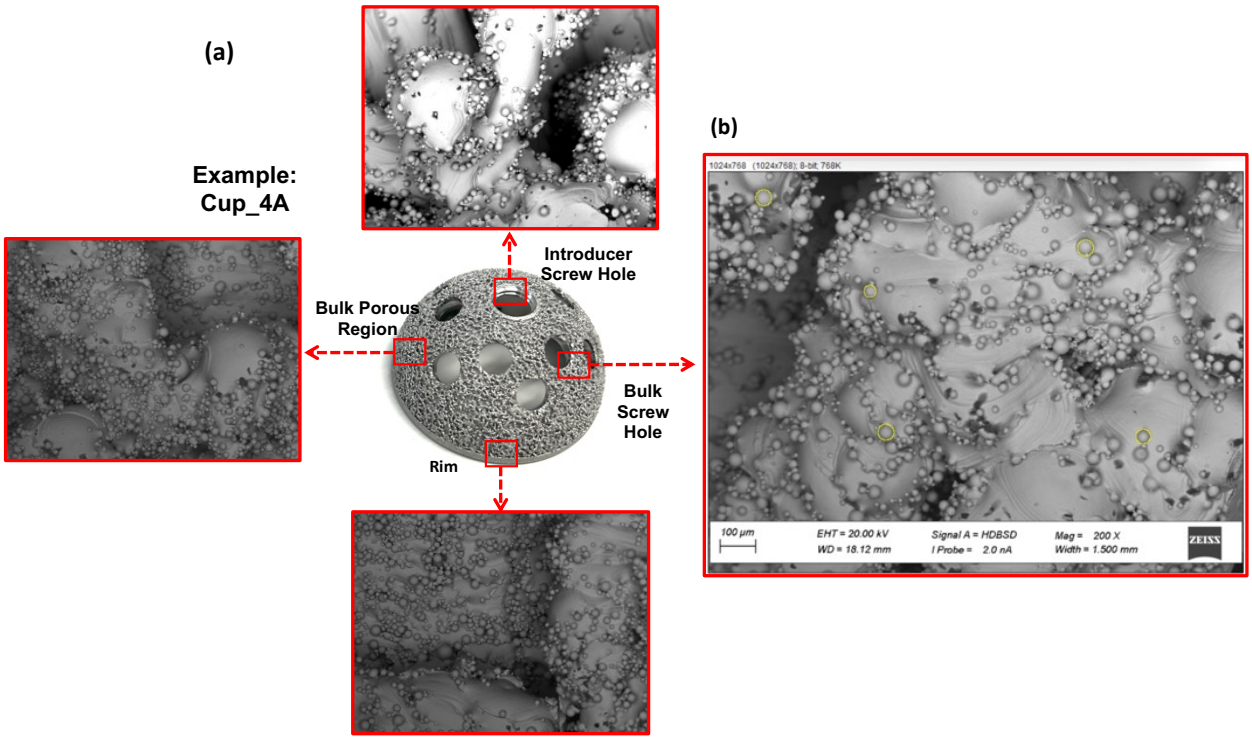

Figure 4.05: (a) The locations at which SEM images were taken using Cup_4A as an example; (b) How ImageJ was used to identify surface adhered particles and measure their area, from which the particle diameter was determined [125].

printing of the implants and post-processing. The images were captured at 200x magnification, with 8 images taken in total per implant.

200x magnification was chosen after comparing different levels of magnification to observe these particles (Figure 4.05 (b)). Lower magnifications (50-150x) allowed for broader observation of the porous structure design of the implant, but the field of view was too large for precise identification of particles, particularly with implants with smaller and numerous particles present. Higher magnifications (>250x) had a small field of view which would not be representative of the particular region being imaged.

4.4.3 | Identification of Surface Adhered Particles

In this study both a manual and a partially automated method were explored for the identification of the surface adhered particles within the porous structures of the implants, as described below. The SEM images were imported into the respective

softwares and following identification of the particles on the scans of each region of interest, two outcome measures were evaluated.

1. The diameter of each particle
2. The number of particles per mm^2.

4.4.4 ImageJ Manual Methodology

The SEM images at 200x magnification were imported into the image analysis software, ImageJ, which was used to manually identify, count and measure the particles characterised in this study. ImageJ is an openly available software that was suitable in this case for characterisation of the features of the porous region, including the determination of the dimensions of the pores and struts of the lattice structure on the porous backsides of these acetabular cups, as well as the identification of surface adhered particles. The steps taken for manual identification of the particles in ImageJ can be found in Appendix II.

This was a purely manual method, and it is likely that it could be susceptible to human error such as repeating or missing counting of particles. This error could be manageable when fewer and / or larger particles are measured but when there are significantly more particles present in the image which are also smaller in size, the potential for error becomes much more significant. These are some of the potential challenges associated with a manual method and could provide some argument for the development and application of an automated or partially automated methodology. Additionally, counting manually is very time consuming, and a computerised technique could increase the speed of identification and quantification.

4.4.5 Python Computerised Methodology

In order to improve the speed and reduce the human error associated with manually identifying and counting the particles present on the struts of the porous structures, a partially automated method was tested and developed. This was facilitated by Python code using Spyder. Spyder is an open-source cross-platform and an integrated development environment for scientific programming and facilitates Python, which is a widely used coding language. It should be noted that this study is the first, when benchmarking with literature surrounding the interrogation of 3D printed implants, to consult the use of a computerised and partially automated method to identify and evaluate surface adhered particles within the porous layer of 3D printed implants. Similar Python scripts have been experimented in more biological settings [148,149], but this is the first in the context of metal particles on 3D printed structures for medical applications.

Through using online tutorials and sample pieces of code, an initial code can be constructed based on the types of functions we wanted to complete, and mesh together sets of code openly available to achieve this (See Appendix II, Figure 4.G). Then the code was adapted by experimenting with different clauses and actions to carry out functions as below. An explanation of the Python script and respective functions, and a detailed methodology describing the use of this code in the identification and measurement of the particles in this study can be found in Appendix II.

When a non-existent particle was identified by the code, this is termed a false positive. This can occur when the parameters of the code are such that they are very sensitive and then begin to pick up undulations or ‘edges’ in the colour of the image and mistakenly identify a particle. This is prevented and minimised to an extent by trialling the code several times with different strengths and combinations of

parameters (Appendix II). However, it is not possible to ensure all false positives are avoided, and the same is true for the opposite case of ensuring all of the particles are identified. Therefore, the remaining particles are identified and counted manually in ImageJ.

This partially automated process was validated by comparing these measurements with those determined by the manual method using ImageJ.

4.4.6 Validation of Computerised Method

Validation of the computerised method was established by carrying out several steps (Figure 4.06 and in Appendix II) and comparing results with the manual method. The respective agreement/disagreement in these data sets were assessed by finding the

A

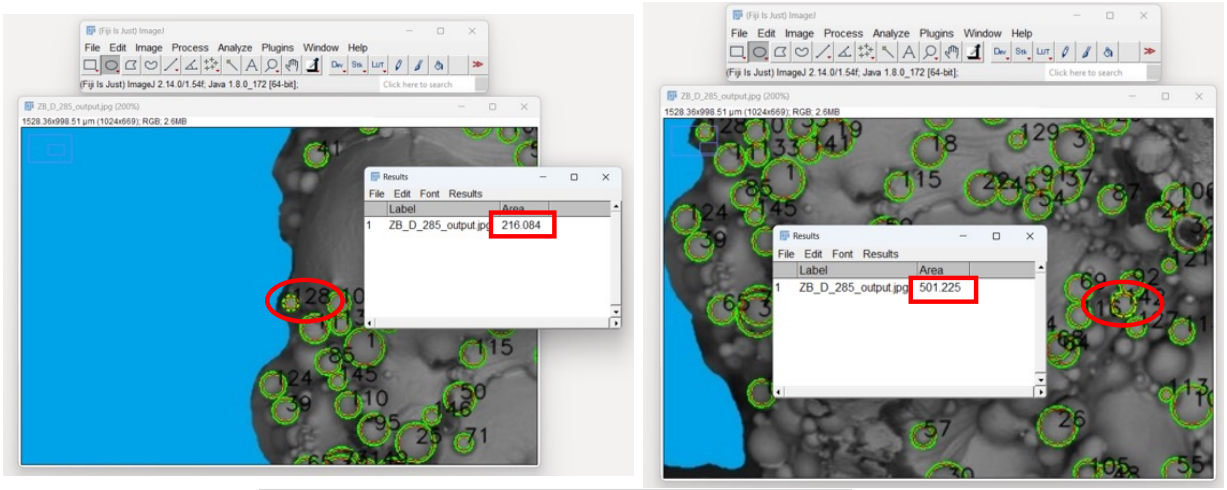

B

ImageJ				Code
Particle No.	Area	Radius	Diameter	Diameter
4	652.707	14.41399	28.82798	28.65672
14	1481.399	21.71506	43.43013	42.98507
21	997.995	17.82335	35.64669	36.1194
36	1285.364	20.22731	40.45462	39.40298
52	777.456	15.73124	31.46248	31.64179
77	652.707	14.41399	28.82798	28.65672
90	501.225	12.63111	25.26221	25.07463
94	855.424	16.50121	33.00242	32.83582
128	216.084	8.293472	16.58694	16.41791
142	501.225	12.63111	25.26221	25.07463

Figure 4.06: A) Examples using the circle tool in ImageJ to measure the specific particles. B) The areas measured for the 10 chosen particles were converted into diameters and compared with the measurements found by the code to check for concurrent values. Examples in (A) are indicated. These steps were applied to all cups counted and measured using the computerised method.

Intra-class Correlation Coefficient (ICC) between the tested particles (Figure 4.06) using the statistical software package, IBM SPSS Statistics 29 (IBM).

4.4.7 | Statistical Analysis

Following identification of the particles utilising the methods outlined above, we were able to evaluate the two outcome measures:

1. The diameter of each particle
2. The number of particles per mm^2.

These parameters were then used to compare between the different designs, manufacturers and 3D-printing methods, and also investigated the differences in the presence of particles at the surface and sub-surface level within the porous structure of each cup. All statistical analysis was completed using Prism 9 (GraphPad Software, Boston, USA).

4.4.8 | Reproducibility Studies

An intra-observer and inter-observer study was performed to interrogate the reliability and repeatability of the identification and quantification of the particles. This was carried out on a sub-set of the images analysed in this study (x2 images for 2 regions for each implant), involving the original examiner repeating the original measurements and a second independent observer quantifying the particles.

The repeatability of particle diameter was also evaluated by using a sub-set of images with a numbered sequence of particles on each image, identified independently by two examiners.

The respective agreement/disagreement in these data sets were assessed by finding the Intra-class Correlation Coefficient (ICC) in SPSS.

4.4.9 | Comparison with Data from Custom 3D Printed Implants

The porous structures of the custom 3D printed implants that were also investigated in the previous chapter have also previously been analysed and any surface adhered particles present have been characterised. This data will be compared with the results collected in this study for an additional comparison between different types of porous structures and inclusion between more manufacturers.

4.5 | Results

4.5.1 | Validation Tests

The method for validating the measurement of the diameter of the identified particles is outlined in Appendix II, and this was carried out on several images to test the was agreement between the values generated computationally through the code and manually in ImageJ. Examples of the values produced by both methods for visual comparison can be observed in Figure 4.06.

ICC analysis was conducted on the values obtained by manually measuring particle diameter in ImageJ in comparison with the values obtained via the partially automated method in Python. The values measured exhibited excellent agreement (>0.9) between these two measurement techniques, which supports the validation of the computational method to measure particle diameter.

4.5.2 | Reproducibility Studies

ICC analysis was conducted for the intra-observer study and the inter-observer study on particles per mm^2, using measurements taken by two different observers for the surface and subsurface of each implant. The values calculated indicated excellent agreement (>0.9) for both studies.

The ICC values were also calculated to evaluate the method used to determine particle diameter, through an intra and inter observer study. The analysis also exhibited excellent agreement (>0.9).

4.5.3 | Number of Particles per mm^2

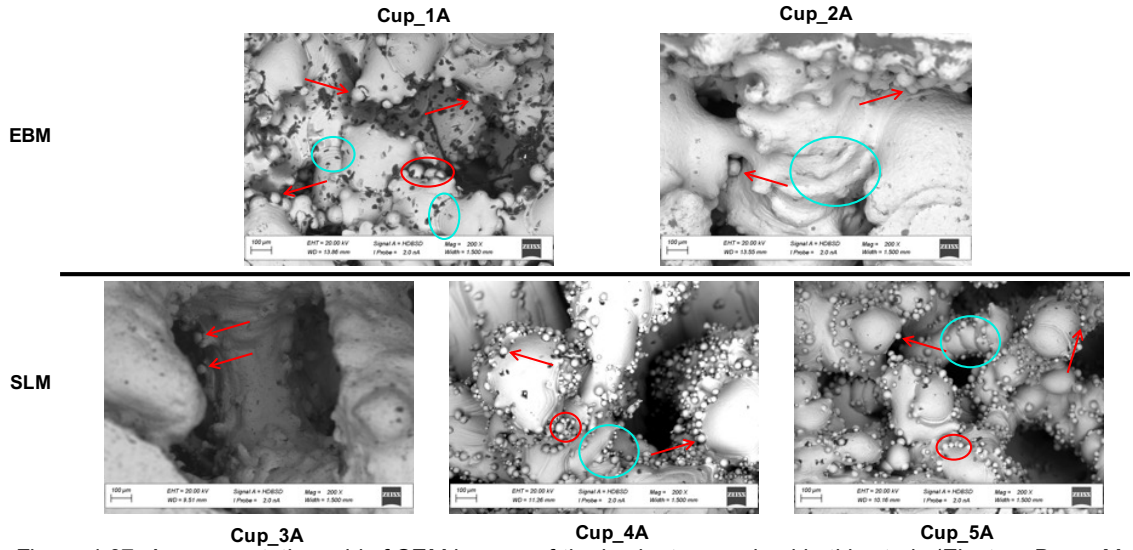

Figure 4.07: A representative grid of SEM images of the implants examined in this study (Electron Beam Melting (EBM) vs Selective Laser Melting (SLM)). Surface adhered particles (SAP) are indicated by arrows. All images are at 200x magnification and were taken at the Introducer Screw hole location. Blue circles highlight an additional observation of undulations in the struts potentially indicating layer thickness.

Surface adhered particles were found within the porous structures of all the cups examined in this study (Figures 4.07 – 4.10). There was a large variability between the designs from different manufacturers in the size and number of particles per mm^2

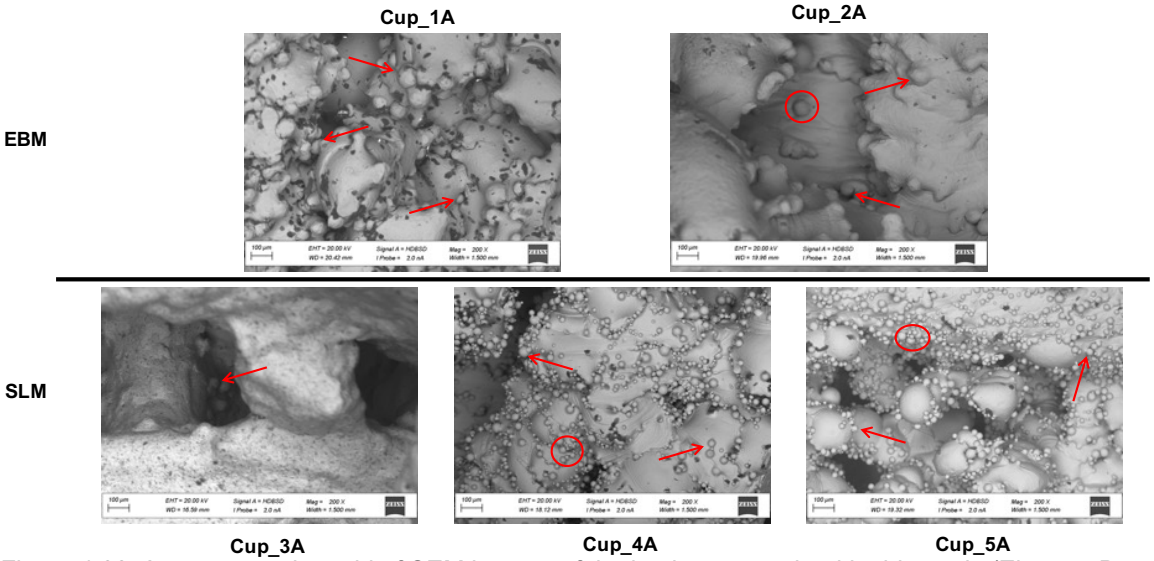

Figure 4.08: A representative grid of SEM images of the implants examined in this study (Electron Beam Melting (EBM) vs Selective Laser Melting (SLM)). Surface adhered particles (SAP) are indicated by arrows. All images are at 200x magnification and were taken at the Bulk Screw hole location.

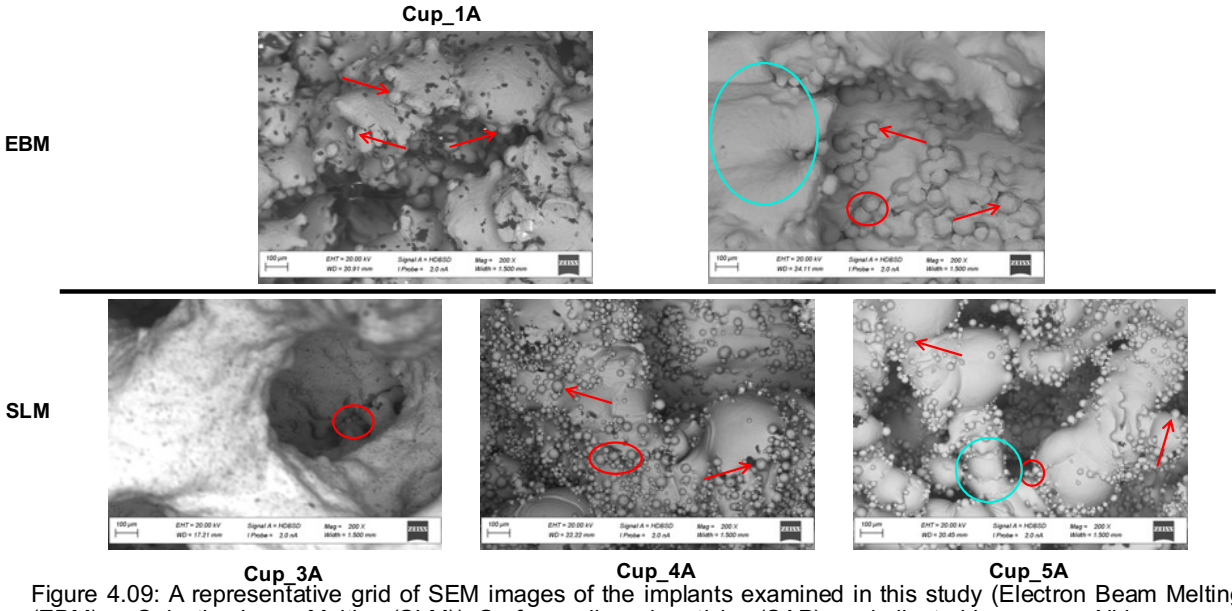

Figure 4.09: A representative grid of SEM images of the implants examined in this study (Electron Beam Melting (EBM) vs Selective Laser Melting (SLM)). Surface adhered particles (SAP) are indicated by arrows. All images are at 200x magnification and were taken at the Bulk Porosity location. Blue circles highlight an additional observation of undulations in the struts potentially indicating layer thickness.

($p<0.01$), and also in the extent of the adherence of the particles to the struts of the porous lattice. The median (range) particles per mm^2 for both the surface and sub-surface level of the struts of the porous structure were 53.7 (7.61-761) particles per mm^2 and 105 (21.3-717) particles per mm^2 respectively.

The median (range) of the number of particles per mm^2 on all the implants in the study was 89.1 (7.61-761) particles per mm^2. Additionally, a Kruskal-Wallis test showed there to be a significant variability between the five manufacturers at the surface and sub-surface level ($p<0.01$), and this is demonstrated visually in Figure 4.11.

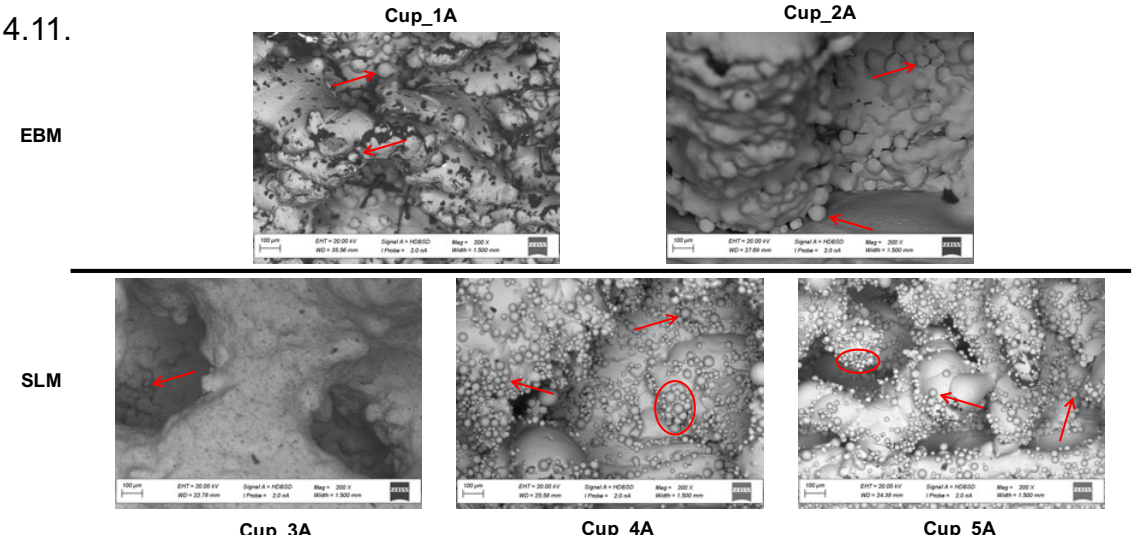

Figure 4.10: A representative grid of SEM images of the implants examined in this study (Electron Beam Melting (EBM) vs Selective Laser Melting (SLM)). Surface adhered particles (SAP) are indicated by arrows. All images are at 200x magnification and were taken at the Rim location.

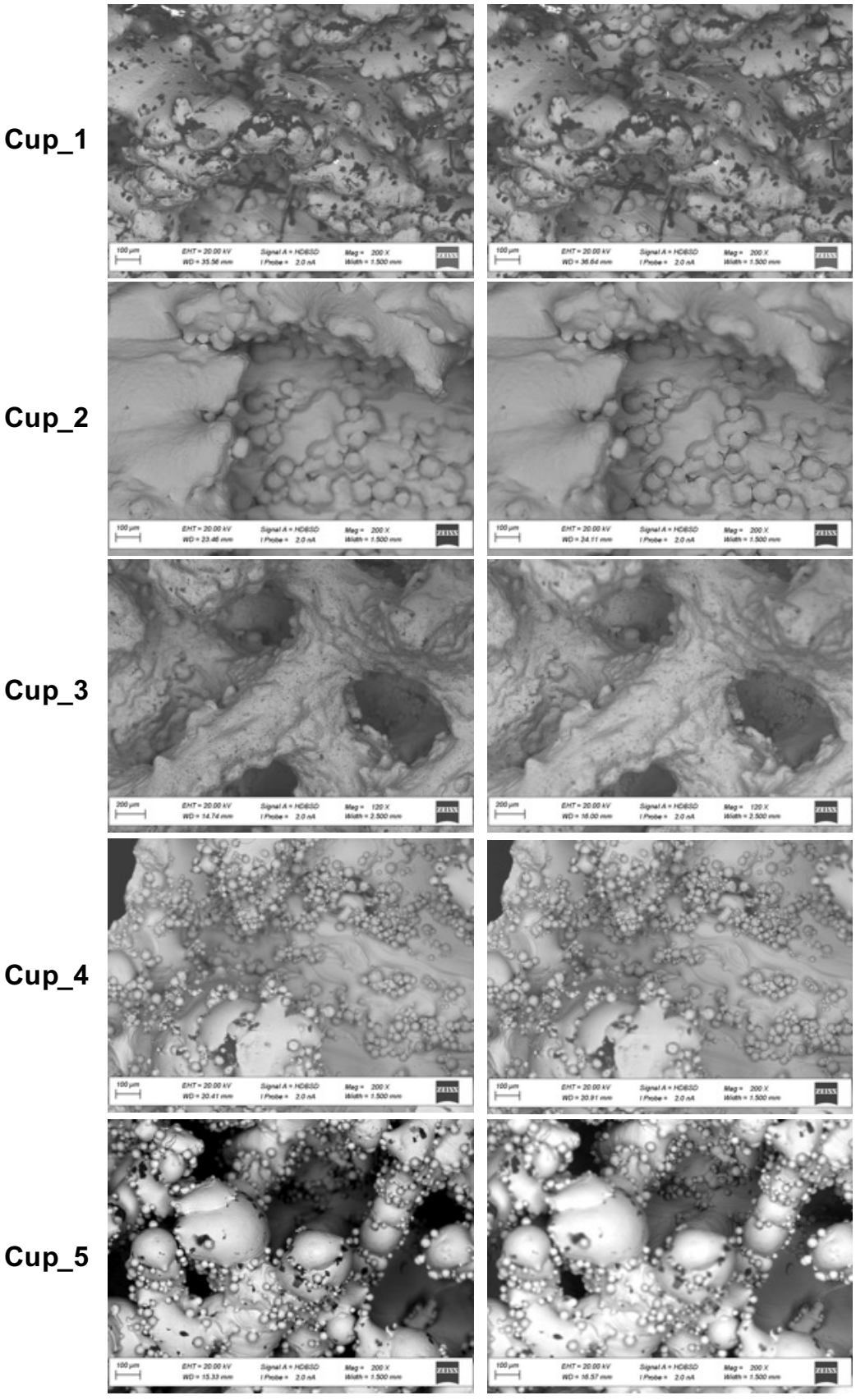

Figure 4.11: A panel of SEM Images demonstrating the change of focus to highlight the particles present at the surface and subsurface for the different cups. All images taken at 200x magnification.

The boxplot in Figure 4.12 shows the variability in number of particles per mm^2 at the surface level for each cup design. A Kruskal-Wallis test demonstrated there to be a difference in the number of particles per mm^2 on the surface of each cup (p=0.0001), and a post-hoc Dunn's multiple comparisons test indicated statistically significant differences between Cup_3A and Cup_4A (p=0.0362), Cup_3A and Cup_5A (p=0.0223), Cup_3A and Cup_5B (p=0.0036), and Cup_3B and Cup_5B (p=0.0174). There was also a difference in the number of particles per mm^2 at the sub-surface level of the porous structures (p=0.0004). Post-hoc Dunn's multiple comparisons analysis only found a significant difference between Cup_3A and Cup_5B (p=0.0252).

Table 4.01 demonstrates the difference in the presence of surface adhered particles at the surface and sub-surface level of the porous structure. Some variability in the

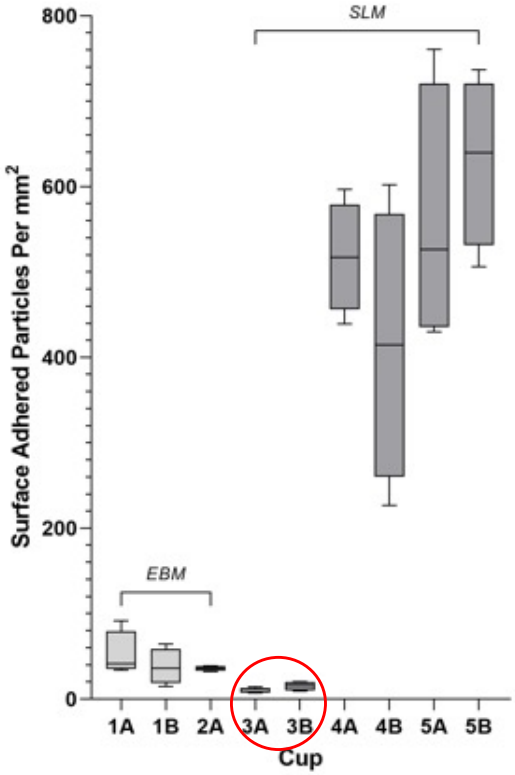

Figure 4.12: A box plot showing the difference in Particles per mm^2 at the surface level between cups manufactured by Electron Beam Melting (EBM) vs Selective Laser (SLM). A Kruskal-Wallis test showed there to be a difference in the number of particles per mm^2 on the surface of each cup (p=0.0001). [125] Cup 3A and 3B are highlighted as they exhibit differing results to the remainder of the SLM cups.

presence of the particles at different regions on the same cup can also be observed in the SEM images (Figures 4.07 – 4.10).

Table 4.01: The Median(Range) for Particles per mm^2 and Diameter at the surface and subsurface levels, and corresponding p-values. Statistically significant p-values are indicated by an asterisk. Cups manufactured by EBM and SLM are also highlighted, as well as the results of Cup 3A and 3B in particular.

			Particles Per mm^2		Diameter (µm)	
	Implant	**Location**	**Median(Range)**	**p-value**	**Median(Range)**	**p-value**
EBM	**Cup_1A**	*Surface*	42(34-92)	0.4857	50.9(25.3-98.7)	0.4841
		Subsurface	54(38-95)		49.4(16.9-86.6)	
	Cup_1B	*Surface*	36(15-64)	0.4857	53.8(23.0-96.9)	0.6831
		Subsurface	59(26-115)		53.8(24.3-92.6)	
	Cup_2A	*Surface*	36(32-39)	0.3429	56.5(37.2-115)	0.4870
		Subsurface	55(21-61)		59.9(35.6-114)	
SLM	**Cup_3A**	*Surface*	9(8-15)	*0.0286**	34.5(25.3-68.7)	*<0.0001**
		Subsurface	45(38-57)		29.9(14.0-59.9)	
	Cup_3B	*Surface*	16(9-20)	*0.0286**	45.1(25.0-64.3)	*<0.0001**
		Subsurface	86(49-123)		27.0(7.72-53.2)	
	Cup_4A	*Surface*	517(439-597)	0.8857	25.1(6.52-43.0)	*0.0010**
		Subsurface	573(310-579)		28.6(7.16-45.1)	
	Cup_4B	*Surface*	415(227-602)	>0.9999	26.3(7.16-49.4)	*0.0016**
		Subsurface	424(129-688)		25.3(5.83-71.5)	
	Cup_5A	*Surface*	526(4310-761)	0.8857	25.1(7.16-45.9)	*<0.0001**
		Subsurface	511(371-631)		22.1(7.72-52.1)	
	Cup_5B	*Surface*	640(506-737)	0.8857	22.1(5.05-41.8)	*<0.0001**
		Subsurface	662(515-717)		21.0(5.05-43.4)	

Individual Mann-Whitney comparisons of the number of particles per mm^2 in Table 4.01 demonstrates the difference in the presence of surface adhered particles at the surface and subsurface level of the porous structure, revealing significant differences; Cup_3A (p=0.0286) and Cup_3B (p=0.0286). The remaining cups did not have such statistical significance (Table 4.01). Additionally, notably in Figure 4.12, Cups 3A and 3B exhibited the least particles per mm^2 of all cups examined in this study, which in some part could be due to the type or level of post processing applied to the porous regions of these cups.

4.5.4 | SLM vs EBM

The SLM cups were found to have approximately twelve times the number of surface adhered particles than EBM at the surface level, with medians of 446 and 38.1 particles per mm^2, respectively, and a Mann-Whitney comparison shows that these values are statistically different. At the subsurface level approximately an eight-fold difference in these values were found; the median number of particles per mm^2 were 424 and 55.5 particles per mm^2 for SLM and EBM, respectively. This is shown in a boxplot in Figure 4.12, where there is a clear distinction in the number of surface adhered particles per mm^2 between cups manufactured by EBM and SLM. This is also illustrated in Figures 4.07 – 4.10 and 4.13, where the difference in presence of particles between the manufacture methods can be compared visually.

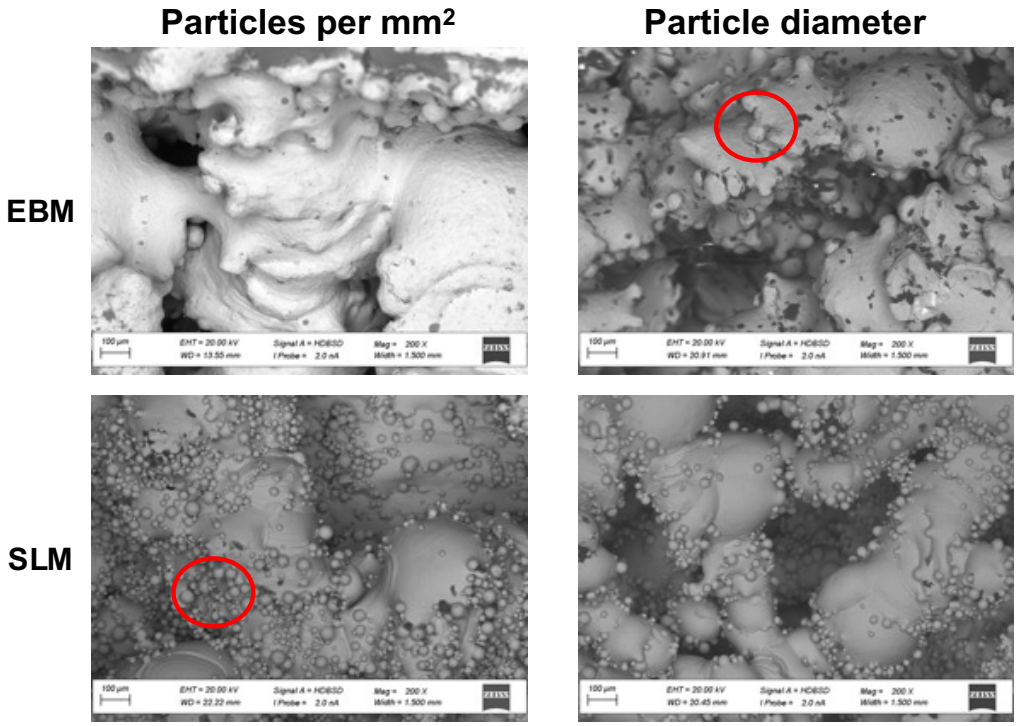

Figure 4.13: A panel of cups manufactured by EBM and SLM, showing stark differences between the particles per mm^2 and particle diameter between the manufacture methods. The contrast in level of adhesion of the particles is also highlighted in the red circles. All images are taken at 200x magnification.

This contrast also increased further in SLM cups with an irregular bone-facing porous structure; a median at the surface level of up to 517 particles per mm^2, compared with 10.9 particles per mm^2 for a repeating cell lattice. Irregularity of the structure does not appear to have the same effect with EBM cups (41.1 particles per mm^2, compared with 36.3 particles per mm^2 for irregular and regular at the surface level, respectively). This contrast can also be observed macroscopically in Figures 4.02, where the design of cups Cup_3A and Cup_3B has a repeating cell porous lattice, and the remaining SLM cups have irregular porous structures.

4.5.5 | Particle Diameter

The EBM particles exhibited a larger diameter than SLM particles; the median (range) particle diameters were 53.8 (16.9-115) μm and 24.3 (5.05-71.5) μm, respectively. A Mann-Whitney comparison between diameters of the EBM and SLM cups shows that they are significantly different ($p<0.001$). This contrast in diameters between each cup and between manufacture methods can be observed in Figures 4.14 and 4.15, respectively, and this is illustrated visually in Figure 4.13. A Kruskal-

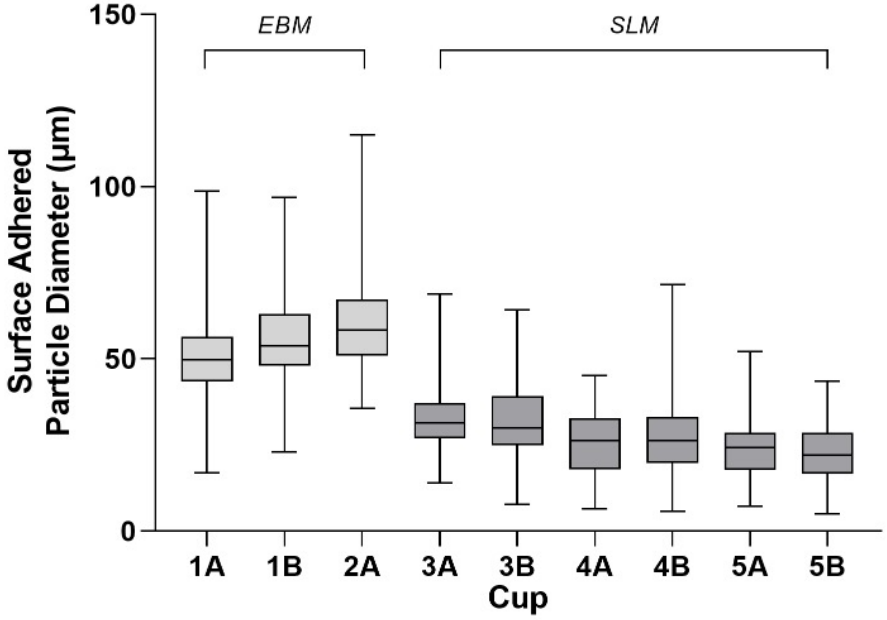

Figure 4.14: A box plot to show the significant spread of particle diameters between all the cups examined in this study. There is a clear decrease in particle diameter in the cups manufactured via Selective Laser Melting (SLM) when compared with the Electron Beam Melting (EBM) cups [125].

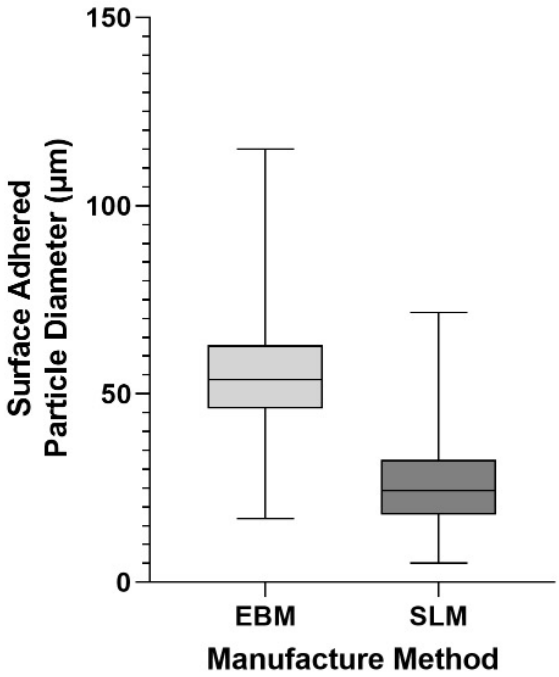

Figure 4.15: A box plot to illustrate the significant difference in particle diameter between the cups manufactured via Electron Beam Melting (EBM) vs Selective Laser (SLM) [125].

Wallis test showed there to be a difference in the diameters surface of each cup ($p<0.0001$), and a post-hoc Dunn's multiple comparisons test demonstrated significant differences between the majority of cups, except for Cup_1A and Cup_1B, Cup_1A and Cup_2A, Cup_1B and Cup_2A, Cup_3A and Cup_3B, and Cup_4A and Cup_4B, and this is reassuring as these are comparisons within the same manufacture method, manufacturer and design.

Individual Mann-Whitney comparisons were also completed on each cup individually at the surface and subsurface level of the porous structure, to examine the difference in particle diameter (Table 4.01). Cups manufactured via EBM were did not demonstrate significantly different particle diameters at the surface and subsurface level, in contrast to those manufactured by SLM, which exhibited statistically significant differences in all cups (Table 4.01).

4.5.6 | Level of Adhesion

Visually, particles observed on the SLM shells were more complete spheres, with less adhesion to the main component, in contrast to those found on the EBM shells, which were more hemispherical and fused with the strut surface to a greater extent. The differences in levels of adhesion can be observed and are indicated in Figure 4.13.

4.5.7 | Comparison with Custom Implants

The data obtained in this study was then compared with previously presented data on surface adhered particles found within the porous structures on the backsides of custom 3D printed acetabular cups.

The median (range) particles per mm^2 on 3D printed off-the-shelf cups were higher, both at the surface and subsurface; 34 (1-227) vs 53.7 (7.61-761), and 70 (1-423) vs 105 (21.3-717) particles/mm^2, respectively. Also, the median (range) diameter of the particles on the 3D-printed off-the-shelf implants (25.3 (5.05-115) μm) is comparatively similar to those found in 3D-printed custom implants (36 (10-122) μm),

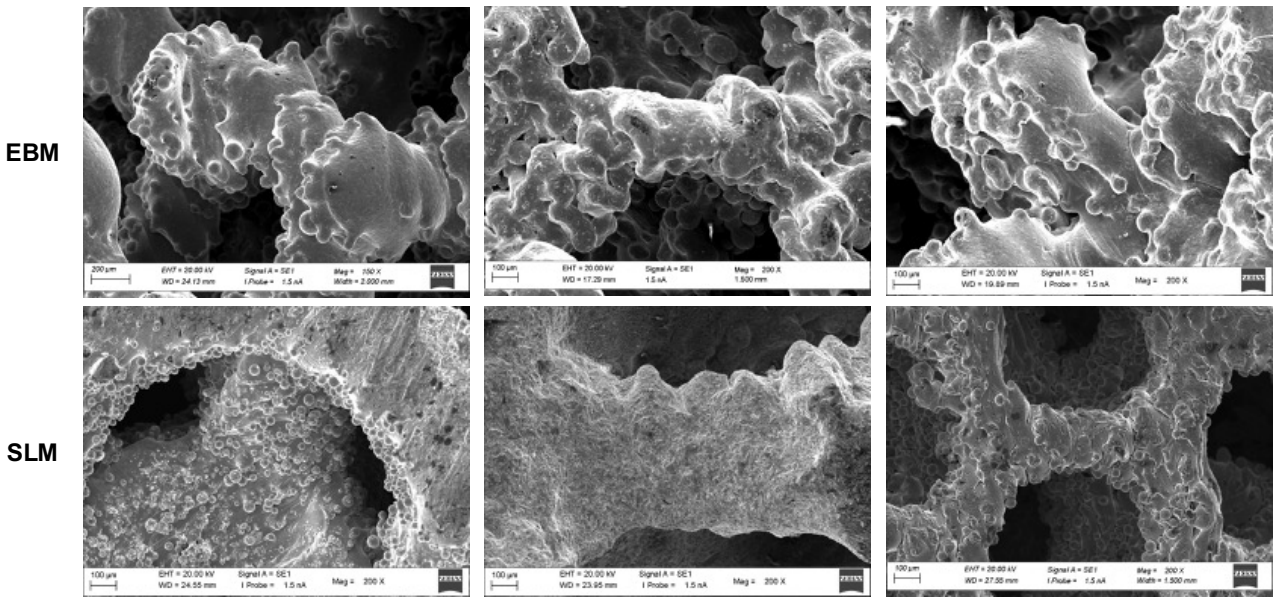

Figure 4.16: Panel of SEM Images from the porous structures of 6 3D printed custom acetabular cups manufactured by EBM and SLM from 6 different implant manufacturers. The differences in particles per mm^2, diameter and level of adhesion, as well as the variability in levels of post-processing can all be observed. All images are taken at 200x magnification using secondary electron radiation.

and this is reassuring as the implants used in this study were manufactured by SLM and EBM. Some examples of SEM images taken of the porous structure of these cups can be observed in Figure 4.16, which can be compared to the 3D printed off-the-shelf designs in Figures 4.07 – 4.10.

4.6 | Discussion

This is one of the first studies to evaluate the presence of surface adhered particles on off-the-shelf 3D printed implants. An important finding was the presence of surface adhere particles on all implants examined, irrespective of 3D printing method, implant design or manufacturer. Secondly, there was a notable variability in the number of particles per mm^2, where there were significantly more on implants manufactured via SLM versus EBM, additionally with particles of a much smaller diameter. Also, another key finding in this study is that Cup_3 exhibited the lowest particles per mm^2 of all cups examined (Figure 4.12), despite being manufactured via SLM, which highlights the impact of post-processing on the final presence of surface adhered particles in the porous structure.

The diameter of powder particles used in EBM is also significantly larger than those used in SLM, to accommodate a larger energy beam and ensure optimisation of each process for a high-quality printed component. Typically powders with approximate diameter ranges of 15-45μm and 45-106μm are used in SLM and EBM [57], respectively. This is consistent with the diameter median(range) of the powder particles identified on implants in this study. There is often a powder size distribution in the powder feedstock, including powder particles smaller than the expected range. Three manufacturers in this study publicly disclose their choice of method, and this is supported by the particle diameter measurements. This, together with optimised

parameters, results in a higher density final part [150], and could provide an explanation for the considerable range of powder particle sizes observed in this study.

Cups manufactured using SLM were found to have a significantly more surface-adhered particles than EBM, which also appears to increase further with an irregular design (Table 4.01). Additionally, visually, particles observed on the SLM shells were also more complete spheres, with less adhesion to the main component, versus particles on the EBM shells, which were more hemispherical and fused to a greater extent to the strut surface.

Upon inspection of the SEM images, two thirds of the cups exhibited structures of considerable irregularity, and there was a notable visible presence of surface adhered particles in those manufactured by SLM. This observation is supported by the data in Table 4.01. The remaining third of cups demonstrated regular porous structures made up of a repeating unit cell. Additionally, it is important to note that the 3D printing parameters including build angle and direction can impact the presence of surface adhered particles and their distribution across the struts within the porous structures, and this therefore also highlights the importance of optimising printing parameters [151]. However, this is challenging to characterise fully without obtaining samples from the implants destructively, and by visual inspection alone.

Manufacturer 3's implants exhibited the lowest surface level median particles per mm^2 of all implants analysed in this study, despite being manufactured via SLM (Table 4.01). While the specific methods are not publicly disclosed, this suggests that

post-processing in this case was responsible for the small number surface adhered particles, which we assume has been undertaken by all manufacturers. Common post-processing for particle removal includes both mechanical and chemical techniques.

In previous literature, it has been reported that the selection and combination of process parameters affect the final surface quality of the struts in the lattice. These parameters include the intensity of the laser power and the scanning speed, which have been found to impact the generation of defects including lack of fusion, as well as influencing the quality of the surface of components printed via SLM. This impact was found to be particularly important on down-facing surfaces where the higher energy input generates a larger melt pool leading to increased particle adhesion and entrapment, resulting in a poor finished surface [151].

Mechanical methods include abrasive machining and cavitation abrasive finishing for physical material removal within the complex internal channels of additively manufactured structures. The polishing media is often made up of micron-sized ceramic or metallic particles [152] which are pumped at high pressure through the porous structure. These methods are effective in the ‘line-of-sight’, but any residual abrasive remaining within the structure could negatively affect osseointegration. Chemical methods are also common for the removal of these particles and require less tooling than mechanical techniques [152]. Examples include chemical treatment or electrochemical polishing where a thin layer of material is removed to smoothen the surface, where the device acts as the anode alongside a corresponding cathode and an electrolyte of sulphuric and phosphoric acid and distilled water [153]. One of the major advantages of electrochemical over mechanical polishing is that no tool

contact is required, and this method does not face issues posed by line-of-sight and can therefore handle potentially much more complex geometries. However, these methods may lead to a reduction in thickness from the part when prolonged treatment times are applied, which could be counterproductive [152]. Therefore, there are challenges with post-processing of such structures, where most methods are only achieved in the 'line-of-sight' and poorly address the sub-surfaces, providing a potential explanation for the increased presence of these particles at the sub-surface levels.

When comparing with 3D printed custom acetabular shells [124], the is comparatively similar to those found in 3D printed custom implants, and this is reassuring as the implants used in this study were also manufactured by SLM and EBM [124].

This therefore suggests that a more complex implant design does not necessarily result in more surface adhered particles on the struts of the porous structure, and we can also assume that the custom 3D-printed implants had undergone a form of post-processing.

Another interesting observation of this manufacture method that was demonstrated in this study was the speculation of the build direction of the 3D printing process for the implants. This can be observed in Figures 4.07-4.11 and 4.13, where undulations in the struts (as indicated) can suggest the layer thickness and the change in location of the melt pool, as the part was undergoing printing. This kind of uneven surface is another known limitation of 3D printing, often referred to as the 'staircase'

or ‘stair-stepping effect’, and occurs when curved surfaces, or surfaces built in a plane almost parallel to that of the build direction, as is the case here in the struts of the porous structure [116].

There are currently no guidelines on optimal parameters for the number of surface adhered particles, the material, complexity of the part and 3D printing method to minimise the initial generation of surface adhered particles [52]. The results of this study suggests that post-processing of the porous structure of these implants has not been sufficiently optimised, leading to a substantial variation in the presence of surface adhered particles amongst implants, and from this study it is evident that there is no specific standard across this industry that guide acceptable tolerances of surface adhered particles. Therefore, there is now the need to evaluate the clinical and long-term effect of these particles such as the use of blood metal level testing, as conducted in previous studies to monitor the performance of other large titanium implants in vivo and prevent premature failure [154].

When considering the surface adhered particles found in this study it is important to note their clinical relevance in orthopaedics. This has been evidenced extensively in previous literature concerning the release of metal particles and ions from orthopaedic implants (Table 4.02). An immune response is often dictated by the size, concentration and composition of the particle, whereby smaller instead of larger and Titanium versus polyethylene (PE) would trigger a higher level of bio-reactivity [155].

From the data in Table 4.02, we can compare surface adhered particles with the characteristics of other particles important in orthopaedics. Surface adhered particles

appear to be larger than particulates caused by wear of metal-on-metal implants and PE. The critical size of a particle to incite problematic bioreactivity is still unknown, but based on in vitro data, it is suggested that a size of <10μm or between 0.24-7.2μm can promote an inflammatory reaction [155]. Therefore, it is conceivable that the particles evaluated in this study could elicit an immune response post implantation. It should also be noted that in Table 4.02, only surface adhered particles are present on implantation and could become debris upon breakage, unlike the other types which arise due to wear of the implant, post-implantation.

Additionally, if the metal particles are released on implantation or over time, it is conceivable that they could give rise to third body wear. This situation occurs when the hard particles such as ceramic or bone debris, or in this case metal particles, become trapped between the articulating bearing surfaces within the hip prosthesis, and can potentially lead to accelerated overall wear of the implant, possibly leading to early failure of the implant [147]. Particles of a similar size to those found in this study have demonstrated the potential for third-body wear in simulation studies in different types of bearing interfaces [156]. This could be particularly applicable to the

Table 4.02: Types and sizes of other clinically relevant particles in orthopaedics, e.g. wear debris from certain hip implant components and combinations. The particles observed and measured in this study are italicised [52,106,125,154–156].

Type of Debris	**Diameter (μm)**	**Shape of Debris**
Surface Adhered Particles (3D Printed Implants)	***5.05-115***	***Spherical***
Metal-on-Metal Particulate Debris	0.1-5	Spherical or agglomerates
Conventional Polyethylene (CPE) Debris	0.5-5	Rounded or elongated, >90% of the particles are granular or ellipsoidal
Highly Crosslinked Polyethylene (HXLPE) Debris	0.2-0.8	

case of using a ceramic-on-ceramic bearing with 3D-printed cups, given the history of third-body wear with this type of bearing couple.

The manufacturers of the 3D-printed acetabular cups in this study include Zimmer Biomet, BBraun, Implantcast, Stryker and Medacta.

We acknowledge the limitations of this study. While the range of manufacturers and implant designs captured in this study included commercially available implants distributed by 5 of the largest manufacturers, future studies would benefit from analysing more implant designs, sizes and manufacturers, to evaluate the variability between prints and post-processing.

Additionally, the investigation methods in this study were limited to non-destructive testing, limiting the inspection and measurements to only what was visible via microscopy. This technique is also prone to interference by surface contamination and obstructions by the foreground struts. Destructive testing and observation would improve in analysis of these particles and may overcome some of the challenges of 'line-of-sight'. However, an automated or computational method to characterise the presence of these particles in these porous structures three-dimensionally could be most beneficial, preventing interference by contamination and obstruction of the foreground struts for a more accurate measurement of particle density, and avoiding any discrepancy in particle diameter measurements with distance from the detector (when using SEM).

Despite these issues, this study still offers an initial insight into the presence of surface adhered particles on 3D-printed implants.

4.7 | Conclusion

In this study, evidence of surface adhered particles was found across the surfaces of all final-production 3D printed acetabular shells examined, which are the most commonly used 3D-printed implant shells and distributed by 5 of the largest manufacturers. SLM shells had a significantly greater number of particles present in the porous structures, that also were smaller in diameter compared to EBM shells. There is the potential for concern surrounding the particles left by the SLM process as these appear visually less consolidated to the strut surface than those found in the EBM cups.

The clinical impact of these particles in relation to their potential breakage in-vivo include third body wear and adverse body response, which should be further monitored at pre-clinical testing and through post-market surveillance. Blood metal ion testing could provide a potential metric for the performance of these implants in-vivo.

5 | Clinical Relevance

It is important to consider the broader significance of the results in this report in terms of different time periods. In the short and midterm, the studies completed in this thesis begin to build an important bank of knowledge of the features of the porous structures of 3D printed orthopaedic implants from a primarily engineering perspective and then moving on to the long-term clinical impacts and any potential implications.

It is important to consider the clinical relevance of the results found in this report, as the use of 3D printed implants for hip arthroplasty continues to rise and become more accepted in orthopaedics. One of the most common reasons for revision and re-revision hip arthroplasty with conventionally manufactured implants is aseptic loosening [13]. A key benefit of 3D printed implants is the potential to reduce the prevalence of loosening by providing enhanced fixation with the host bone stick, due to the porous structure designed to mimic that of bone and the higher coefficient of friction with this porous layer versus conventionally produced designs [82]. Recent literature and registry data has reported positive clinical outcomes of 3D printed acetabular implants for data regarding short and mid-term in vivo, comparable to conventionally manufactured porous acetabular implants. However, long-term performance and monitoring data are yet to be collected and reported.

Micro-CT was used to characterise the porous structures of 12 custom 3D printed acetabular cups from 6 different manufacturers. Synopsys Simpleware was then utilised to analyse the raw data and take dimensional measurements of the struts that make up this porous structure. The results of this study indicate that all manufacturers have a different approach to the design and construction of the porous structures, with some exhibiting regular lattices with consistent pore sizes,

and others with irregular architectures with inconsistent pore sizes and strut lengths. The method of manufacture also varied with some produced by SLM and other by EBM. At the moment, we know that the different manufacturers and their porous structures have the same key aim of enhancing bone ingrowth and the current clinical evidence suggests that those which are currently commercially available are achieving with some level of success and there are no obvious cases or reports of a particular design becoming loose in patients. The data from this study will help guide understanding of how these structures are different, and as long-term data is generated for these designs, it will help indicate which types of designs and manufacture method, if any, perform are better poorer in terms of bony fixation. Currently, it is apparent that all manufacturers have their own set approach and standard designs for the porous structure on the backside of 3D printed acetabular cups. Going forward, there is the consideration if there is any value in customising the porosity of the porous layer to match the bone quality and stock for the specific patient, especially in the case of a custom implant for a massive acetabular defect where there is often already reduced and low-quality bone stock. This would entail much longer design and development stages and production times for manufacturers as well as increasing costs for these already expensive custom devices. However, this argument also raises the question if this layer was any kind of porous holey structure with no particular design, if bone will just effectively integrate into the structure over time.

While it is evident that the optimal design of the porous structure in terms of pore size, porosity, strut length and thickness, has not yet been determined, the optimal depth of the porous layer is also unknown. In both cases, there is the concern of additively manufactured structures being more susceptible to the risk of infection in

vivo in the vacant spaces within the structure where bone is yet to grow or will not grow at all. It is possible that this could occur as there is such a wide variation in the designs of structures that are commercially available, all with different dimensional features and porosity levels. Therefore, it is possible that some designs could inadvertently become a breeding ground for bacteria or cells which can lead to infection, and some custom devices have exhibited higher infection rates [157]. However, a recent study has addressed this potential risk through biofunctionalization of the surfaces using silver particles [158].

The porous structures were interrogated further using SEM and ImageJ and a partially automated method to identify, quantify and measure the presence of surface adhered particles within the porous layer of nine 3D printed off-the-shelf acetabular cups from five different manufacturers. The results of this study demonstrated that a form of surface adhered particles was present in the porous structures of all the cups that were analysed, regardless of lattice design, level of regularity or choice of 3D printing method.

When considering the potential clinical impact of the particles there are several aspects to consider. It is possible that their presence could have a positive initial impact by increasing the roughness and coefficient of friction of the porous structure providing a better initial fixation with the surrounding bone. However, there are also many potential clinical risks associated with these particles including the possibility that some particles could break off from the backside in the cups and could result in the mechanical issue of third body wear between the bearing surfaces (between the femoral head and acetabular liner), leading to the generation of more debris at this interface and several other problems later in the life of the implant. A recent study

has also investigated the orientation of printing these structures to reduce the generation of surface adhered particles which occur more significantly with higher angled surfaces. This was done by looking to improve the roughness of the surfaces (reduce surface adhered particle generation) for enhanced biological response and fixation and reduce the possibility of infection [157].

Another potential risk of these particles are the increased blood metal ion levels, if they break off and are able to circulate round body in the blood, including the ions present in the constituent alloy (Ti-6Al-4V). When looking at Table 4.02 and considering previous clinically relevant particles and particulates in orthopaedics, it is apparent that these particles are larger than metal ions and will be too large to circulate within the blood stream but could cause third body wear, and their increased surface area could elevate the blood metal ion levels in vivo.

Blood metal ion levels have been used in previous studies to monitor the performance of orthopaedic implants and can be used to indicate a failing implant to complement the corresponding medical imaging. Post-implantation, wear and corrosion often generate metal particles and ions which are released into the surrounding tissue and bloodstream and may cause a range of adverse local and systemic effects in patients, such as inflammation and pain, and cytotoxicity [145]. A recent study investigated the potential of using blood titanium ion levels as a biomarker for function for large and sliding titanium implants, including spine rods, 3D custom acetabular cups for massive acetabular defects and tumour implants. This data was the compared with standard conventionally manufactured primary titanium hip implants, and the spine rods and massive 3D printed acetabular cups exhibited higher levels of blood titanium ions compared to the standard hips [159].

Reassuringly, this study found that there appeared to be no adverse effects as a result of these elevated blood titanium levels [159].

In any case, we need to understand how much patients are exposed to with increasing blood metal ion levels, and best way to approach the evaluation of blood metal ion levels within patients would be to conduct a prospective longitudinal study.

6 | Future Work

While both studies would benefit from a larger range of implants and sample sizes of each implant, the aspects of the porous layer of 3D printed acetabular cups explored in both research chapters establish a clear foundation for several future studies to continue the investigation of complex medical devices.

Chapter 3

Building on the parameters characterised in the porous layer in this study, other metrics such as pore size, and circularity of the struts, as well as a range of undetermined the features of retrieved implants that have also undergone Micro-CT scanning. Also, further investigating how Simpleware evaluates these parameters, such as the reliability of modelling the circularity of the cross-section of struts and determining node-to-node distance corresponding to the length of the struts in the centreline network. This could be completed using an object with a similar level of complexity and known dimensions that make up the structure (e.g. a phantom), to ensure and validate the reliability and reproducibility of analysis of Micro-CT scans in Simpleware.

Additionally, the Simpleware software could be implemented, as it has been previously in clinical settings, to perform Statistical Shape Modelling (SSM) on these implants, particularly those with a repeating unit cell, to investigate the repeatability when considering the transition between the design and final print of the product.

SSM could also be used to understand the extent of irregularity of the manufacturer designs that are more intentionally irregular. Also, to evaluate the mechanical integrity of the porous layer, compression or impact testing could provide invaluable insights and reassurance.

Chapter 4

Future work could also investigate the properties of retrieved 3D printed implants to evaluate the real in vivo performance of these components and their respective porous layers. This could also include the consideration of the biological impact of surface adhered particles.

Levels of blood titanium could form the basis of an investigation into monitoring the function of these implants, in comparison to the levels found for the conventionally produced counterparts, and if this can be used as a biomarker for failure. This would include samples taken using a blood test at regular intervals in the lifetime of the implant (such as 6 months or a year), as well as pre-operative and post-operative tests as control samples for comparison later in the study. For a full and exhaustive study, this should be conducted on a set of patients with 3D printed acetabular cups and also a comparative set of patients implanted with conventionally manufactured acetabular cups. This study would also evaluate and measure all of the ions present in the constituent titanium alloy of the implant. This includes titanium ions as well as both vanadium and aluminium. It is important to note that the measurements of titanium levels are not necessarily for adverse reactions or toxicity, but to be used as a monitor of the implant performance in vivo and an indication of failure. This investigation will allow the observation of how to levels of titanium levels vary in patents over time and assist in identifying anomalies and low performing implants.

Going forward, data from these studies can then inform the development of standardised protocols and facilitate improved quality control processes, which will become increasingly more important as 3D printing becomes more prevalent in orthopaedics.

Additionally, other parameters that could be considered for future work include that of the 3D printing process itself and looking at minimising its resulting surface finish errors such as surface adhered particles and ‘stair-stepping’ due to curvature. These are known limitations and are often rectified in other industries relatively simply through post-processing, which is more challenging in medical applications with complex porous structures. Therefore, the consideration of build direction relative to the part, the quality of the starting powder feedstock, the CAD of the device, programmed parameters of the 3D printer and type of 3D printing method and their impact on the final part should be evaluated to prevent these known errors and specifically in the context of medical applications.

Therefore, several knowledge gaps still remain in this industry surrounding 3D printed implants, but this report provides a reassuring and thorough introduction of this technology as the future of orthopaedics.

7 | Conclusion

The aim of this report was to present both engineers and surgeons with an improved overall understanding of the types of structures that 3D printing has enabled in orthopaedics and also an awareness for what features exist in implants that are currently being used in patients, to ensure patient and clinical safety. The porous structures of 3D printed acetabular cups of both patient-specific and off-the-shelf designs were examined, with a selection from each type of 3D printing method (selective laser melting (SLM) and electron beam melting (EBM)) and from a range of manufacturers (Stryker, Implantcast, Adler Ortho, Zimmer Biomet, Medacta, Lima Corporate, BBraun, Materialise and AK Medical).

From Chapter 3, it was highlighted that despite the significant statistical differences in dimensional measurements of the struts of the porous structures that were analysed on the 3D printed custom and off-the-shelf acetabular cups, this was less considerable between the designs for the overall level of porosity indicating that the approach of all manufacturers is to achieve a comparable value for this important feature. Consistency was also observed within the same manufacturer indicating some extent of repeatability of the structures from the respective manufacturers in their 3D printing processes. From Chapter 4, evidence of surface adhered particles was found across the surfaces of all final-production 3D printed acetabular cups examined, which are distributed by 5 of the largest manufacturers. Those manufactured by SLM exhibited smaller and a significantly greater number of particles on the surfaces of the struts within the porous structures than the EBM cups.

In order to interrogate these implants, several different analysis techniques and software’s were utilised. Micro-CT was extremely useful, alongside Synopsys

Simpleware to create a network of the structure for each cup that was analysed, and to find the dimensional features of these struts and a value for the overall porosity. Also, SEM and ImageJ, combined with the partial automation using Python was a novel and useful way to characterise the presence of particles within these porous structures. However, there were apparent limitations with these methods. Going forward, it would be effective to use higher resolution micro-CT and incorporate statistical shape modelling to assess the consistency of the lattices, in the prints and in the designs, both regular and irregular. Higher resolution micro-CT could also enable the visualisation of surface adhered particles in a complementing software, for quantification and characterisation. This would also overcome the challenge of 'line-of-sight' with SEM in this study, and analysis methods for studies of this feature in the future should look to minimise this so the complete, unobscured surfaces of the struts can be examined.

This thesis has investigated and presented brand new information on important features within the porous structures of 3D printed custom and off-the-shelf acetabular cups. It has found new results with which to educate implant manufacturers, engineers, surgeons and the wider orthopaedics community. The findings of this report will also be useful to regulatory bodies when considering revisions to existing guidelines and standards as well as during the development of new advice, in order to close the gap between the current regulation and the rapid uptake of this technology.

8 | List of current publications, conferences and awards

1 | Publications

- **Nicum A**, Di Laura A, Hothi H, Henckel J, Schlueter-Brust K, Hart A. Surface adhered titanium particles on 3D printed off-the-shelf acetabular cups. Journal of Orthopaedic Research® 2024;42:2817–25.
- **Nicum A,** Hothi H, Henckel J, Di Laura A, Schlueter-Brust K, Hart A. Characterisation of 3D-printed acetabular hip implants. EFORT Open Reviews 2024;9:862–72. https://doi.org/10.1530/eor-23-0182.
- Hothi H, Henckel J, **Nicum A**, Di Laura A, Schlueter-Brust K, Hart A. Comparative analysis of conventionally and additively manufactured acetabular shells from a single manufacturer. 3D Print Med 2024;10:1–11. https://doi.org/10.1186/S41205-024-00233-Y/FIGURES/7.

2 | Conferences

- **Nicum, A.**, Hothi, H., Di Laura, A., Davies, A., Henckel, J., Schlueter-Brust, K., Hart, A. *Loose Titanium Particles On 3D-Printed Acetabular Shells*. Paper presented as a podium talk at the **European Federation of National Associations of Orthopaedic and Traumatology (EFORT)**, Hamburg 2024
- **Nicum, A.**, Hothi, H., Di Laura, A., Schlueter-Brust, K. Henckel, J., Hart, A. *The Impact of SLM and EBM 3D-Printers on Surface Adhered Titanium Particles on Acetabular Implants*. Paper presented as a podium talk at the **International Society for Technology in Arthroplasty (ISTA)**, Nashville 2024

- **Nicum, A.**, Hothi, H., Di Laura, A., Schlueter-Brust, K. Henckel, J., Hart, A. Variability of the Porous Structure in 3D-Printed Acetabular Implants. Paper presented as a poster at the **International Society for Technology in Arthroplasty (ISTA)**, Nashville 2024
- **Nicum, A.,** Hothi, H., Di Laura, A., Henckel, J., Schlueter-Brust, K., Hart, A. *The Effect of 3D-Printing Type on the Surface Characteristics of 3D-Printed Acetabular Shells.* Paper presented as a poster at **BioMedEng24**, London 2024

3 | Awards

- UCL *'Robert Brown Travel Award'*, May 2024

9 | Bibliography

[1] Evans JT, Evans JP, Walker RW, Blom AW, Whitehouse MR, Sayers A. How long does a hip replacement last? A systematic review and meta-analysis of case series and national registry reports with more than 15 years of follow-up. Lancet 2019;393:647–54. https://doi.org/10.1016/S0140-6736(18)31665-9.

[2] Affatato S. “The history of total hip arthroplasty (THA).” Perspectives in Total Hip Arthroplasty. First Edition, Waltham, MA, US: Woodhead Publishing (Elsevier); 2014, p. 3–18.

[3] Thompson JC. “Chapter 8 - Thigh/Hip.” O’Grady, E. and Thiel, M. (Eds.), Netter’s Concise Orthopaedic Anatomy. Second Edition, Philadelphia, PA, US: Saunders Elsevier; 2010, p. 249–84.

[4] Świątkowska I, Sabah SA, Horga LM, Hart AJ. Introduction to hip implants and biomarker testing. Biomarkers of Hip Implant Function 2023:3–39. https://doi.org/10.1016/B978-0-12-821596-8.00003-3.

[5] Bergmann G, Graichen F, Rohlmann A, Bender A, Heinlein B, Duda GN, et al. Realistic loads for testing hip implants. Biomed Mater Eng 2010;20:65–75. https://doi.org/10.3233/BME-2010-0616.

[6] Cooper C, Inskip H, Croft P, Campbell L, Smith G, McLaren M, et al. Individual risk factors for hip osteoarthritis: obesity, hip injury, and physical activity. Am J Epidemiol 1998;147:516–22. https://doi.org/10.1093/OXFORDJOURNALS.AJE.A009482.

[7] Fagerson TL, Babatunde OM, Safran MR. Hip Pathologies : Diagnosis and Intervention. Pathology and Intervention in Musculoskeletal Rehabilitation. Second Edition, Maryland Heights, MO, US: Elsevier Inc.; 2016, p. 651–91.

[8] Karlson EW, Mandl LA, Aweh GN, Sangha O, Liang MH, Grodstein F. Total hip replacement due to osteoarthritis: The importance of age, obesity, and other modifiable risk factors. American Journal of Medicine 2003;114:93–8. https://doi.org/10.1016/S0002-9343(02)01447-X.

[9] Lespasio MJ, Sultan AA, Piuzzi NS, Khlopas A, Husni ME, Muschler GF, et al. Hip Osteoarthritis: A Primer. Perm J 2018;22. https://doi.org/10.7812/TPP/17-084.

[10] AJRR. Sixth American Joint Replacement Registry (AJRR) Annual Report on Hip and Knee Arthroplasty Data. 2019.

[11] AOANJRR. Australian Orthopaedic Association National Joint Replacement Registry - 20th Annual Report. 2019.

[12] Lübbeke A, Silman AJ, Barea C, Prieto-Alhambra D, Carr AJ. Mapping existing hip and knee replacement registries in Europe. Health Policy 2018;122:548–57. https://doi.org/10.1016/J.HEALTHPOL.2018.03.010.

[13] NJR. National Joint Registry for England, Wales, Northern Ireland and Isle of Man: 16th Annual Report. 2019.

[14] R.I.P.O. Regional Register of Orthopaedic Prosthetic Implantology - Overall Data Hip, Knee and Shoulder Arthroplasty in Emilia-Romagna Region (Italy). 2019.

[15] SHAR. Swedish Hip Arthroplasty Register - Annual Report. 2018.

[16] Ganz R, Leunig M, Leunig-Ganz K, Harris WH. The Etiology of Osteoarthritis of the Hip: An Integrated Mechanical Concept. Clin Orthop Relat Res 2008;466:264. https://doi.org/10.1007/S11999-007-0060-Z.

[17] Babis GC, Soucacos PN. Effectiveness of total hip arthroplasty in the management of hip osteonecrosis. Orthopedic Clinics of North America 2004;35:359–64. https://doi.org/10.1016/j.ocl.2004.02.007.
[18] Baig SA, Baig M. Osteonecrosis of the Femoral Head: Etiology, Investigations, and Management. Cureus 2018;10. https://doi.org/10.7759/CUREUS.3171.
[19] Yang S, Cui Q. Total hip arthroplasty in developmental dysplasia of the hip: Review of anatomy, techniques and outcomes. World J Orthop 2012;3:42–8. https://doi.org/10.5312/WJO.V3.I5.42.
[20] Johansson T. Internal fixation compared with total hip replacement for displaced femoral neck fractures: a minimum fifteen-year follow-up study of a previously reported randomized trial. J Bone Joint Surg Am 2014;96:e46(1). https://doi.org/10.2106/JBJS.K.00244.
[21] Ranawat A, Zelken J, Helfet D, Buly R. Total Hip Arthroplasty for Posttraumatic Arthritis after Acetabular Fracture. Journal of Arthroplasty 2009;24:759–67. https://doi.org/10.1016/j.arth.2008.04.004.
[22] Eskelinen A, Paavolainen P, Helenius I, Pulkkinen P, Remes V. Total hip arthroplasty for rheumatoid arthritis in younger patients: 2,557 replacements in the Finnish Arthroplasty Register followed for 0-24 years. Acta Orthop 2006;77:853–65. https://doi.org/10.1080/17453670610013132.
[23] Tang WM, Chiu KY. Primary total hip arthroplasty in patients with ankylosing spondylitis. J Arthroplasty 2000;15:52–8. https://doi.org/10.1016/S0883-5403(00)91155-0.
[24] Learmonth ID, Young C, Rorabeck C. The operation of the century: total hip replacement. Lancet 2007;370:1508–19. https://doi.org/10.1016/S0140-6736(07)60457-7.
[25] Abdel Jaber S, Affatato S. An overview of in vitro mechanical and structural characterization of hip prosthesis components. Biomaterials in Clinical Practice: Advances in Clinical Research and Medical Devices 2017:585–99. https://doi.org/10.1007/978-3-319-68025-5_22.
[26] Patel A, Pavlou G, Mújica-Mota RE, Toms AD. The epidemiology of revision total knee and hip arthroplasty in England and Wales: a comparative analysis with projections for the United States. A study using the National Joint Registry dataset. Bone Joint J 2015;97-B:1076–81. https://doi.org/10.1302/0301-620X.97B8.35170.
[27] Wyatt S, Bailey R, Moore P, Revell M. Equity of access to NHS-funded hip replacements in England and Wales: Trends from 2006 to 2016. The Lancet Regional Health - Europe 2022;21:100475. https://doi.org/10.1016/j.lanepe.2022.100475.
[28] Patient Profile - NHS England Digital n.d. https://digital.nhs.uk/data-and-information/publications/statistical/patient-reported-outcome-measures-proms/finalised-hip--knee-replacements-april-2018---march-2019/patient-profile (accessed April 15, 2024).
[29] Health at a Glance 2021 2021. https://doi.org/10.1787/AE3016B9-EN.
[30] Bozic KJ, Kurtz SM, Lau E, Ong K, Vail DTP, Berry DJ. The epidemiology of revision total hip arthroplasty in the United States. J Bone Joint Surg Am 2009;91:128–33. https://doi.org/10.2106/JBJS.H.00155.
[31] Hip Joint Replacement Surgery | cemented, uncemented, artificial n.d. https://www.healthpages.org/surgical-care/hip-joint-replacement-surgery/ (accessed November 28, 2024).

[32] Fuchs RK, TWR and WSJ. “Bone biology.” Bone Repair Biomaterials. Second Edition, Cambridge, MA, US: Woodhead Publishing (Elsevier); 2019, p. 15–52.
[33] Currey J. “The Structure of Bone Tissue.” Bone: Structure and Mechanics. Second Edition, Princeton University Press; 2002, p. 3–26.
[34] Keaveny TM, Morgan EF, Niebur GL, Yeh OC. Biomechanics of trabecular bone. Annu Rev Biomed Eng 2001;3:307–33. https://doi.org/10.1146/ANNUREV.BIOENG.3.1.307.
[35] Rho JY, Kuhn-Spearing L, Zioupos P. Mechanical properties and the hierarchical structure of bone. Med Eng Phys 1998;20:92–102. https://doi.org/10.1016/S1350-4533(98)00007-1.
[36] Vanhegan IS, Malik AK, Jayakumar P, Ul Islam S, Haddad FS. A financial analysis of revision hip arthroplasty: the economic burden in relation to the national tariff. J Bone Joint Surg Br 2012;94:619–23. https://doi.org/10.1302/0301-620X.94B5.27073.
[37] Sivananthan S, Goodman SB, Burke M. Failure mechanisms in joint replacement. Joint Replacement Technology 2021:373–402. https://doi.org/10.1016/B978-0-12-821082-6.00017-0.
[38] Affatato S. “Recent developments and future trends in total hip arthroplasty (THA).” Perspective in Total Hip Arthroplasty. First Edition, Waltham, MA, US: Woodhead Publishing; 2014, p. 76–95.
[39] Raphel J, Holodniy M, Goodman SB, Heilshorn SC. Multifunctional coatings to simultaneously promote osseointegration and prevent infection of orthopaedic implants. Biomaterials 2016;84:301–14. https://doi.org/10.1016/J.BIOMATERIALS.2016.01.016.
[40] Fitzgerald RH, Nolan DR, Ilstrup DM, Van Scoy RE, Washington IInd JA, Coventry MB. Deep wound sepsis following total hip arthroplasty. J Bone Joint Surg Am 1977;59:847–55. https://doi.org/10.2106/00004623-197759070-00001.
[41] Tande AJ, Patel R. Prosthetic joint infection. Clin Microbiol Rev 2014;27:302–45. https://doi.org/10.1128/CMR.00111-13/ASSET/C146EE26-F6EF-476D-9B09-0469C9A24FB8/ASSETS/GRAPHIC/ZCM9990924590004.JPEG.
[42] Ratner B, HNJ and JJJ. Orthopedic Applications. Biomaterials Science: An Introduction to Materials in Medicine. Third Edition, Waltham, MA, US: Elsevier Inc.; 2013, p. 841–82.
[43] Murr LE, Quinones SA, Gaytan SM, Lopez MI, Rodela A, Martinez EY, et al. Microstructure and mechanical behavior of Ti–6Al–4V produced by rapid-layer manufacturing, for biomedical applications. J Mech Behav Biomed Mater 2009;2:20–32. https://doi.org/10.1016/J.JMBBM.2008.05.004.
[44] McTighe T, BD and BW. “Metallic Alloys in Total Hip Arthroplasty.” The Hip: Preservation, Replacement and Revision. First Edition, Brooklandville, MD, USA: Data Trace Publishing Company; 2015, p. 1–12.
[45] Chen Q, Thouas GA. Metallic implant biomaterials. Materials Science and Engineering: R: Reports 2015;87:1–57. https://doi.org/10.1016/J.MSER.2014.10.001.
[46] Long M, Rack HJ. Titanium alloys in total joint replacement—a materials science perspective. Biomaterials 1998;19:1621–39. https://doi.org/10.1016/S0142-9612(97)00146-4.
[47] Malahias MA, Kostretzis L, Greenberg A, Nikolaou VS, Atrey A, Sculco PK. Highly Porous Titanium Acetabular Components in Primary and Revision Total

Hip Arthroplasty: A Systematic Review. J Arthroplasty 2020;35:1737–49. https://doi.org/10.1016/J.ARTH.2020.01.052.
[48] Banerjee S, Issa K, Kapadia BH, Pivec R, Khanuja HS, Mont MA. Systematic review on outcomes of acetabular revisions with highly-porous metals. Int Orthop 2014;38:689–702. https://doi.org/10.1007/S00264-013-2145-5.
[49] Zivic F, LK, WR and SJ. “Porous metals in orthopedics.” Biomaterials in Clinical Practice: Advances in Clinical Research and Medical Devices. First Edition, Cham, CH, USA: Springer International Publishing; 2017, p. 281–301.
[50] ISO/ASTM 52900:2021 - Additive manufacturing — General principles — Fundamentals and vocabulary n.d. https://www.iso.org/standard/74514.html (accessed January 17, 2024).
[51] Karkun MS, Dharmalingam S. 3D Printing Technology in Aerospace Industry – A Review. International Journal of Aviation, Aeronautics, and Aerospace 2022;9:4. https://doi.org/https://doi.org/10.15394/ijaaa.2022.1708.
[52] Gokuldoss PK, Kolla S, Eckert J. Additive Manufacturing Processes: Selective Laser Melting, Electron Beam Melting and Binder Jetting—Selection Guidelines. Materials 2017, Vol 10, Page 672 2017;10:672. https://doi.org/10.3390/MA10060672.
[53] Dall’Ava L, Hothi H, Di Laura A, Henckel J, Hart A. 3D printed acetabular cups for total hip arthroplasty: A review article. Metals (Basel) 2019;9. https://doi.org/10.3390/met9070729.
[54] Ryan G, Pandit A, Apatsidis DP. Fabrication methods of porous metals for use in orthopaedic applications. Biomaterials 2006;27:2651–70. https://doi.org/10.1016/J.BIOMATERIALS.2005.12.002.
[55] Slotwinski JA, Garboczi EJ, Stutzman PE, Ferraris CF, Watson SS, Peltz MA. Characterization of Metal Powders Used for Additive Manufacturing. J Res Natl Inst Stand Technol 2014;119:460. https://doi.org/10.6028/JRES.119.018.
[56] Herzog D, Seyda V, Wycisk E, Emmelmann C. Additive manufacturing of metals. Acta Mater 2016;117:371–92. https://doi.org/10.1016/J.ACTAMAT.2016.07.019.
[57] Dawes J, Bowerman R, Trepleton R. Introduction to the additive manufacturing powder metallurgy supply chain. Johnson Matthey Technology Review 2015;59:243–56. https://doi.org/10.1595/205651315X688686.
[58] Gibson I, Rosen D, Stucker B. Powder Bed Fusion Processes. Additive Manufacturing Technologies 2015:107–45. https://doi.org/10.1007/978-1-4939-2113-3_5.
[59] Tang HP, Qian M, Liu N, Zhang XZ, Yang GY, Wang J, et al. Effect of Powder Reuse Times on Additive Manufacturing of Ti-6Al-4V by Selective Electron Beam Melting. JOM 2015;67:555–63. https://doi.org/10.1007/S11837-015-1300-4.
[60] Trevisan F, Calignano F, Aversa A, Marchese G, Lombardi M, Biamino S, et al. Additive manufacturing of titanium alloys in the biomedical field: processes, properties and applications. J Appl Biomater Funct Mater 2018;16:57–67. https://doi.org/10.5301/JABFM.5000371.
[61] Leary M. Design of titanium implants for additive manufacturing. Titanium in Medical and Dental Applications 2018:203–24. https://doi.org/10.1016/B978-0-12-812456-7.00009-3.
[62] Huotilainen E, Jaanimets R, Valášek J, Marcián P, Salmi M, Tuomi J, et al. Inaccuracies in additive manufactured medical skull models caused by the

DICOM to STL conversion process. Journal of Cranio-Maxillofacial Surgery 2014;42:e259–65. https://doi.org/10.1016/J.JCMS.2013.10.001.
[63] Murr LE, Gaytan SM, Martinez E, Medina F, Wicker RB. Next generation orthopaedic implants by additive manufacturing using electron beam melting. Int J Biomater 2012. https://doi.org/10.1155/2012/245727.
[64] Murr LE, Martinez E, Amato KN, Gaytan SM, Hernandez J, Ramirez DA, et al. Fabrication of Metal and Alloy Components by Additive Manufacturing: Examples of 3D Materials Science. Journal of Materials Research and Technology 2012;1:42–54. https://doi.org/10.1016/S2238-7854(12)70009-1.
[65] Sames WJ, List FA, Pannala S, Dehoff RR, Babu SS. The metallurgy and processing science of metal additive manufacturing. International Materials Reviews 2016;61:315–60. https://doi.org/10.1080/09506608.2015.1116649.
[66] Sing SL, An J, Yeong WY, Wiria FE. Laser and electron-beam powder-bed additive manufacturing of metallic implants: A review on processes, materials and designs. Journal of Orthopaedic Research 2016;34:369–85. https://doi.org/10.1002/JOR.23075.
[67] Wang P, Sin WJ, Nai MLS, Wei J. Effects of Processing Parameters on Surface Roughness of Additive Manufactured Ti-6Al-4V via Electron Beam Melting. Materials 2017, Vol 10, Page 1121 2017;10:1121. https://doi.org/10.3390/MA10101121.
[68] Murr LE, Gaytan SM, Ramirez DA, Martinez E, Hernandez J, Amato KN, et al. Metal Fabrication by Additive Manufacturing Using Laser and Electron Beam Melting Technologies. J Mater Sci Technol 2012;28:1–14. https://doi.org/10.1016/S1005-0302(12)60016-4.
[69] Murr LE, Gaytan SM, Medina F, Lopez H, Martinez E, MacHado BI, et al. Next-generation biomedical implants using additive manufacturing of complex, cellular and functional mesh arrays. Philos Trans A Math Phys Eng Sci 2010;368:1999–2032. https://doi.org/10.1098/RSTA.2010.0010.
[70] Frazier WE. Metal additive manufacturing: A review. J Mater Eng Perform 2014;23:1917–28. https://doi.org/10.1007/S11665-014-0958-Z/FIGURES/9.
[71] Dennis DA. Management of massive acetabular defects in revision total hip arthroplasty. Journal of Arthroplasty 2003;18:121–5. https://doi.org/10.1054/arth.2003.50105.
[72] Hart A, PV and HJ. “Personalised orthopaedics – using 3D printing for tailor-made technical teaching , preoperative planning and precise placement of implants.” Orthopaedic Products News 2017.
[73] Jain S, Grogan RJ, Giannoudis P V. Options for managing severe acetabular bone loss in revision hip arthroplasty. A systematic review. Hip Int 2014;24:109–22. https://doi.org/10.5301/HIPINT.5000101.
[74] Moore KD, McClenny MD, Wills BW. Custom Triflange Acetabular Components for Large Acetabular Defects: Minimum 10-Year Follow-up. Orthopedics 2018;41:E316–20. https://doi.org/10.3928/01477447-20180213-11.
[75] Sheth NP, Nelson CL, Springer BD, Fehring TK, Paprosky WG. Acetabular bone loss in revision total hip arthroplasty: evaluation and management. J Am Acad Orthop Surg 2013;21:128–39. https://doi.org/10.5435/JAAOS-21-03-128.
[76] Wyatt MC. Custom 3D-printed acetabular implants in hip surgery--innovative breakthrough or expensive bespoke upgrade? Hip Int 2015;25:375–9. https://doi.org/10.5301/HIPINT.5000294.
[77] Barlow BT, Oi KK, Lee Y yu, Carli A V., Choi DS, Bostrom MP. Outcomes of Custom Flange Acetabular Components in Revision Total Hip Arthroplasty and

Predictors of Failure. Journal of Arthroplasty 2016;31:1057–64. https://doi.org/10.1016/j.arth.2015.11.016.
[78] Berry DJ, Muller ME. Revision arthroplasty using an anti-protrusio cage for massive acetabular bone deficiency. J Bone Joint Surg Br 1992;74:711–5. https://doi.org/10.1302/0301-620X.74B5.1527119.
[79] Durand-Hill M, Henckel J, Di Laura A, Hart AJ. Can custom 3D printed implants successfully reconstruct massive acetabular defects? A 3D-CT assessment. Journal of Orthopaedic Research® 2020;38:2640–8. https://doi.org/10.1002/JOR.24752.
[80] Citak M, Kochsiek L, Gehrke T, Haasper C, Suero EM, Mau H. Preliminary results of a 3D-printed acetabular component in the management of extensive defects. Hip Int 2018;28:266–71. https://doi.org/10.5301/HIPINT.5000561.
[81] Paprosky WG, Perona PG, Lawrence JM. Acetabular defect classification and surgical reconstruction in revision arthroplasty. A 6-year follow-up evaluation. J Arthroplasty 1994;9:33–44. https://doi.org/10.1016/0883-5403(94)90135-X.
[82] Lowther M, Louth S, Davey A, Hussain A, Ginestra P, Carter L, et al. Clinical, industrial, and research perspectives on powder bed fusion additively manufactured metal implants. Addit Manuf 2019;28:565–84. https://doi.org/10.1016/J.ADDMA.2019.05.033.
[83] Wang X, Xu S, Zhou S, Xu W, Leary M, Choong P, et al. Topological design and additive manufacturing of porous metals for bone scaffolds and orthopaedic implants: A review. Biomaterials 2016;83:127–41. https://doi.org/10.1016/J.BIOMATERIALS.2016.01.012.
[84] Vanmeensel K, Lietaert K, Vrancken B, Dadbakhsh S, Li X, Kruth JP, et al. Additively manufactured metals for medical applications. Additive Manufacturing: Materials, Processes, Quantifications and Applications 2018:261–309. https://doi.org/10.1016/B978-0-12-812155-9.00008-6.
[85] Berry DJ, Von Knoch M, Schleck CD, Harmsen WS. Effect of femoral head diameter and operative approach on risk of dislocation after primary total hip arthroplasty. J Bone Joint Surg Am 2005;87:2456–63. https://doi.org/10.2106/JBJS.D.02860.
[86] Burroughs BR, Hallstrom B, Golladay GJ, Hoeffel D, Harris WH. Range of motion and stability in total hip arthroplasty with 28-, 32-, 38-, and 44-mm femoral head sizes: An in vitro study. Journal of Arthroplasty 2005;20:11–9. https://doi.org/10.1016/j.arth.2004.07.008.
[87] Cho M-R, Choi WK, Kim JJ. Current Concepts of Using Large Femoral Heads in Total Hip Arthroplasty. Hip Pelvis 2016;28:134. https://doi.org/10.5371/HP.2016.28.3.134.
[88] Weller C, Kleer R, Piller FT. Economic implications of 3D printing: Market structure models in light of additive manufacturing revisited. Int J Prod Econ 2015;164:43–56. https://doi.org/10.1016/J.IJPE.2015.02.020.
[89] Zhai Y, Lados DA, Lagoy JL. Additive Manufacturing: Making imagination the major Limitation. JOM 2014;66:808–16. https://doi.org/10.1007/S11837-014-0886-2/TABLES/2.
[90] Orthopedic 3D printed devices market size to grow by USD 1.35 billion from 2023 to 2028 | North America to account for 40% of market growth- Technavio - Ortho Spine News n.d. https://orthospinenews.com/2023/12/14/orthopedic-3d-printed-devices-market-size-to-grow-by-usd-1-35-billion-from-2023-to-2028-north-america-to-account-for-40-of-market-growth-technavio/ (accessed April 15, 2024).

[91] Lin AY, Yarholar LM. Plastic Surgery Innovation with 3D Printing for Craniomaxillofacial Operations. Mo Med 2020;117:136.
[92] Ginestra P, Ferraro RM, Zohar-Hauber K, Abeni A, Giliani S, Ceretti E. Selective laser melting and electron beam melting of Ti6Al4V for orthopedic applications: A comparative study on the applied building direction. Materials 2020;13:1–23. https://doi.org/10.3390/ma13235584.
[93] Popov V V., Muller-Kamskii G, Kovalevsky A, Dzhenzhera G, Strokin E, Kolomiets A, et al. Design and 3D-printing of titanium bone implants: brief review of approach and clinical cases. Biomed Eng Lett 2018;8:337–44. https://doi.org/10.1007/s13534-018-0080-5.
[94] Mukherjee T, DebRoy T. Mitigation of lack of fusion defects in powder bed fusion additive manufacturing. J Manuf Process 2018;36:442–9. https://doi.org/10.1016/J.JMAPRO.2018.10.028.
[95] Murr LE. Additive manufacturing of biomedical devices: an overview. Materials Technology 2018;33:57–70. https://doi.org/10.1080/10667857.2017.1389052.
[96] Ryan G, Pandit A, Apatsidis DP. Fabrication methods of porous metals for use in orthopaedic applications. Biomaterials 2006;27:2651–70. https://doi.org/10.1016/J.BIOMATERIALS.2005.12.002.
[97] Pałka K, Pokrowiecki R. Porous Titanium Implants: A Review. Adv Eng Mater 2018;20. https://doi.org/10.1002/ADEM.201700648.
[98] Di Laura A, Henckel J, Hart A. Custom 3D-Printed Implants for Acetabular Reconstruction: Intermediate-Term Functional and Radiographic Results. JBJS Open Access 2023;8:e22.00120. https://doi.org/10.2106/JBJS.OA.22.00120.
[99] Castagnini F, Caternicchia F, Biondi F, Masetti C, Faldini C, Traina F. Off-the-shelf 3D printed titanium cups in primary total hip arthroplasty. World J Orthop 2021;12:376. https://doi.org/10.5312/WJO.V12.I6.376.
[100] Dall'Ava L, Hothi H, Henckel J, Di Laura A, Shearing P, Hart A. Comparative analysis of current 3D printed acetabular titanium implants. 3D Print Med 2019;5. https://doi.org/10.1186/s41205-019-0052-0.
[101] Dall'ava L, Hothi H, Henckel J, Laura A Di, Tirabosco R, Eskelinen A, et al. Osseointegration of retrieved 3D-printed, off-the-shelf acetabular implants Aims. Bone Joint Res 2021;10:388–400. https://doi.org/10.1302/2046-3758.107.BJR.
[102] Nicum A, Hothi H, Henckel J, di Laura A, Schlueter-Brust K, Hart A. Characterisation of 3D-printed acetabular hip implants. EFORT Open Rev 2024;9:862–72. https://doi.org/10.1530/eor-23-0182.
[103] Jiao J, Hong Q, Zhang D, Wang M, Tang H, Yang J, et al. Influence of porosity on osteogenesis, bone growth and osteointegration in trabecular tantalum scaffolds fabricated by additive manufacturing. Front Bioeng Biotechnol 2023;11:1117954. https://doi.org/10.3389/FBIOE.2023.1117954/BIBTEX.
[104] Dall'Ava L, Hothi H, Henckel J, Di Laura A, Shearing P, Hart A. Characterization of dimensional, morphological and morphometric features of retrieved 3D-printed acetabular cups for hip arthroplasty. J Orthop Surg Res 2020;15. https://doi.org/10.1186/s13018-020-01665-y.
[105] Blakey-Milner B, Gradl P, Snedden G, Brooks M, Pitot J, Lopez E, et al. Metal additive manufacturing in aerospace: A review. Mater Des 2021;209:110008. https://doi.org/10.1016/J.MATDES.2021.110008.
[106] Hothi H, Henckel J, Bergiers S, Di Laura A, Schlueter-Brust K, Hart A. The analysis of defects in custom 3D-printed acetabular cups: A comparative study

of commercially available implants from six manufacturers. Journal of Orthopaedic Research 2022. https://doi.org/10.1002/jor.25483.
[107] Hothi H, Henckel J, Bergiers S, Di Laura A, Schlueter-Brust K, Hart A. Morphometric analysis of patient-specific 3D-printed acetabular cups: a comparative study of commercially available implants from 6 manufacturers. 3D Print Med 2022;8. https://doi.org/10.1186/s41205-022-00160-w.
[108] Song P, Hu C, Pei X, Sun J, Sun H, Wu L, et al. Dual modulation of crystallinity and macro-/microstructures of 3D printed porous titanium implants to enhance stability and osseointegration. J Mater Chem B 2019;7:2865–77. https://doi.org/10.1039/C9TB00093C.
[109] Chen C, Hao Y, Bai X, Ni J, Chung SM, Liu F, et al. 3D printed porous Ti6Al4V cage: Effects of additive angle on surface properties and biocompatibility; bone ingrowth in Beagle tibia model. Mater Des 2019;175:107824. https://doi.org/10.1016/J.MATDES.2019.107824.
[110] Xie K, Guo Y, Zhao S, Wang L, Wu J, Tan J, et al. Partially Melted Ti6Al4V Particles Increase Bacterial Adhesion and Inhibit Osteogenic Activity on 3D-printed Implants: An In Vitro Study. Clin Orthop Relat Res 2019;477:2772. https://doi.org/10.1097/CORR.0000000000000954.
[111] Whitehead KA, Colligon J, Verran J. Retention of microbial cells in substratum surface features of micrometer and sub-micrometer dimensions. Colloids Surf B Biointerfaces 2005;41:129–38. https://doi.org/10.1016/J.COLSURFB.2004.11.010.
[112] McGee OM, Geraghty S, Hughes C, Jamshidi P, Kenny DP, Attallah MM, et al. An investigation into patient-specific 3D printed titanium stents and the use of etching to overcome Selective Laser Melting design constraints. J Mech Behav Biomed Mater 2022;134. https://doi.org/10.1016/j.jmbbm.2022.105388.
[113] Ye C, Zhang C, Zhao J, Dong Y. Effects of Post-processing on the Surface Finish, Porosity, Residual Stresses, and Fatigue Performance of Additive Manufactured Metals: A Review. J Mater Eng Perform 2021;30:6407–25. https://doi.org/10.1007/s11665-021-06021-7.
[114] Pyka G, Burakowski A, Kerckhofs G, Moesen M, Van Bael S, Schrooten J, et al. Surface Modification of Ti6Al4V Open Porous Structures Produced by Additive Manufacturing. Adv Eng Mater 2012;14:363–70. https://doi.org/10.1002/ADEM.201100344.
[115] Uriondo A, Esperon-Miguez M, Perinpanayagam S. The present and future of additive manufacturing in the aerospace sector: A review of important aspects. Proc Inst Mech Eng G J Aerosp Eng 2015;229:2132–47. https://doi.org/10.1177/0954410014568797.
[116] Chahal V, Taylor RM. A review of geometric sensitivities in laser metal 3D printing. Https://DoiOrg/101080/1745275920191709255 2020;15:227–41. https://doi.org/10.1080/17452759.2019.1709255.
[117] Gao W, Zhang Y, Ramanujan D, Ramani K, Chen Y, Williams CB, et al. The status, challenges, and future of additive manufacturing in engineering. Computer-Aided Design 2015;69:65–89. https://doi.org/10.1016/J.CAD.2015.04.001.
[118] DebRoy T, Wei HL, Zuback JS, Mukherjee T, Elmer JW, Milewski JO, et al. Additive manufacturing of metallic components – Process, structure and properties. Prog Mater Sci 2018;92:112–224. https://doi.org/10.1016/J.PMATSCI.2017.10.001.

[119] Blakey-Milner B, Gradl P, Snedden G, Brooks M, Pitot J, Lopez E, et al. Metal additive manufacturing in aerospace: A review. Mater Des 2021;209:110008. https://doi.org/10.1016/J.MATDES.2021.110008.
[120] Leuders S, Thöne M, Riemer A, Niendorf T, Tröster T, Richard HA, et al. On the mechanical behaviour of titanium alloy TiAl6V4 manufactured by selective laser melting: Fatigue resistance and crack growth performance. Int J Fatigue 2013;48:300–7. https://doi.org/10.1016/J.IJFATIGUE.2012.11.011.
[121] Hothi H, Dall'Ava L, Henckel J, Di Laura A, Iacoviello F, Shearing P, et al. Evidence of structural cavities in 3D printed acetabular cups for total hip arthroplasty. J Biomed Mater Res B Appl Biomater 2020;108:1779–89. https://doi.org/10.1002/jbm.b.34520.
[122] Kumar GR, Sathishkumar M, Vignesh M, Manikandan M, Rajyalakshmi G, Ramanujam R, et al. Metal additive manufacturing of commercial aerospace components – A comprehensive review. Proceedings of the Institution of Mechanical Engineers, Part E: Journal of Process Mechanical Engineering 2022. https://doi.org/10.1177/09544089221104070/ASSET/IMAGES/LARGE/10.1177_09544089221104070-FIG9.JPEG.
[123] Carter LN, Villapún VM, Grover L, Cox SC. Exploring the duality of powder adhesion and underlying surface roughness in laser powder bed fusion processed Ti-6Al-4V. J Manuf Process 2022;81:14–26. https://doi.org/10.1016/J.JMAPRO.2022.06.057.
[124] Hothi H, Henckel J, Di Laura A, Hart A. Evidence of Partially Molten Titanium Particles on 3D Printed Acetabular Cups. Podium Talk presented at the European Hip Society Meeting, Bern, Switzerland: 2023.
[125] Nicum A, Di Laura A, Hothi H, Henckel J, Schlueter-Brust K, Hart A. Surface adhered titanium particles on 3D printed off-the-shelf acetabular cups. Journal of Orthopaedic Research® 2024;42:2817–25. https://doi.org/10.1002/JOR.25958.
[126] Dall'Ava L, Hothi H, Henckel J, Di Laura A, Bergiers S, Shearing P, et al. Dimensional analysis of 3D-printed acetabular cups for hip arthroplasty using X-ray microcomputed tomography. Rapid Prototyp J 2020;26:567–76. https://doi.org/10.1108/RPJ-06-2019-0175.
[127] Liu H, Liu LL, Tan JH, Yan YG, Xue JB. Definition of Pore Size in 3D-Printed Porous Implants: A Review. ChemBioEng Reviews 2023;10:167–73. https://doi.org/10.1002/CBEN.202200043.
[128] EcoFit® EPORE® cup n.d. https://www.implantcast.de/en/for-medical-professionals/products/standard-/-tumour-prosthetics/pelvis-and-hip-endoprosthetics/primary-endoprosthetics-femoral-heads-/-acetabulum/ecofitr-eporer-cup/ (accessed November 12, 2024).
[129] Acetabular System | Stryker n.d. https://www.stryker.com/us/en/joint-replacement/products/trident-ii.html (accessed November 12, 2024).
[130] ODEP is the Orthopaedic Data Evaluation Panel n.d. https://www.odep.org.uk/ (accessed February 5, 2024).
[131] ODEP Rating System - NEC ODEP n.d. https://www.odep.org.uk/about/rating-system/ (accessed January 24, 2024).
[132] 3D Printing of Medical Devices | FDA n.d. https://www.fda.gov/medical-devices/products-and-medical-procedures/3d-printing-medical-devices (accessed January 17, 2024).

[133] 3D printing (additive manufacturing) of medical devices or component parts during the coronavirus (COVID-19) pandemic - GOV.UK n.d. https://www.gov.uk/guidance/3d-printing-additive-manufacturing-of-medical-devices-or-component-parts-during-the-coronavirus-covid-19-pandemic#advice-for-those-using-3d-printing (accessed January 17, 2024).
[134] ISO 22441:2022 - Sterilization of health care products — Low temperature vaporized hydrogen peroxide — Requirements for the development, validation and routine control of a sterilization process for medical devices n.d. https://www.iso.org/standard/73214.html (accessed January 17, 2024).
[135] ISO 17664-1:2021 - Processing of health care products — Information to be provided by the medical device manufacturer for the processing of medical devices — Part 1: Critical and semi-critical medical devices n.d. https://www.iso.org/standard/81720.html (accessed January 17, 2024).
[136] ISO 14971:2019(en), Medical devices — Application of risk management to medical devices n.d. https://www.iso.org/obp/ui/#iso:std:iso:14971:ed-3:v1:en (accessed January 17, 2024).
[137] ISO 10993-1:2018 - Biological evaluation of medical devices — Part 1: Evaluation and testing within a risk management process n.d. https://www.iso.org/standard/68936.html (accessed January 17, 2024).
[138] CDRH. Technical Considerations for Additive Manufactured Medical Devices Guidance for Industry and Food and Drug Administration Staff. FDA 2016.
[139] Medical Devices Medical Device Coordination Group Document MDCG 2021-3 Questions and Answers on Custom-Made Devices & considerations on Adaptable medical devices and Patient-matched medical devices Medical Devices. 2021.
[140] Carl AK, Hochmann D. Impact of the new European medical device regulation: a two-year comparison. Biomedizinische Technik 2023. https://doi.org/10.1515/bmt-2023-0325.
[141] Committee F42 on Additive Manufacturing Technologies n.d. https://www.astm.org/committee-f42 (accessed January 18, 2024).
[142] Swiatkowska I, Martin NG, Henckel J, Apthorp H, Hamshere J, Hart AJ. Blood and plasma titanium levels associated with well-functioning hip implants. Journal of Trace Elements in Medicine and Biology 2020;57:9–17. https://doi.org/10.1016/J.JTEMB.2019.09.005.
[143] Tognini M, Hothi H, Tucker S, Broomfield E, Shafafy M, Gikas P, et al. Blood titanium levels in patients with large and sliding titanium implants. BMC Musculoskelet Disord 2022;23:1–10. https://doi.org/10.1186/S12891-022-05717-8/FIGURES/4.
[144] Hothi H, Henckel J, Nicum A, Di Laura A, Schlueter-Brust K, Hart A. Comparative analysis of conventionally and additively manufactured acetabular shells from a single manufacturer. 3D Print Med 2024;10:1–11. https://doi.org/10.1186/S41205-024-00233-Y/FIGURES/7.
[145] Swiatkowska I, Martin N, Hart AJ. Blood titanium level as a biomarker of orthopaedic implant wear. Journal of Trace Elements in Medicine and Biology 2019;53:120–8. https://doi.org/10.1016/J.JTEMB.2019.02.013.
[146] Xie K, Guo Y, Zhao S, Wang L, Wu J, Tan J, et al. Partially Melted Ti6Al4V Particles Increase Bacterial Adhesion and Inhibit Osteogenic Activity on 3D-printed Implants: An In Vitro Study. Clin Orthop Relat Res 2019;477:2772. https://doi.org/10.1097/CORR.0000000000000954.

[147] Cowie RM, Jennings LM. Third body damage and wear in arthroplasty bearing materials: A review of laboratory methods. Biomaterials and Biosystems 2021;4. https://doi.org/10.1016/J.BBIOSY.2021.100028.
[148] Meimban RJ, Fernando AR, Monsura A, Ranada J, Apduhan JC. Blood Cells Counting using Python OpenCV. International Conference on Signal Processing Proceedings, ICSP 2019;2018-August:50–3. https://doi.org/10.1109/ICSP.2018.8652384.
[149] Conrad R, Narayan K. Instance segmentation of mitochondria in electron microscopy images with a generalist deep learning model trained on a diverse dataset. Cell Syst 2023;14:58-71.e5. https://doi.org/10.1016/J.CELS.2022.12.006.
[150] Kumar S. Selective Laser Sintering/Melting. Comprehensive Materials Processing: Thirteen Volume Set 2014;10:93–134. https://doi.org/10.1016/B978-0-08-096532-1.01003-7.
[151] Cao X, Carter LN, Man K, Villapún VM, Giangiorgi L, Cox SC. Improving predictability of additively manufactured Ti-6Al-4 V lattices for orthopaedic devices: A parametric and struts angle study. Mater Des 2024;243:113043. https://doi.org/10.1016/J.MATDES.2024.113043.
[152] Lee JY, Nagalingam AP, Yeo SH. A review on the state-of-the-art of surface finishing processes and related ISO/ASTM standards for metal additive manufactured components. Virtual Phys Prototyp 2021;16:68–96. https://doi.org/10.1080/17452759.2020.1830346.
[153] Kim US, Park JW. High-Quality Surface Finishing of Industrial Three-Dimensional Metal Additive Manufacturing Using Electrochemical Polishing. International Journal of Precision Engineering and Manufacturing - Green Technology 2019;6:11–21. https://doi.org/10.1007/S40684-019-00019-2/FIGURES/12.
[154] Swiatkowska I, Martin NG, Henckel J, Apthorp H, Hamshere J, Hart AJ. Blood and plasma titanium levels associated with well-functioning hip implants. Journal of Trace Elements in Medicine and Biology 2020;57:9–17. https://doi.org/10.1016/J.JTEMB.2019.09.005.
[155] Bitar D, Parvizi J. Biological response to prosthetic debris. World J Orthop 2015;6:172. https://doi.org/10.5312/WJO.V6.I2.172.
[156] De Fine M, Terrando S, Hintner M, Porporati AA, Pignatti G. Pushing Ceramic-on-Ceramic in the most extreme wear conditions: A hip simulator study. Orthopaedics & Traumatology: Surgery & Research 2021;107:102643. https://doi.org/10.1016/J.OTSR.2020.05.003.
[157] Villapún VM, Carter LN, Gao N, Addison O, Webber MA, Shepherd DET, et al. A design approach to facilitate selective attachment of bacteria and mammalian cells to additively manufactured implants. Addit Manuf 2020;36:101528. https://doi.org/10.1016/J.ADDMA.2020.101528.
[158] van Hengel IAJ, van Dijk B, Modaresifar K, Hooning van Duyvenbode JFF, Nurmohamed FRHA, Leeflang MA, et al. In Vivo Prevention of Implant-Associated Infections Caused by Antibiotic-Resistant Bacteria through Biofunctionalization of Additively Manufactured Porous Titanium. J Funct Biomater 2023;14:520. https://doi.org/10.3390/JFB14100520.
[159] Tognini M, Hothi H, Tucker S, Broomfield E, Shafafy M, Gikas P, et al. Blood titanium levels in patients with large and sliding titanium implants. BMC Musculoskelet Disord 2022;23:1–10. https://doi.org/10.1186/S12891-022-05717-8/FIGURES/4.

Appendix I

A | Simpleware Methodology

1. Three samples from the porous structure from the main body were sectioned. Four samples were sectioned using the same method for the off-the-shelf implants. This was done to evaluate the dimensional features of the porous layer in the different areas as defined above. Additionally sectioning of the implant was completed to reduce the specimen size for analysis in Simpleware so the software could run more efficiently. This was achieved via the following steps:
    a. The raw micro-Ct data import of the whole implant was inputted into Simpleware. The implant is now in the mask format within Simpleware
    b. The implant mask was then sectioned into the different samples using the crop tool in Simpleware.
    c. For the customs this was different areas of the porous structure on the main body of the implant.
    d. For the off-the shelf cups these regions were:
        i. The introducer screwhole
        ii. Bulk screwhole
        iii. Bulk porosity
        iv. Cup rim
2. The porous mesh layer was then separated from the dense region of the implant samples by using a filtering tool and some Boolean functions. This was achieved as detailed below:
    a. First a copy is made of the mask of the implant sample. The following steps are then completed on one of these masks, leaving the other for

later operations, as indicated. Also change the colour and name of this mask for ease of use and analysis.

b. The entire lattice structure is removed from the dense region before using a combination of Boolean operations to separate the two regions.
c. An open filter, selected from the ‘Image Processing’ toolbar tab, with a high strength based on the size of the struts (.e.g. X radius = 8-10 pixels) was applied on the mask of the implant. This filter will erode the mask by 8 pixels (remove all features of this magnitude), which essentially deletes the lattice, while also dilating back by 8 pixels, close to the surface of the dense region of the implant sample. It is important to note that this filter is not perfect and will erode other areas of the same magnitude, and the potential loss of data should be reviewed and considered before continuing. This mask now only consists of the dense region of that sample of the implant and the lattice has been removed (Figure 3.A).
d. Then create another copy of the original mask and change its colour and name. Then perform the Boolean operation to separate the porous mesh from the dense region, as below (Figure 3.B):
    i. Right click on the copy of the original mask to be able to select ‘Boolean operations’ from the drop-down options.
    ii. Follow this across and select ‘Subtract with’ and select the mask where the open filter has been applied.
e. The dense region has now been removed and the porous region has been isolated.

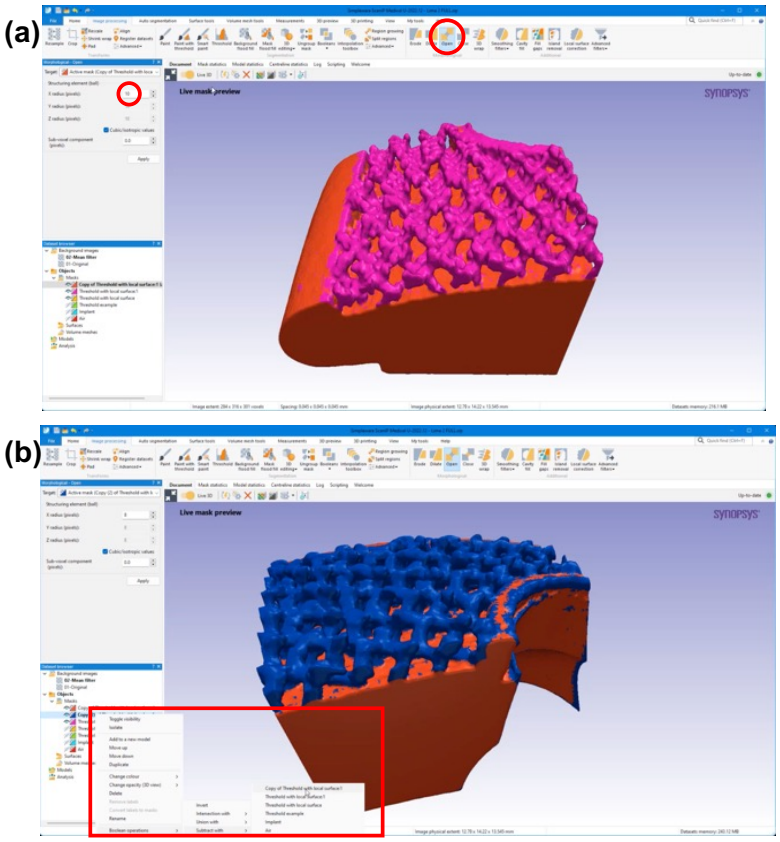

Figure 3.A: The Porous structure being removed using an open filter. (a) Duplicate sample mask (red mask). Using a high strength 'Open Filter' to remove the lattice, as indicated. (b) Boolean subtraction of this mask (red) with the lattice removed, from a copy of the original (blue), to leave the lattice.

f. This mask will require some cleaning to remove the areas that are not part of the lattice, using another open filter of a lower strength (e.g. 1-3 pixels). 'Mask floodfill' in the Image processing tab of Simpleware can

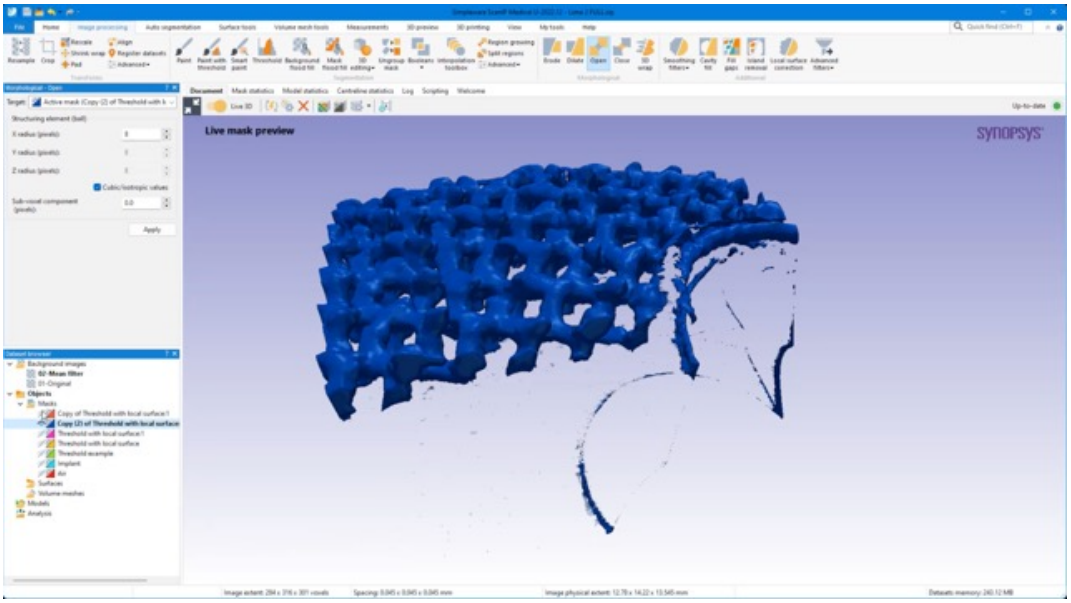

Figure 3.B: The isolated porous structure after the Boolean subtraction operation.

also be used, by left-clicking on the region to apply, and this ensures the lattice is one body (Figure 3.C).

The samples of the implant porous structures were then ready for analysis, as outlined below.

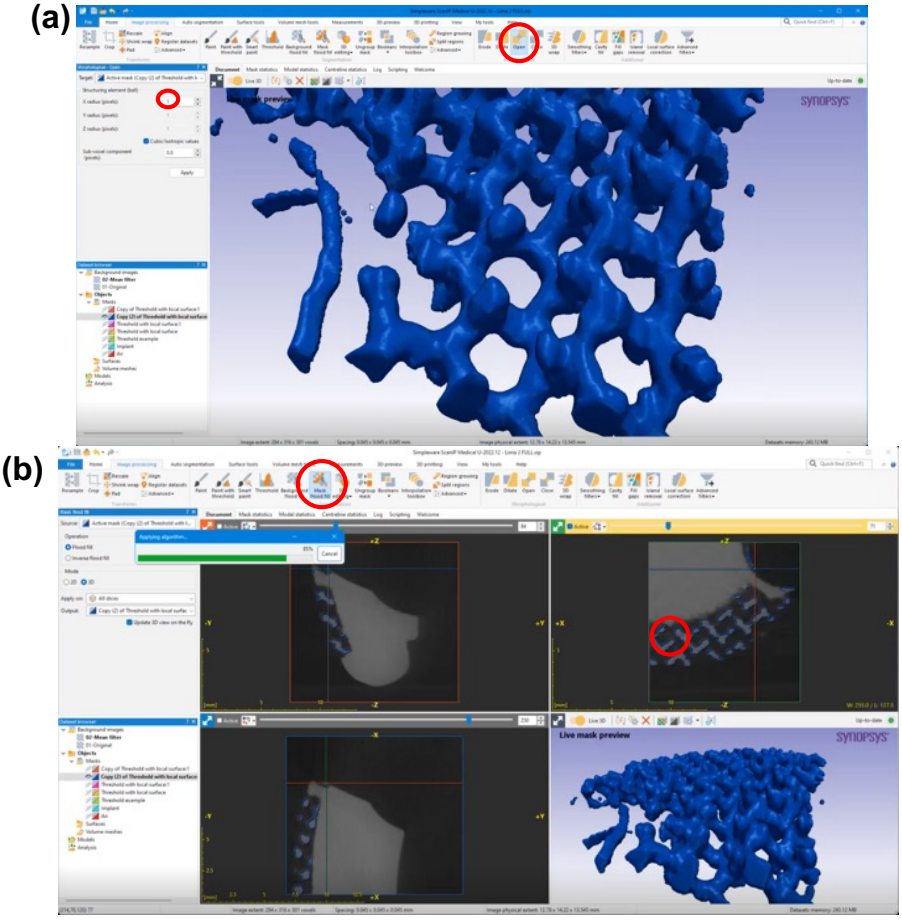

Figure 3.C: Cleaning the mask of the isolated lattice using (a) an Open filter with a lower strength or (b) the mask floodfill tool by left-clicking on the area to fill, leaving a cleaner final mask of the porous structure for analysis.

Length

Within Simpleware,

1. The centrelines tool was used to generate a network of nodes and lines on the isolated porous structures from the sectioned implant samples (Figure 3.D).

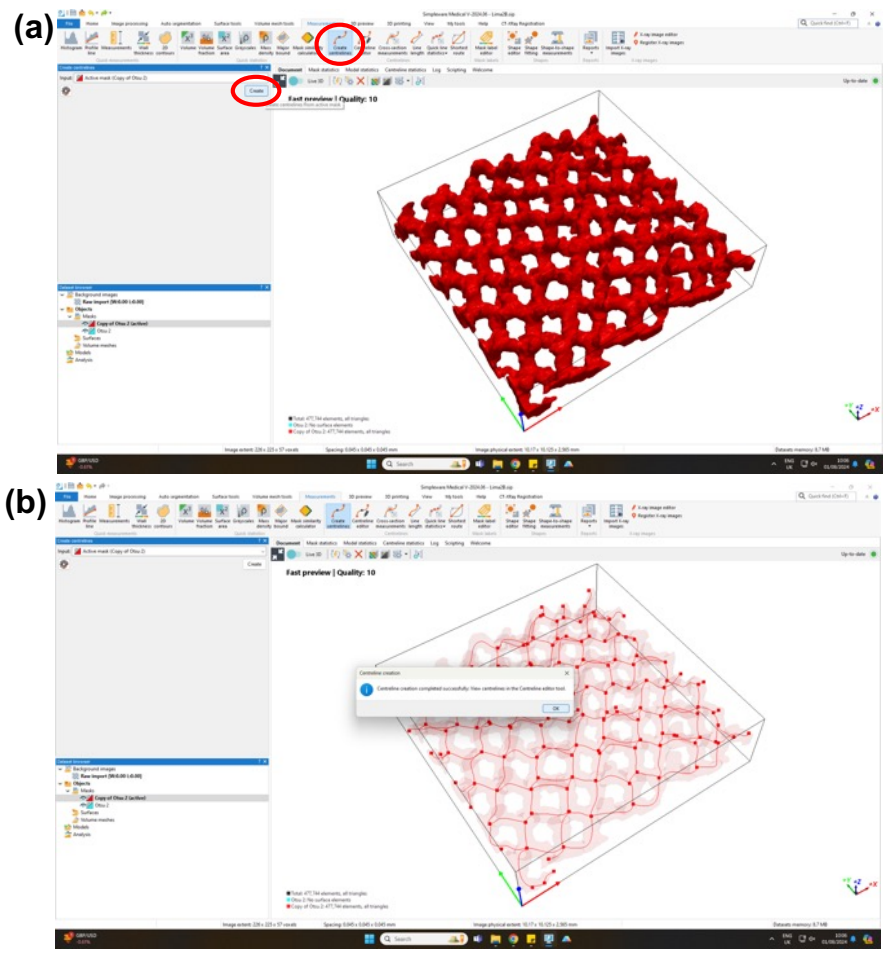

Figure 3.D: How to create a centreline network in Simpleware. (a) Select the ‘Create Centreline’ tool under the ‘Measurements’ tab. Select ‘Create’ to generate the network. (b) Generation is complete.

2. The network generated was then corrected for any false nodes that were identified (Figure 3.E). This was achieved by manually identifying and selecting disconnected or duplicate nodes, therefore there is likely some human error associated with this method. However, this step is necessary to improve the accuracy of the dimensional features measured from the corrected struts such as length and radius.
3. The **Length** of the lines in millimetres were then exported (Figure 3.F).

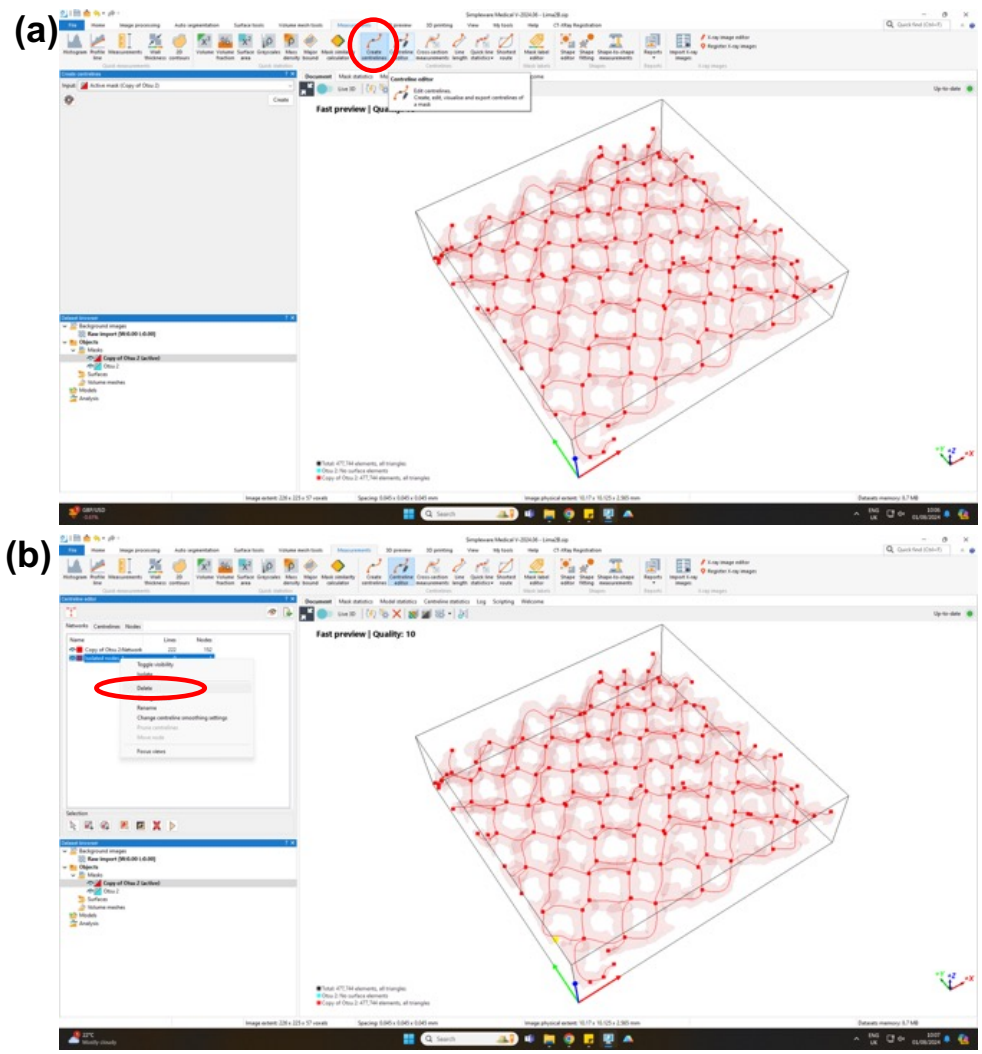

Figure 3.E: Removal of false nodes and islands. (a) Select the ‘Centreline Editor’ tool. (b) Right-click on the island and delete. Also delete disconnected nodes on the centreline network.

a. Using the export tool, select the following options in the corresponding window before exporting the lengths of the struts as determined by the centreline network;
    i. Export file type - Text / CSV
    ii. Coordinates - Global
    iii. Visible Only
    iv. Data to export – lines
b. After these options are selected, export the file and save in the desired destination.

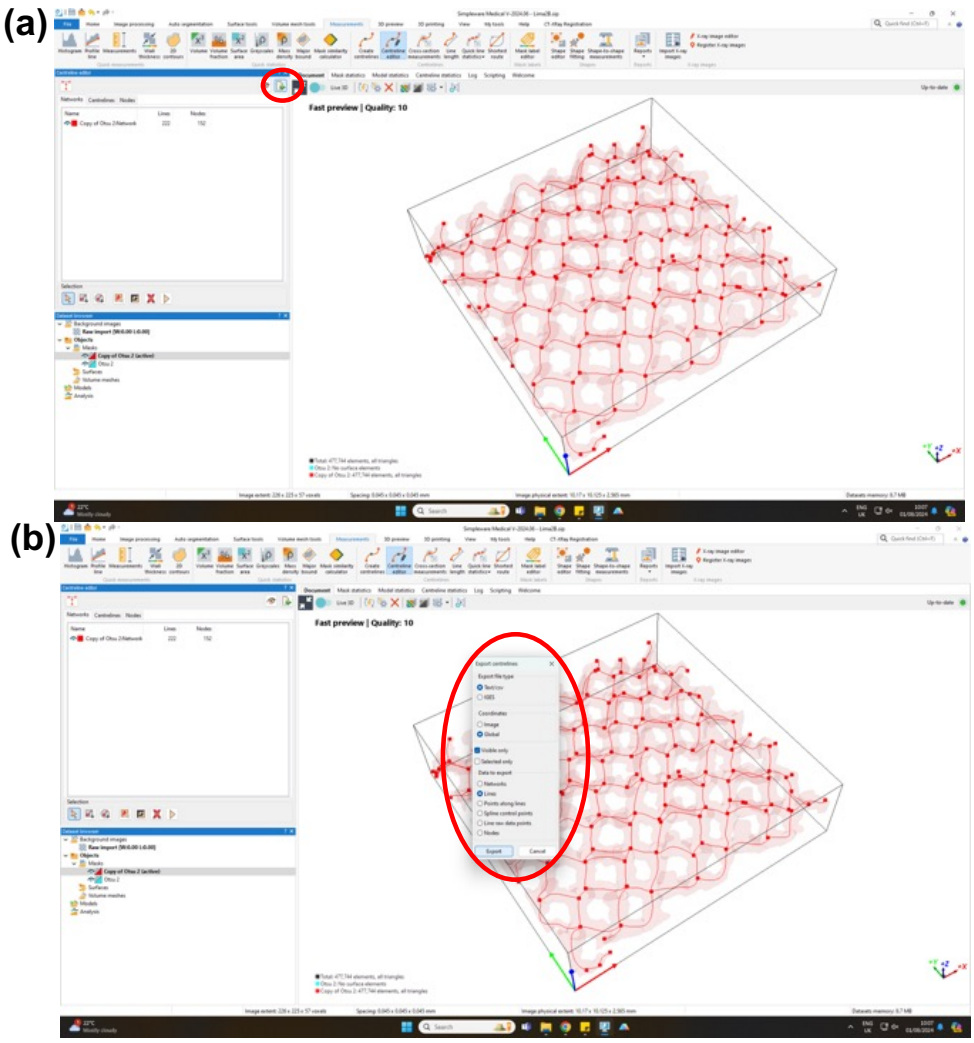

Figure 3.F: Exporting length measurements from Simpleware. (a) Select the export tool. (b) Select these options to export the measurements correctly and save the file in the desired location.

Perimeter, Cross-sectional Area & Radius

To record the measurements for these parameters, a random selection of 15 struts per sample of each of the porous structures was selected from the generated centreline network.

Between 5-10 measurements of strut cross-sectional area, radius and perimeter were collected for each of the 15 struts using the corresponding tool in Simpleware. The steps to do this are as below:

1. Select the Quick line statistics tool in the Measurements tab in Simpleware (Figure 3.G).

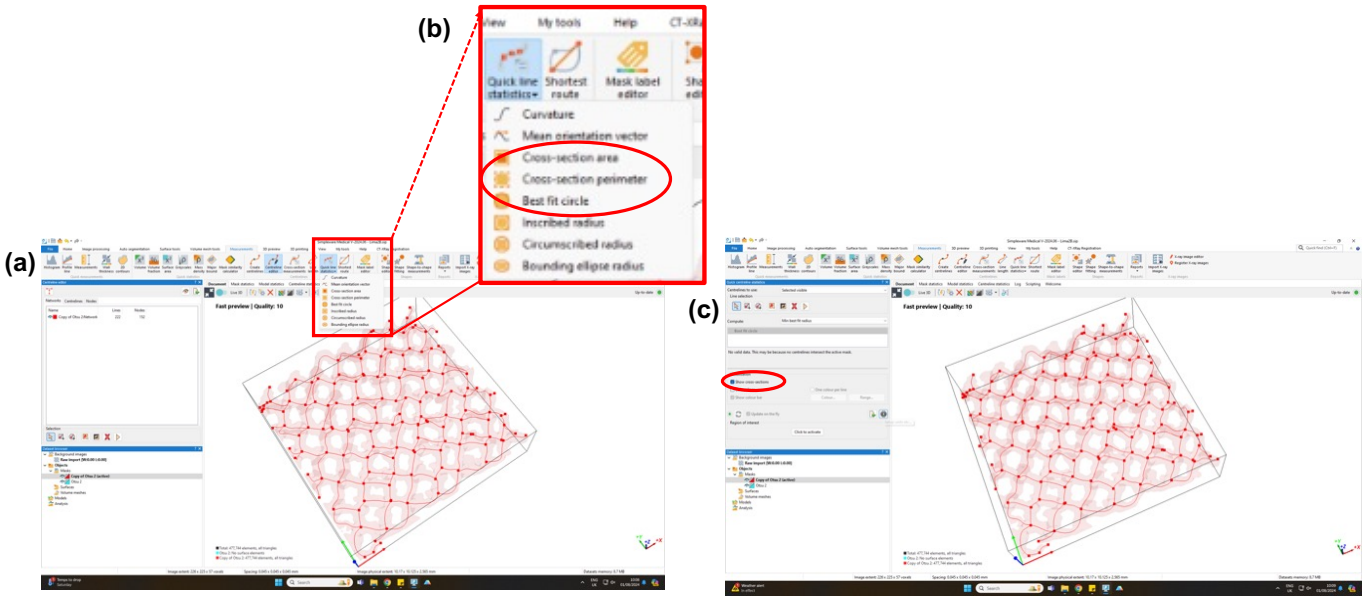

Figure 3.G: Tools to take measurements from the centreline network. (a) Select the 'Quick line Statistics' Tool in Simpleware. (b) Drop down menu, select the parameters are indicated to take the measurements. (c) Show cross sections is ticked to see where the measurements are being taken along the strut and reduce the chance of anomalous results.

2. Select the type of measurement from the drop-down menu, i.e. perimeter, cross-sectional area, best fit circle (Figure 3.G).
3. Ensure 'Show cross-sections' is ticked in Visualisation. This is so the observer is able to view the cross-sections of the strut and provides a quick visual check if there could be anomalies (Figure 3.G).
4. Select settings and change the options as below to ensure the measurements taken are uniform and prevent outlier measurements (Figure 3.H);
    a. Check the boxes to exclude cross-sections touching a boundary and intersected by adjacent lines. (reducing anomalies at strut junctions)

b. Ensure the large outlier false rejection confidence is set to 99.5%. (reducing anomalies at strut junctions and boundaries)

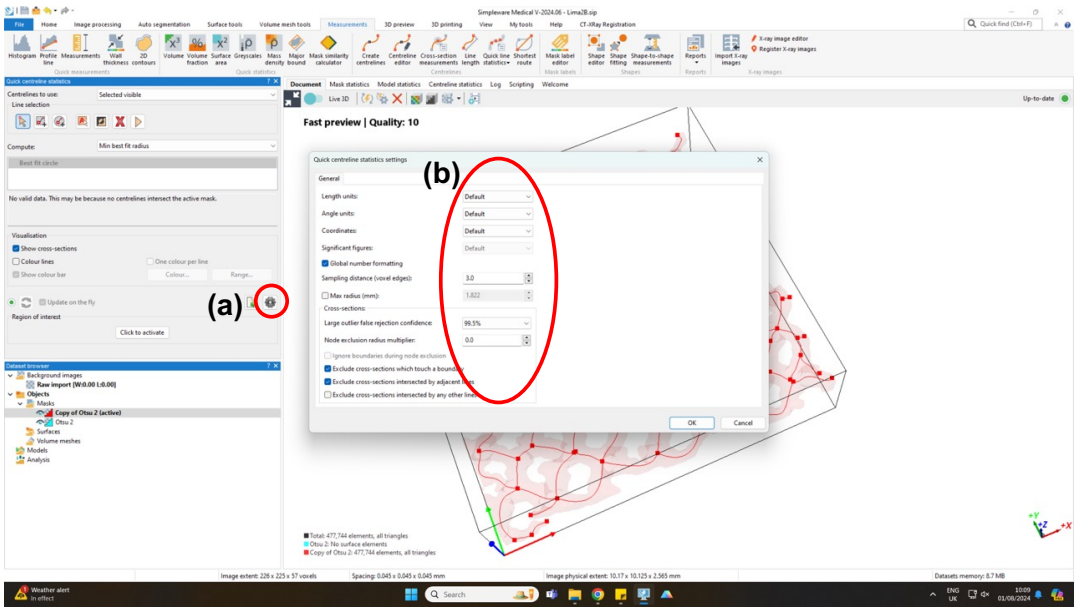

Figure: 3.H: Setting parameters for the measurements. (a) Select the ‘cog’ icon. (b) Select Options to ensure measurements taken are uniform.

c. Set sampling distance to a suitable value to ensure 5-10 readings for each strut. (increasing the readings per strut can improve the reliability and frequency of useful data readings).

5. Select ‘Selected visible’ from the centrelines to use drop-down menu. This is to isolate the readings to one strut, otherwise readings from all mapped-out struts will be exported (Figure 3.I).

6. Select the Export icon and save the file in the desired computer location (Figure 3.I).

7. Keep the existing strut selected and select a second measurement type from the quick statistics drop down menu. This is to ensure the measurements for the three parameters are taken across the same 15 struts for each sample (Figure 3.J).

8. Export and save the file for these measurements, as above.

9. Repeat steps 7-8 for the final measurement type and then repeat steps 1-9 for all implant samples across both the custom and off-the-shelf acetabular cups.

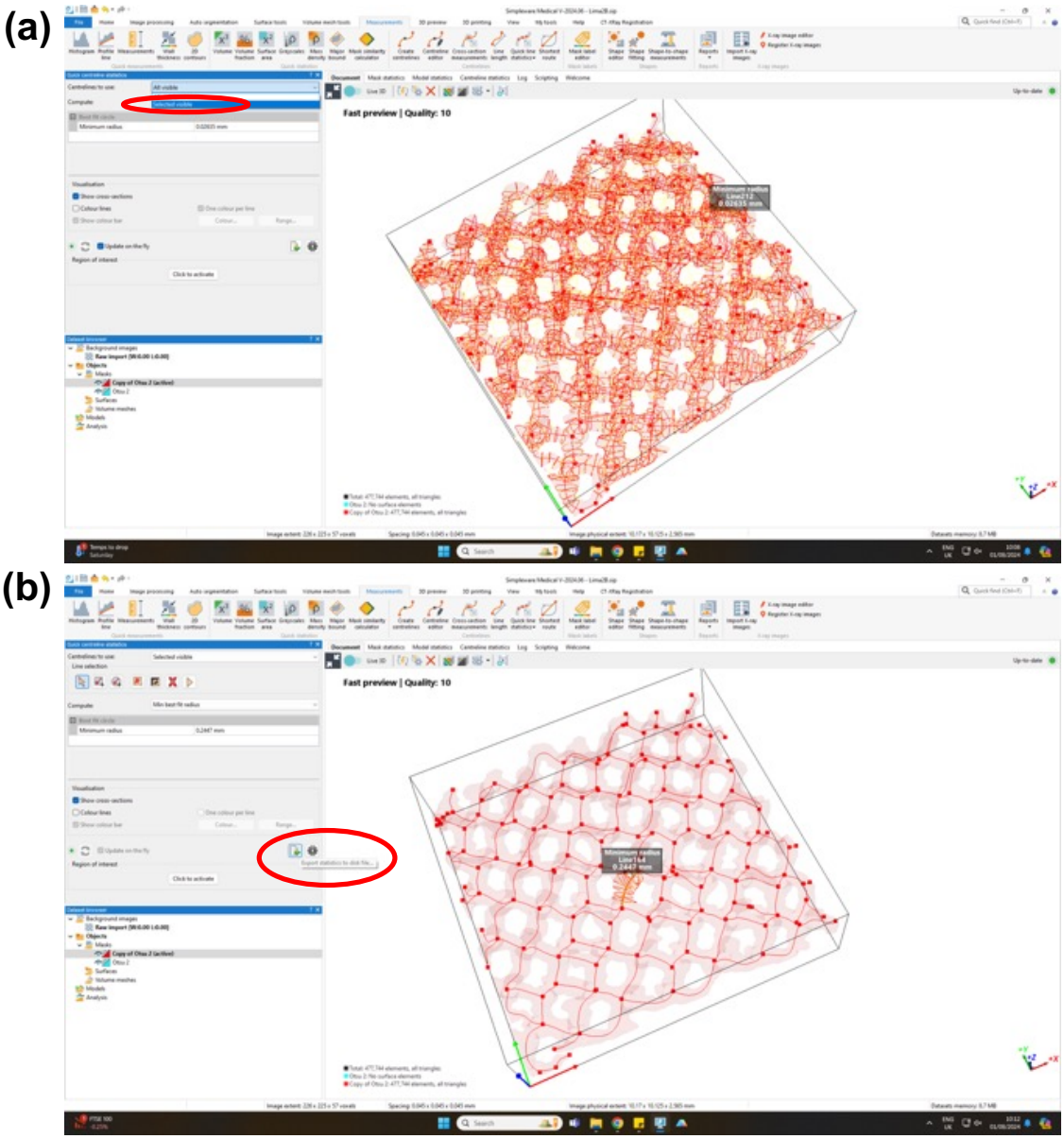

Figure 3.I: Taking measurements and exporting the readings. (a) The specific visible strut is indicated, (b)The specific visible strut is selected, select the indicated export tool to export the measurements.

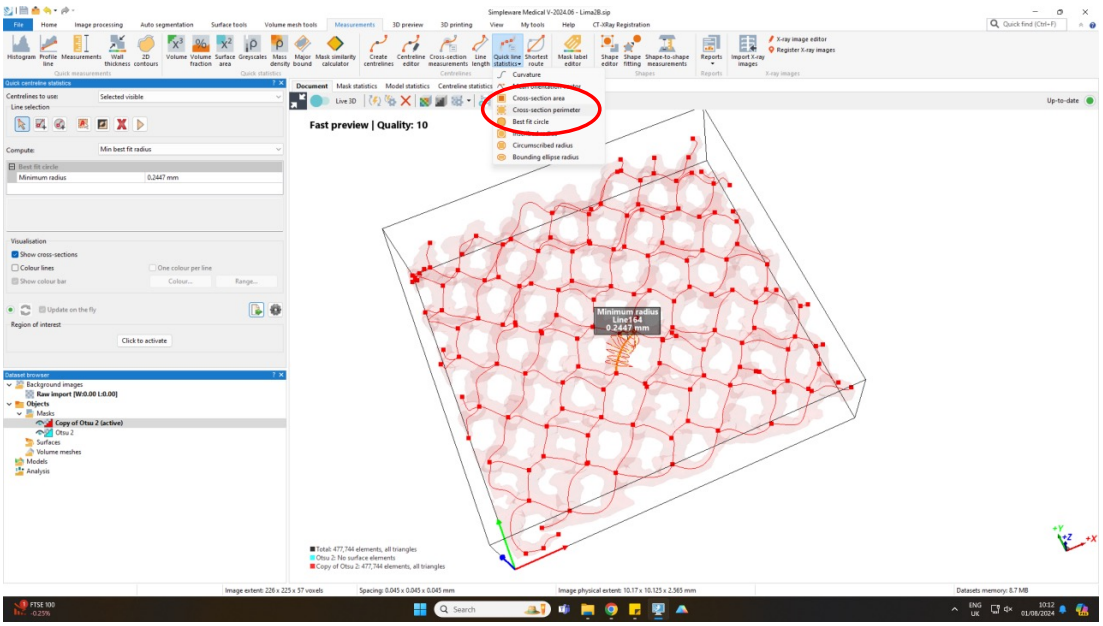

Figure 3.J: Taking the other measurements while still selecting the specific strut in Simpleware. Selecting the next measurement to be taken from the dropdown menu, as indicated.

Porosity

The porosity of the lattice was determined by using the following steps in Simpleware:

1. Generate a cuboid mask of a fixed volume and save this as a separate file (Figure 3.K).

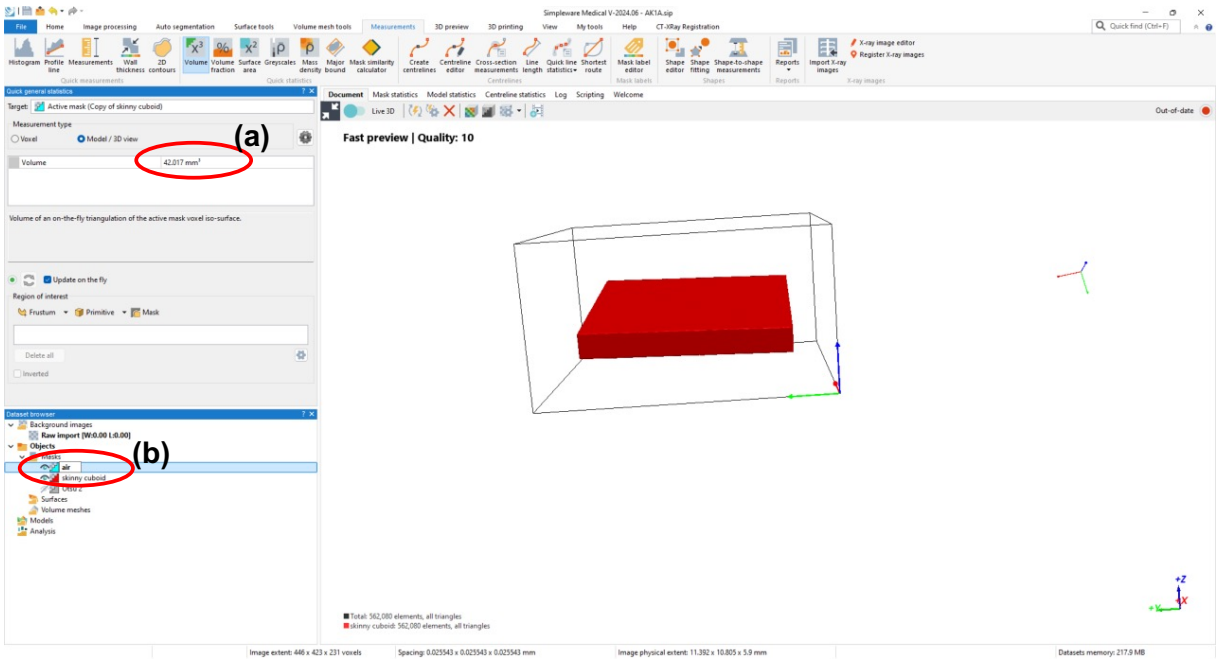

Figure 3.K: Simpleware generation of a cuboid mask. (a) Note the volume of the cuboid. (b) Duplicate the cuboid and rename the copy as ‘air’.

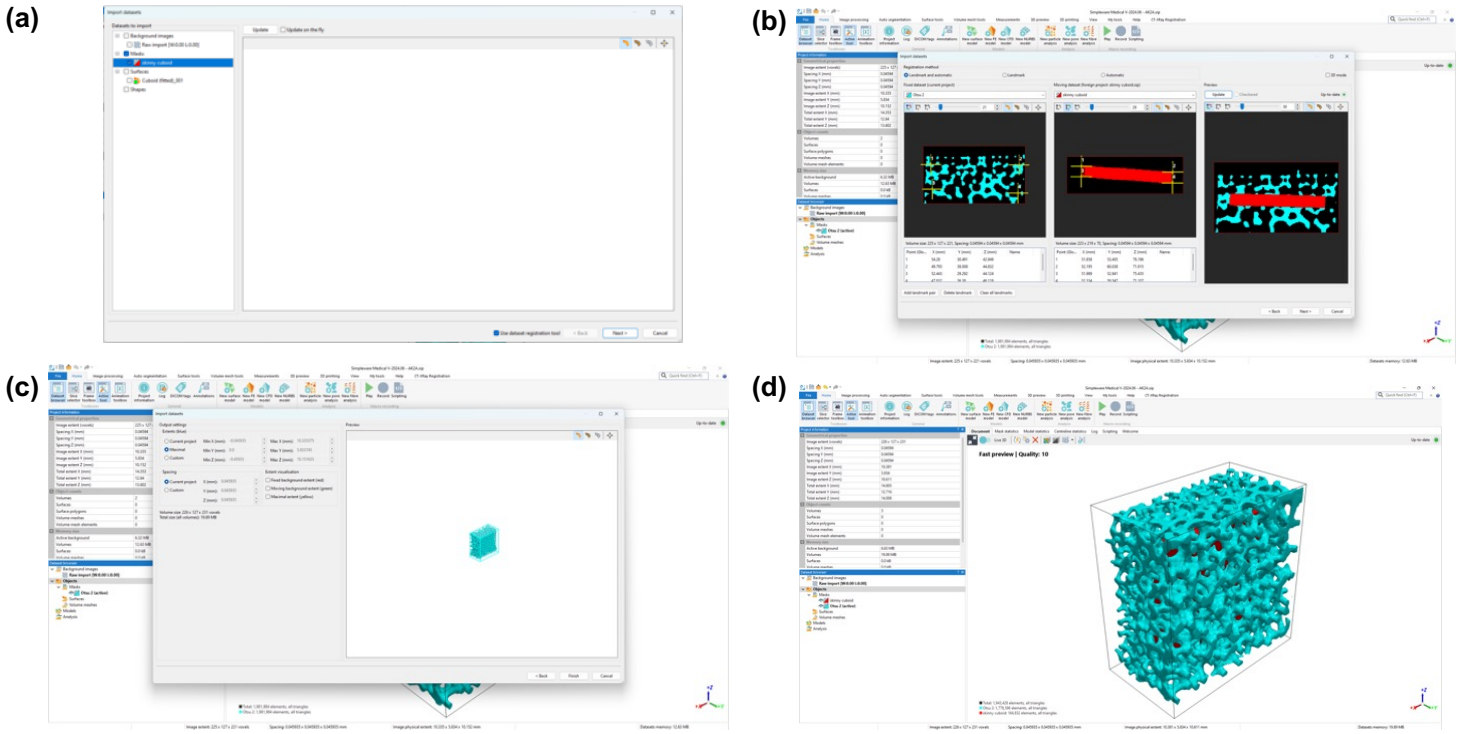

Figure 3.L: Aligning cuboid within porous structure. (a) Uploading Cuboid into same file as porous structure sample. (b) Co-registering the cuboid mask within the porous structure sample so that it is fully submerged. (c) Finalising the alignment. (d) Final alignment of cuboid submerged within sample.

2. This mask was then uploaded into the same file as the porous structure samples.
3. Duplicates of the cuboid mask and porous structure sample were made, as described above.
4. The cuboid mask was then co-registered with the implant sample to be submerged within the porous structure (Figure 3.L).
5. Once the alignment of the cuboid within the porous structure was complete, the subtraction Boolean operation (as above) was used to subtract the porous structure from the cuboid (Figure 3.M).
6. This volume, which can be read from Simpleware, was then divided by the whole volume of the cuboid, to find porosity as a percentage (%).
7. This was repeated for all samples across both the custom and off-the-shelf cups involved in this study.

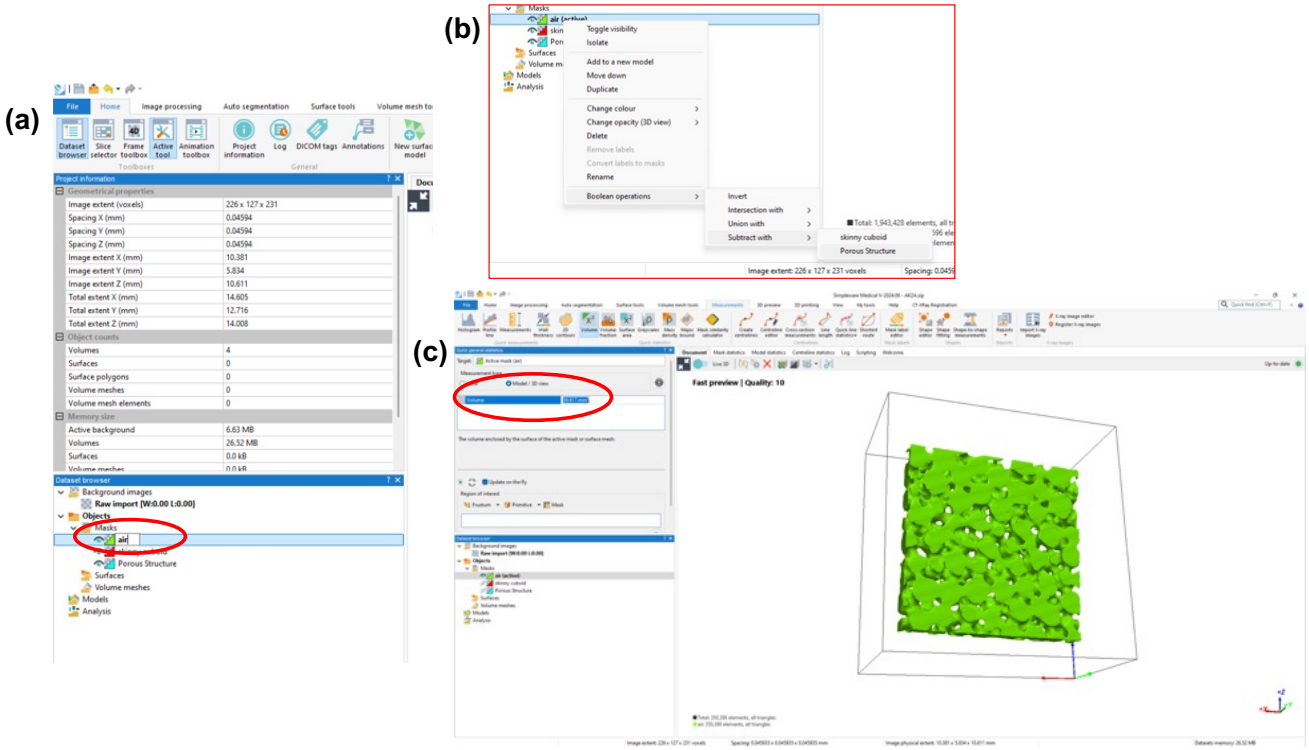

Figure 3.M: (a) Duplicating the cuboid and renaming it ‘air’. (b) Using the Boolean subtraction operation to take the volume of the porous structure from the volume of the cuboid. (c) The final volume of the cuboid (air) to calculate porosity.

Appendix II

A | ImageJ Manual Methodology

The images had been stored on the device according to manufacturer and imaged region for ease of selection. Open ImageJ and open the desired image to upload into ImageJ (Figure 4.A).

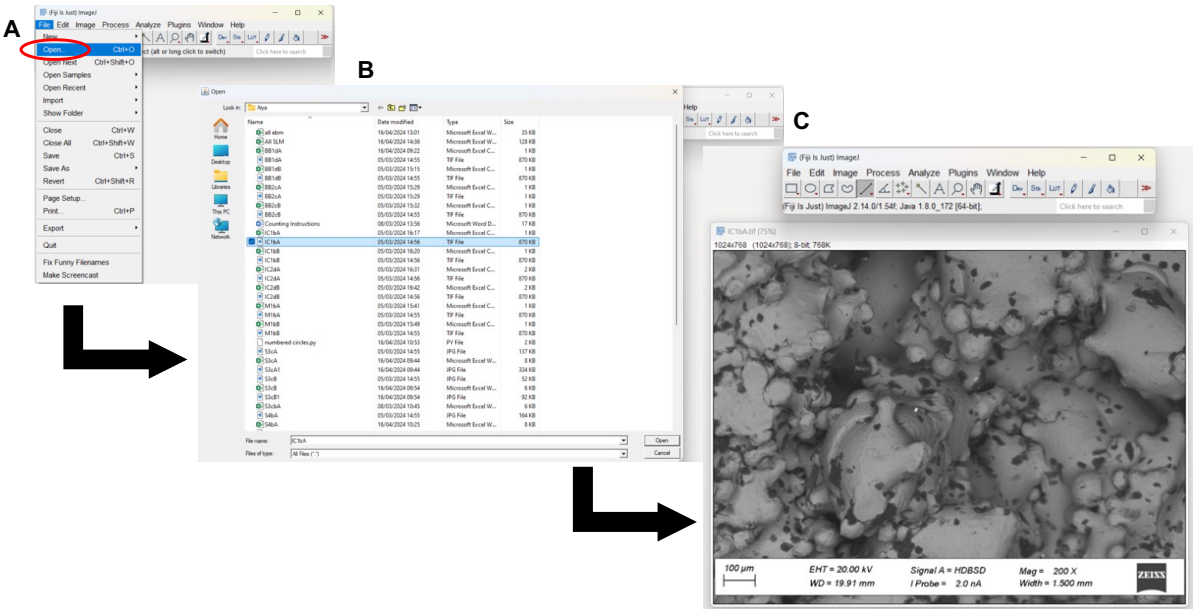

Figure 4.A: Opening ImageJ and uploading desired image into the software.

1. The image scale now needed to be calibrated. This was done by using the line tool and dragging a line across the scale bar embedded in the image (at the bottom left of the SEM image). This length of the line in pixels is then calibrated to the length and unit of the scale bar (here this was 67 pixels to 100 microns for all images at 200x magnification). This step is completed to ensure the measurements of particle radius are taken at the correct scale (Figure 4.B).

2. A grid was then overlayed on the image. This is to help prevent particles being counted more than once by the observer (Figure 4.C).

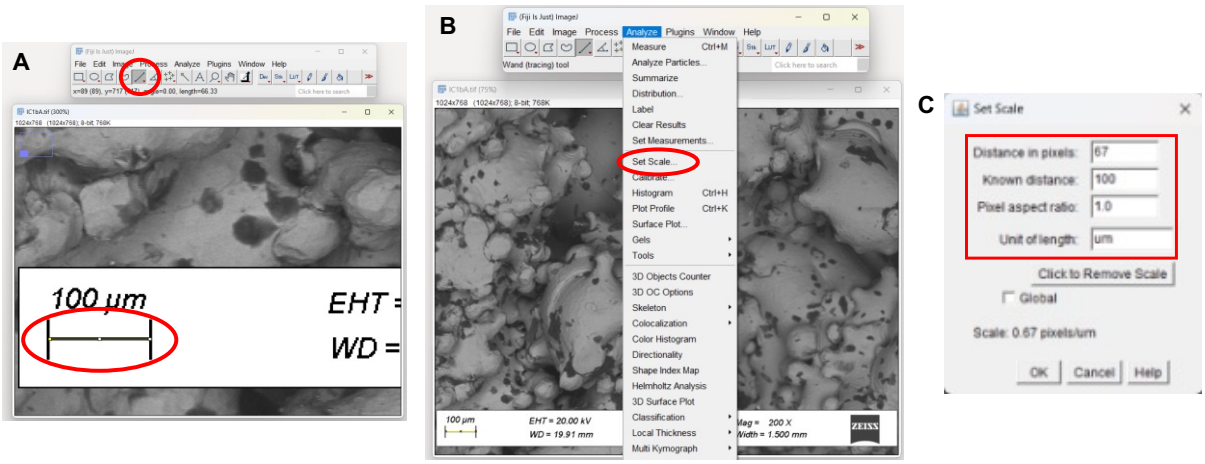

Figure 4.B: How to calibrate the image to the desired scale in ImageJ.

3. Before measuring the particles, go to the 'Analyse' option and select 'Set Measurements…' and check the specific measurement types to be recorded. For this study, 'Area' should be selected as, as diameter can be calculated using the area of a circle. This is so the diameter could then compared across cups (Figure 4.D).
4. The particles were then counted and measured using the circle tool (Figure 4.E).

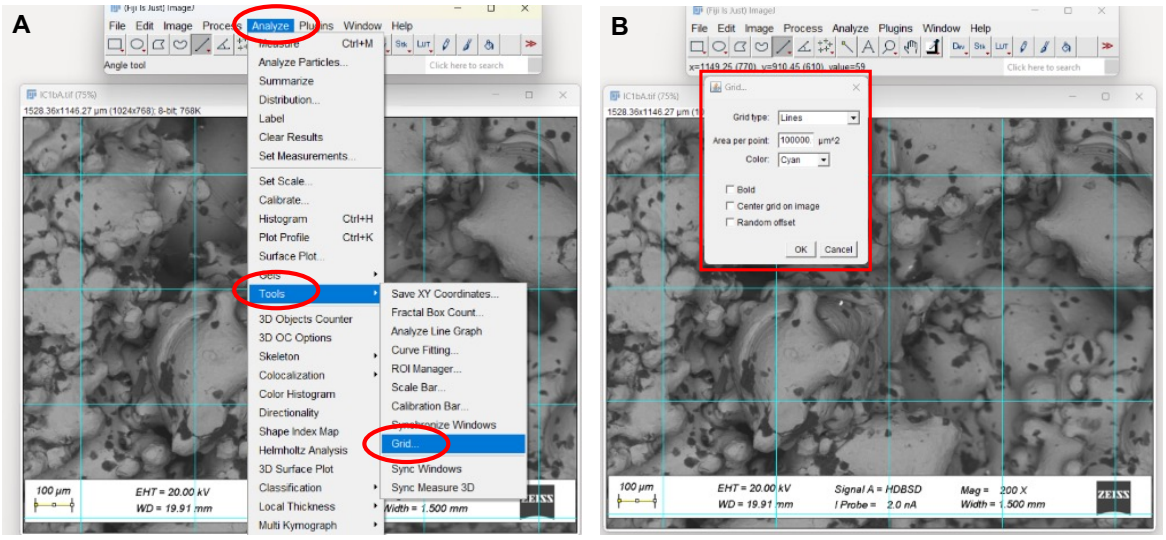

Figure 4.C: Demonstrating how to overlay a grid onto the uploaded image in ImageJ.

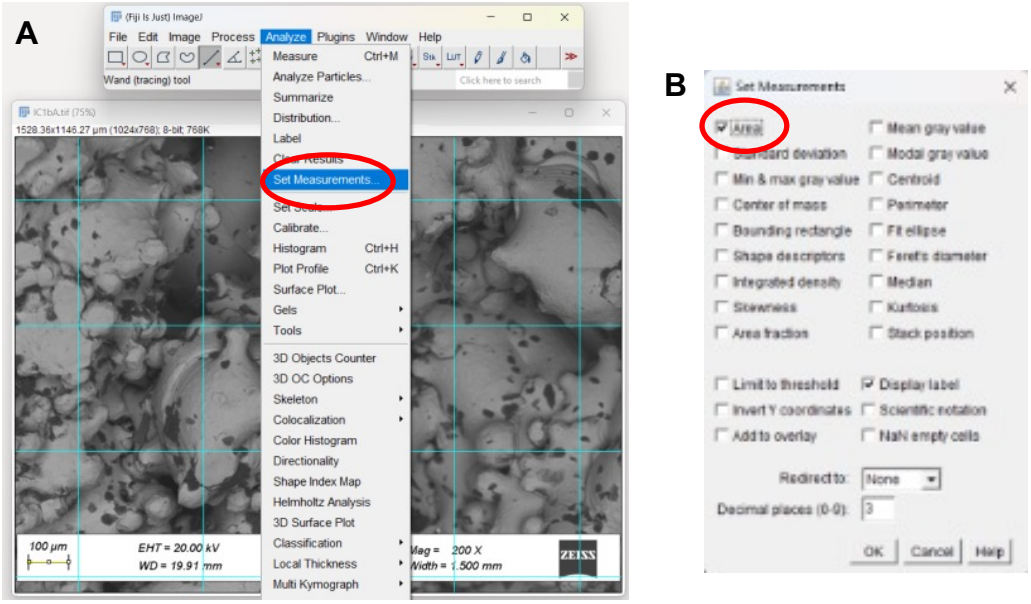

Figure 4.D: Selecting suitable options for the correct parameters for this particular study.

a. Hold down shift while dragging circle tool to maintain the circular shape when using the tool and so it does not change to ellipse when being dragged. If the identified body was a surface adhered particle it is likely to have maintained spherical shape and hence the reason for this step.

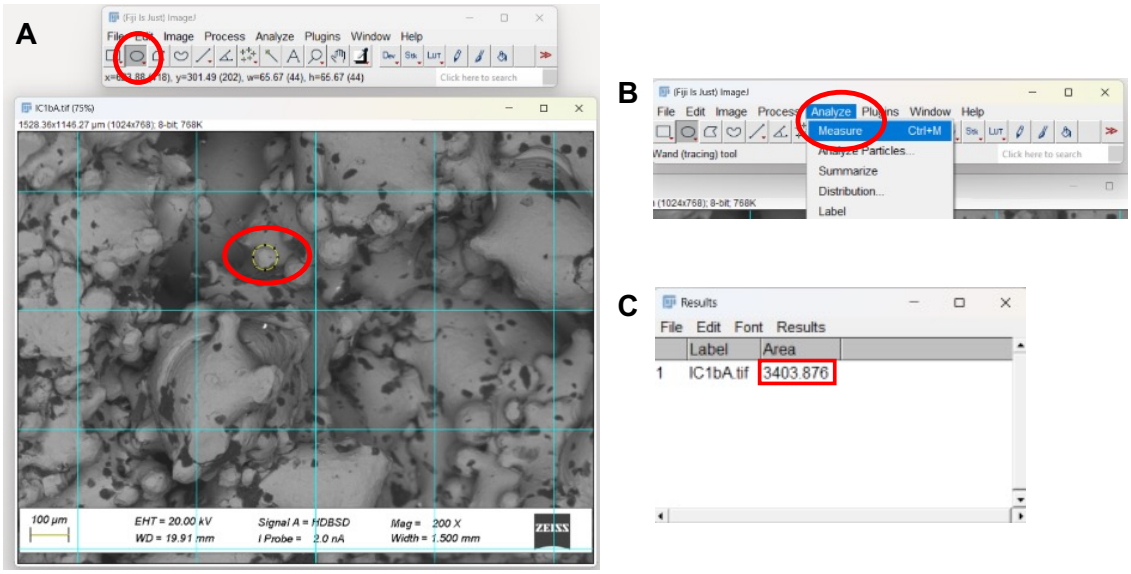

Figure 4.E: How to count particles on the image using the 'Circle' tool in ImageJ.

b. A particle was classified if 3 points of the circle tool could be fitted to the outline of the particle. This was to ensure consistency when identifying particles.

c. Let go of dragging the circle and use the shortcut Ctrl+M to record the measurement in the corresponding window.

d. Click away to remove previous circle. Without this step, using Ctrl+M on the next particle with the previous particle still highlighted will record the cumulative areas of both highlighted particles and therefore result in an incorrect reading when converted to a radius.

e. Steps a-e were repeated for every particle identified in the image.

5. The measurements were then recorded (Figure 4.F):

a. All readings were highlighted in the measurements window.

b. The measurements were then saved by right clicking and saving them as a .csv file in the same name as the corresponding image.

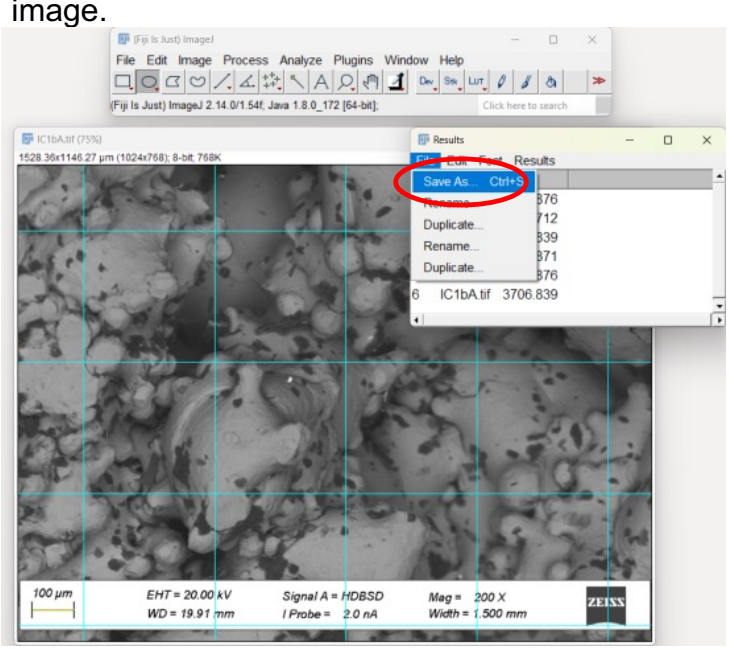

Figure 4.F: Recording and saving the readings in ImageJ.

c. The measurements window and the image window were then closed. This is to refresh the program and ensure all previous recordings had been cleared and not carried over to the next image.

6. Steps 1)-7) were then repeated for all images and implants.

B | Python Computerised Methodology

The code in Figure 4.G functions as explained below:

- Importing the relevant libraries for functions in the code(a).
- To input an image into the code to analyse (b).
- Setting parameters to identify the particles. (c) Measure the radii of the identified particles in pixels. The maximum and minimum radius could be altered to define a range for the size of particles in a particular image. This could potentially reduce the identification of larger clusters of particles such as agglomerates and other debris like impurities smaller than the expected size of the particles.
- Identifying the particles in the image. (d)
- Label the identified particles using numbers (e)
- Save the resulting image of the identified and labelled particles (f)
- Output the radius measurements in an excel spreadsheet, with the values corresponding to the numbered particles (g).
- Save the excel sheet of particle radii in a desired location on the device (h).

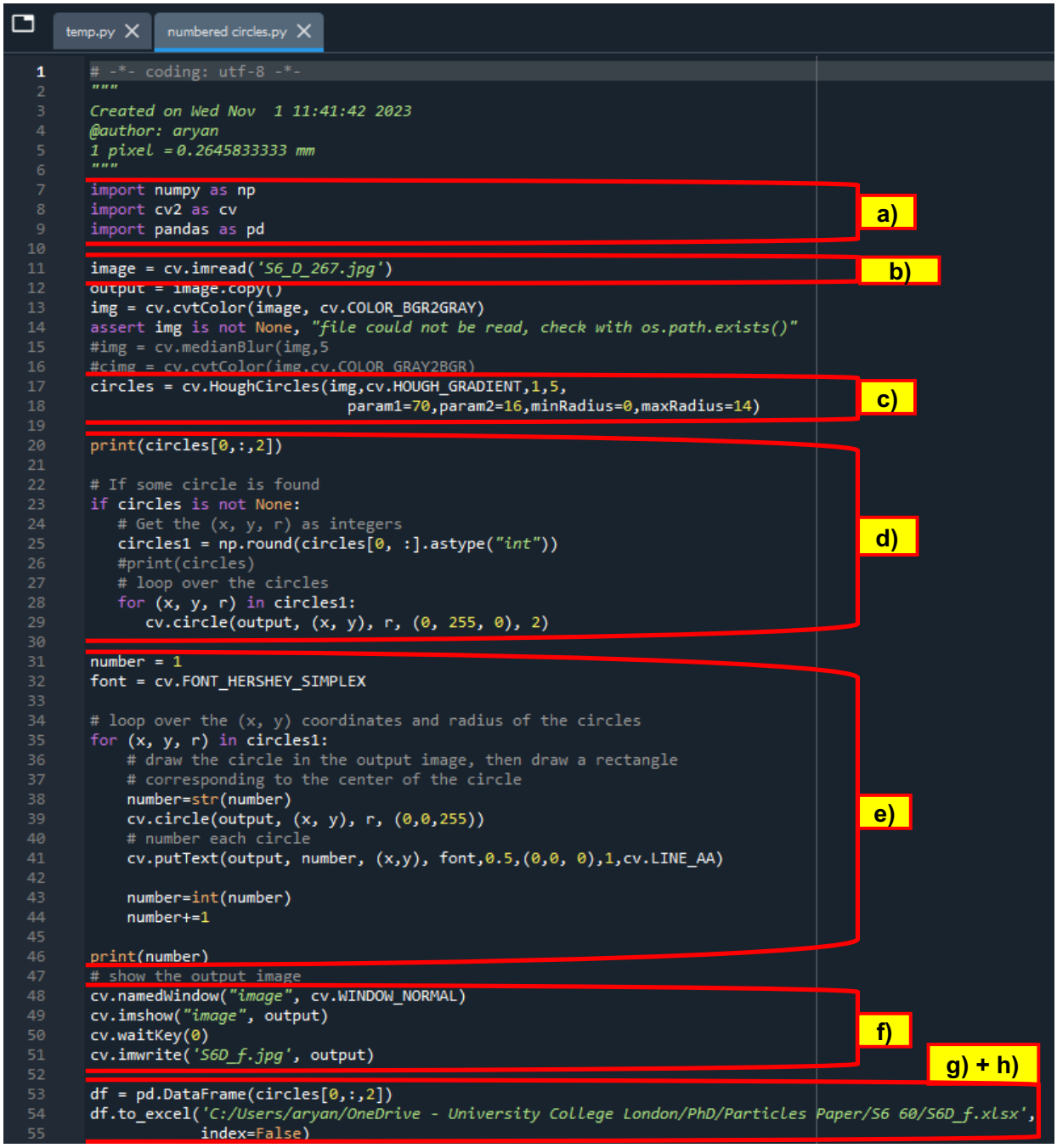

Figure 4.G: The Python code that was used to identify, measure and record the particles in each image. Parameters were able to be altered to make it suitable for the relevant image. Each section ((a) to (h)) is labelled and explained.

The parameters of the code were also refined to ensure the identification of particles and prevent the identification of false positives. This was achieved by experimenting inputting a test image through the code and varying the strength of certain parameters by altering the values (Figure 4.H). These parameters were also refined for each manufacturer to optimise the code and

Figure 4.H: Panel of images showing one image trialling code with different parameters and the outcomes. Examples of some false positives are indicated in A. The parameters are trialled and optimised to prevent these. (B) Parameter 1 is increased to make the code less sensitive. (C) Parameter 2 is increased to make the code less sensitive.

reduce false positives. The methodology consisted of several steps, but still accelerated the counting process:

Step 1: Two SEM images at the selected region were taken at 200x magnification, with the image in focus on the surface and sub-surface levels, respectively, so the particles could be identified by the code at both levels. The particles being in focus will assist the code in identification of the particles due to the more definitive edges of the particles in the image compared to the background. (Figure 4.I (A))

Step 2: The area out of focus was shaded out. (Figure 4.I (B)) This was done in Microsoft Paint where the area in focus was left visible. This was to ensure the code only picked up and identified particles at the desired surface level of the porous structure.

Step 3: The parameters of the different functions in the code were varied and the code was trialled several times with one SEM image for that manufacturer (Figure 4.G). Once optimised for the size and frequency of the particles, the code was ready for the specific images for counting and measuring.

a) Alter parameters (line 18):

   i. Param1 – larger = less sensitive (+/- 5 to 10)

   ii. Param2 – larger = less sensitive (+/- 1 to 5)

   iii. minRadius, maxRadius = Range for size of particles

a) Step 4: This shaded image was then inputted into the formulated Python code. This was done by editing the code to input the correct file location for the specific image that needed to be run through the code (Figure 4.J).

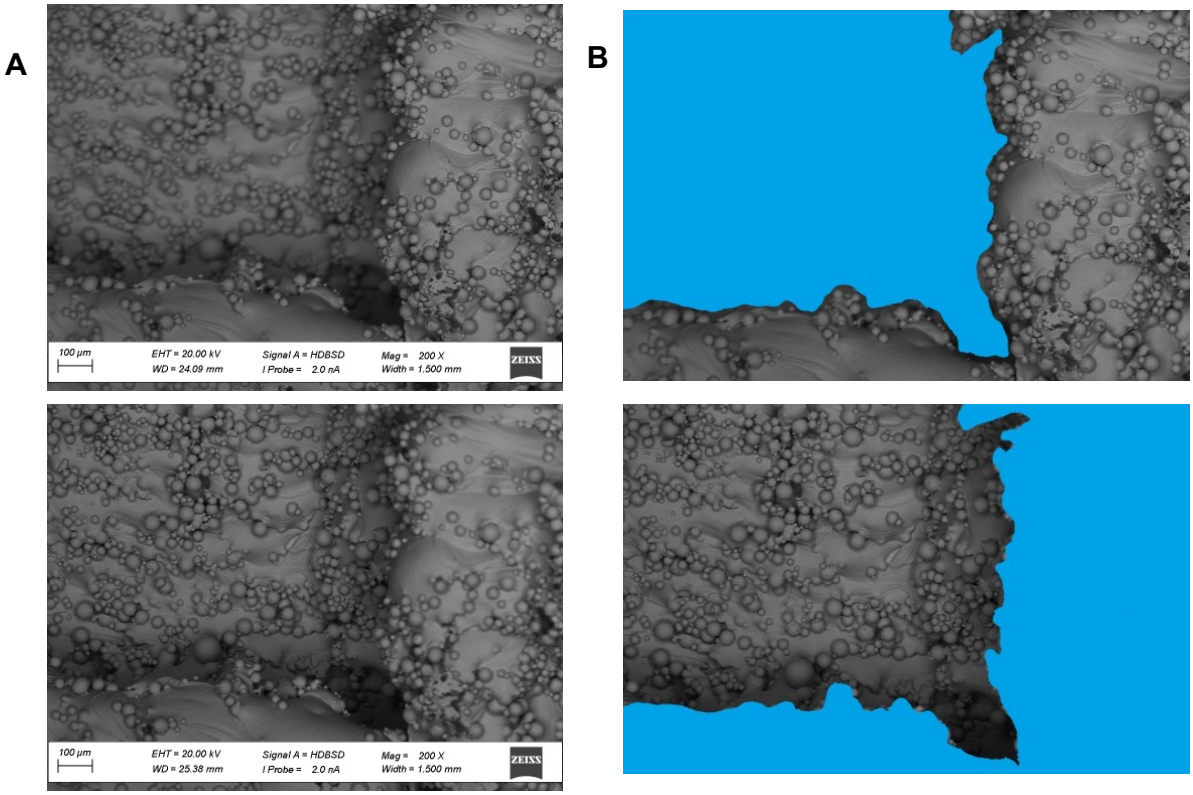

Figure 4.I: A) 2 SEM images of surface and subsurface from Cup_4B. B)The same SEM images have been shaded out for surface and subsurface ready for input into the code.

Step 5: The code both identified and numbered the majority of particles present in the image, as can be observed in the output image once the code has been run. The code then generated an Excel file of the labelled particles and their corresponding radii in pixels (Figure 4.J) and saved this file to the device in the same name as the image as defined in the code. The numbered output image (Figure 4.K) is also saved in the same location as the excel file.

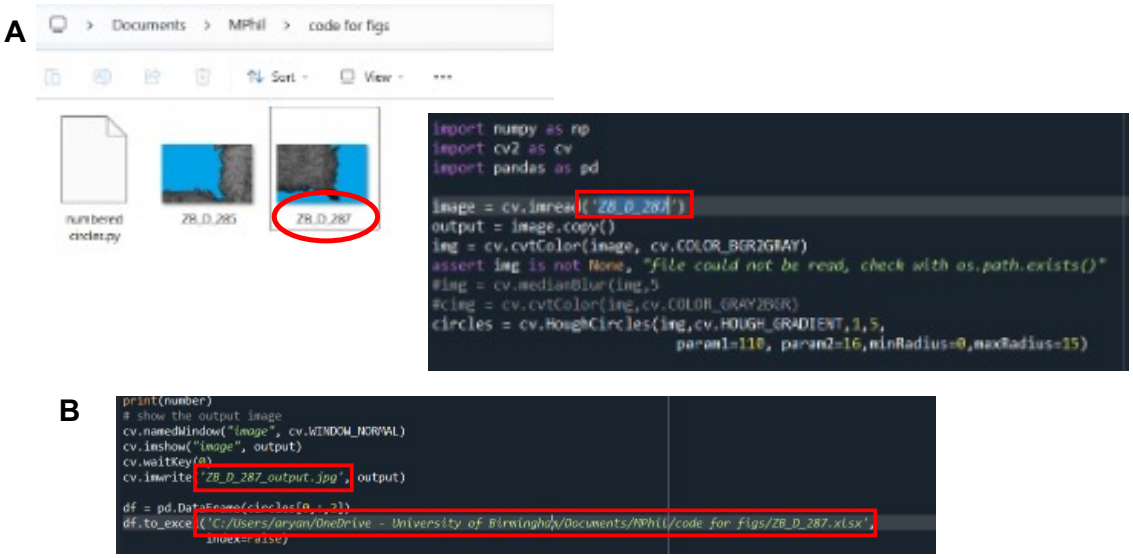

Figure 4.J: Edited code for (A) inputting the desired image using the specific image file name. (B) Saving the output image as the desired name, and saving the identified, counted and measured particles as the desired file type, name and file location.

Step 6: A conversion from pixels to micrometres (microns) was completed in Excel for the diameter for each particle. Using the conversion 67 pixels to 100 microns as defined by the manual method, all radii measured by the code were converted from pixels to micrometres, and this was completed in Microsoft Excel for efficiency.

Step 7: As the code sensitivity and parameters could not be refined to identify all particles in the inputted image without identifying false positives, the

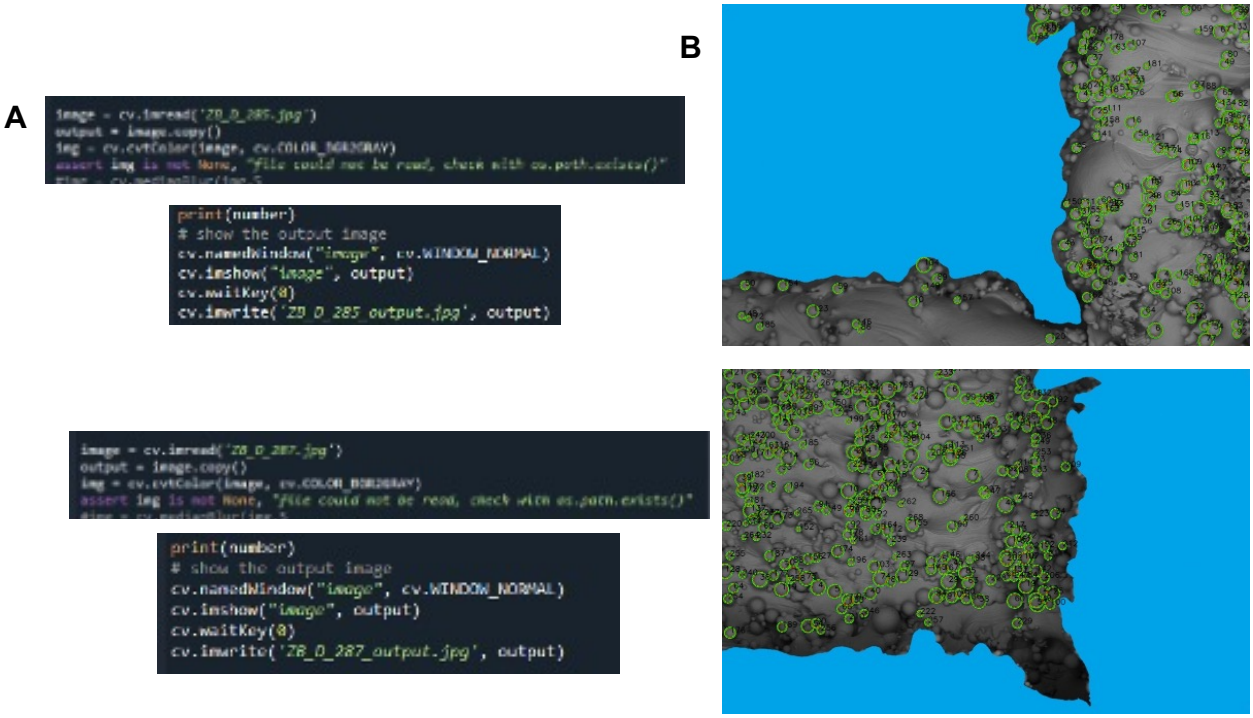

Figure 4.K: Examples of (A) Edited code to read and output saved images from code. (B) The saved resulting output images.

remainder of particles were counted in ImageJ, as per the manual method outlined above.

Step 7: Data collected via both the automated and manual methods were then collated in Excel for data processing and statistical testing.

C | Validation of Computerised Method

1. Using an image that had been put through the code using the steps detailed above, a specific labelled particle was selected on the image (Figure 4.L).
2. This numbered particle was then found on the corresponding output data Excel sheet, with the radius of the particle given in pixel size (Figure 4.L).

A

B

	radius (pixels)	Diameter pixels	Diameter um (from pixels)
1	14.4	28.8	42.9850735
2	9.6	19.2	28.6567176
3	14.4	28.8	42.9850735
4	9.6	19.2	28.6567176
5	9.6	19.2	28.6567176
6	14.4	28.8	42.9850735
7	9.6	19.2	28.6567176
8	13.2	26.4	39.4029845
9	9.6	19.2	28.6567176
10	8.2	16.4	24.4776114
11	10.9	21.8	32.5373123
12	9.6	19.2	28.6567176
13	9.6	19.2	28.6567176
14	14.4	28.8	42.9850735
15	11.3	22.6	33.7313439
16	11	22	32.8358209
17	14.4	28.8	42.9850735
18	11	22	32.8358209
19	13.2	26.4	39.4029845
20	13.2	26.4	39.4029845
21	12.1	24.2	36.1194041
22	11	22	32.8358209

Figure 4.L: A) Identifying particular particles to perform validation. B) Identifying corresponding particle measurement on excel sheet, and the conversion to diameter in microns (radius*2, ANS*67/100).

3. This measurement of the particle radius was then converted into microns, using the conversion as above (Figure 4.L).
4. This same image with the particles labelled (output from the code versus the original image) was then uploaded into ImageJ, following the steps above (Figure 4.M).
5. The radius of the specific labelled particle was then measured in ImageJ, after calibrating the image to the correct scale and using the

A

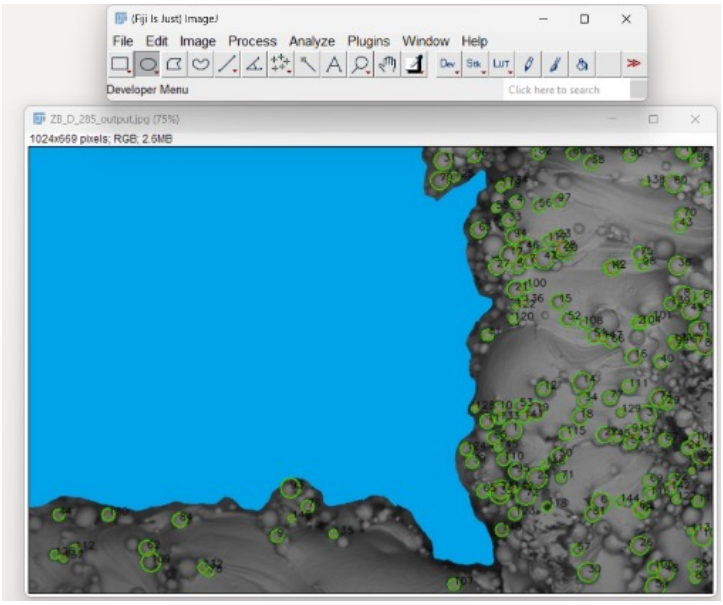

B

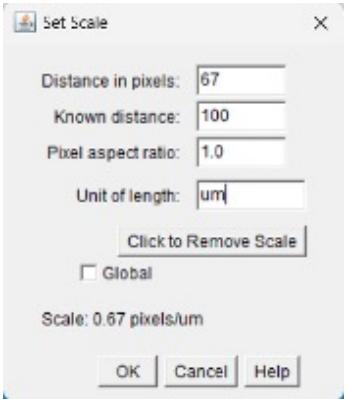

Figure 4.M: A) The code output image was uploaded into ImageJ and B) the scale was calibrated.

circle tool, as detailed above, and a concurrent value was returned, as measured by the code (Figure 4.N).

6. These steps were then completed for several particles on several different images for different implants and manufacturers to ensure sufficient validation of the computerised method (Figure 4.N).

A

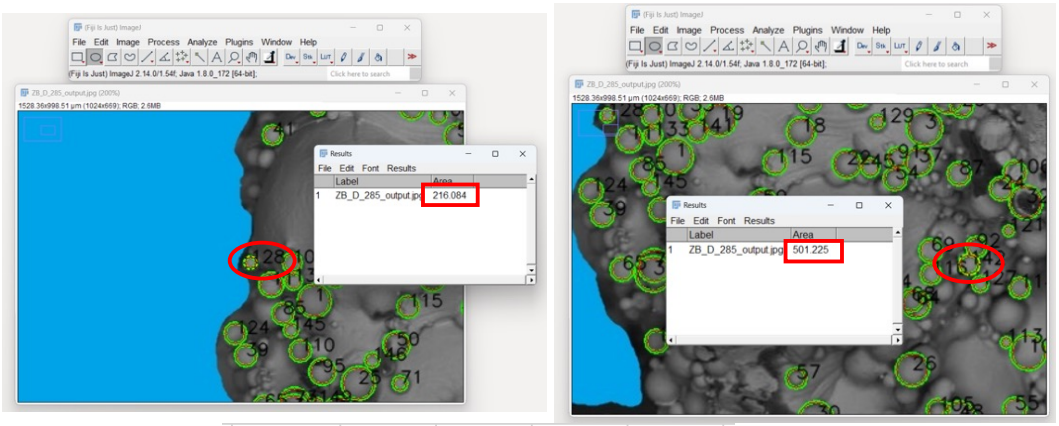

B

ImageJ				Code
Particle No.	Area	Radius	Diameter	Diameter
4	652.707	14.41399	28.82798	28.65672
14	1481.399	21.71506	43.43013	42.98507
21	997.995	17.82335	35.64669	36.1194
36	1285.364	20.22731	40.45462	39.40298
52	777.456	15.73124	31.46248	31.64179
77	652.707	14.41399	28.82798	28.65672
90	501.225	12.63111	25.26221	25.07463
94	855.424	16.50121	33.00242	32.83582
128	216.084	8.293472	16.58694	16.41791
142	501.225	12.63111	25.26221	25.07463

Figure 4.N: A) Examples using the circle tool in ImageJ to measure the specific particles. B) The areas measured for the 10 chosen particles were converted into diameters and compared with the measurements found by the code to check for concurrent values. Examples in (A) are indicated. These steps were applied to all cups counted and measured using the computerised method.